

**HAMMETT STUDY OF THE RESONANCE-ASSISTED HYDROGEN BOND IN
SUBSTITUTED *O*-ACYL NAPHTHOLS
AND
THE DEVELOPMENT OF A COMPUTATIONAL CHEMISTRY EXERCISE FOR
THE FRESHMAN-LEVEL GENERAL CHEMISTRY CURRICULUM**

A Thesis

Presented to

the Faculty of the College of Graduate Studies

Tennessee Technological University

by

Jordan Anthony Jones

In Partial Fulfillment

of the Requirements of the Degree

Master of Science

Chemistry

August 2020

ProQuest Number:28028368

All rights reserved

INFORMATION TO ALL USERS

The quality of this reproduction is dependent on the quality of the copy submitted.

In the unlikely event that the author did not send a complete manuscript and there are missing pages, these will be noted. Also, if material had to be removed, a note will indicate the deletion.



ProQuest 28028368

Published by ProQuest LLC (2020). Copyright of the Dissertation is held by the Author.

All Rights Reserved.

This work is protected against unauthorized copying under Title 17, United States Code
Microform Edition © ProQuest LLC.

ProQuest LLC
789 East Eisenhower Parkway
P.O. Box 1346
Ann Arbor, MI 48106 - 1346

© Jordan A. Jones, David J. Crouse, and Chad E. Rezsnyak 2020.

TABLE OF CONTENTS

AN ABSTRACT OF A THESIS	ix
CERTIFICATE OF APPROVAL OF THESIS	x
DEDICATION.....	xi
ACKNOWLEDGEMENTS.....	xii
LIST OF FIGURES	xiii
LIST OF TABLES.....	xv
PART I: HAMMETT STUDY OF THE RESONANCE-ASSISTED HYDROGEN BOND IN SUBSTITUTED <i>O</i> -ACYL NAPHTHOLS	
CHAPTER 1: INTRODUCTION.....	2
A. Hydrogen Bonds	2
1. The Hydrogen Bond and Methods of Study	2
2. The Hydrogen-Bond Chemical Leitmotifs	5
3. Historical Background of the Resonance-Assisted Hydrogen Bond	6
4. The “Classification” of RAHBs and Some Contemporary Studies Thereof	11
B. Hammett Equation.....	13
1. The Intent of the Hammett Equation and Some Contemporary Uses Thereof.....	17
C. Prior Work on This Project	18
D. Goals	21
CHAPTER 2: EXPERIMENTAL.....	26

A. Materials.....	26
B. Methods.....	28
C. Naphthol Preparations.....	31
1. Preparation of 1-Methyl-1,4-dihydro-1,4-epoxynaphthalene – JAJ1-54-D	31
2. Preparation of 4-Methyl-1-naphthol – JAJ2-39-A.....	32
3. Attempted Preparation of 4-Bromo-1-naphthol – JAJ1-37-A	34
4. Attempted Preparation of 4-Nitro-1-naphthol – JAJ1-69	36
5. Attempted Preparation of 4-Bromo-1-naphthol – JAJ1-71	37
D. Esters.....	39
1. Preparation of 4-Methoxynaphth-1-yl Benzoate – JAJ2-01-A.....	39
2. Preparation of 4-Chloronaphth-1-yl Benzoate – JAJ1-19-A	41
3. Preparation of 4-Nitronaphth-1-yl Benzoate – JAJ2-13-A.....	42
4. Preparation of 4-Bromonaphth-1-yl Benzoate – JAJ2-35-B	43
5. Preparation of 4-Methylnaphth-1-yl Benzoate – JAJ2-56-A.....	43
6. Preparation of 4-Nitronaphth-1-yl <i>p</i> -Toluate – JAJ2-57-A	44
E. Photoreactions	45
1. Preparation of 2-Benzoyl-4-chloro-1-naphthol – JAJ2-19-A	45
2. Preparation of 2-Benzoyl-4-methoxy-1-naphthol – JAJ2-53-B	47
3. Preparation of 2-Benzoyl-4-nitro-1-naphthol – JAJ2-54-B.....	48
4. Preparation of 2-Benzoyl-4-bromo-1-naphthol – JAJ2-58-A.....	49

5. Preparation of 2-Benzoyl-4-methyl-1-naphthol – JAJ2-59-A	50
6. Preparation of 2-(<i>p</i> -Toluoyl)-4-nitro-1-naphthol – JAJ2-60-A	51
CHAPTER 3: DISCUSSION.....	52
A. Analysis of Synthetic Methods	52
1. Synthesis of Naphthols	52
2. Esterification Reactions	55
3. Photo-Fries Reactions	56
B. Hammett Study.....	60
1. Results from Series 2 Compounds.....	60
2. Revision of Previous Results	63
3. Discussion of Hammett Study Data for Series 1 and 2 Compounds	64
CHAPTER 4: CONCLUSIONS	70
A. FUTURE WORK.....	72
PART II: THE DEVELOPMENT OF A COMPUTATIONAL CHEMISTRY EXERCISE FOR THE FRESHMAN-LEVEL GENERAL CHEMISTRY CURRICULUM.....	74
CHAPTER 5: INTRODUCTION	75
A. The Valence Shell Electron Pair Repulsion Model	75
1. History of the Model.....	75
2. Modern Day Classroom Significance	76
B. Computational Chemistry	78

1. The Basics of Computational Chemistry	78
2. Uses of Computational Chemistry in Research and Industry	80
3. Computational Chemistry in the Classroom	81
4. The Avogadro Software	83
C. Goals	84
CHAPTER 6: METHODS	85
A. The Avogadro Exercise	85
B. Data Collection	87
1. Secondary Worksheet Data	87
2. Pre-Quizzes and Post-Quizzes	88
3. Student Survey	89
4. Final Exam Aggregate Data	89
CHAPTER 7: RESULTS	91
A. Secondary Worksheet Data	91
B. Pre-Quizzes and Post-Quizzes	92
C. Student Survey	93
D. Final Exam Aggregate Data	95
CHAPTER 8: DISCUSSION	98
A. The Performance of the Avogadro Software	98
B. Student Satisfaction and Learning Outcomes	99

CHAPTER 9: CONCLUSION	102
A. Future Work	102
APPENDIX A: ¹ H NMR DATA	104
Appendix B: ¹³ C NMR Spectra.....	119
Appendix C: FT-IR Spectra	134
Appendix D: The Avogadro Exercise.....	141
Appendix E: The Avogadro Exercise Pre-Quiz.....	151
Appendix F: The Avogadro Exercise Post-Quiz	153
Appendix G: The Avogadro Exercise Student Survey	155
References.....	156
Vita.....	163

AN ABSTRACT OF A THESIS

HAMMETT STUDY OF THE RESONANCE-ASSISTED HYDROGEN BOND IN SUBSTITUTED *O*-ACYL NAPHTHOLS AND THE DEVELOPMENT OF A COMPUTATIONAL CHEMISTRY EXERCISE FOR THE FRESHMAN-LEVEL GENERAL CHEMISTRY CURRICULUM

Jordan Anthony Jones

Master of Science in Chemistry

Part I

Resonance assisted hydrogen bonds (RAHBs) are among the strongest forms of hydrogen bonding known to occur and are found in specific intramolecular hydrogen-bonding systems. Two series of ortho-acylnaphthols that undergo this type of hydrogen bonding were synthesized. One series was substituted on the 4-naphthol position (Y), and the other substituted on the *p*-benzoyl position (X), where X or Y = OCH₃, CH₃, H, Br, Cl, or NO₂. A Hammett study was carried out using ¹H NMR and ¹³C NMR to determine the nature of the electronic effects on the RAHB in this system. Previous research has shown that *p*-benzoyl substituents cause the enolic ¹H NMR shift to increase when electron-donating groups are in the *para* position, exhibiting shifts up to 14.01ppm. The opposite trend has now been observed with 4-naphthyl substituents; the enolic ¹H NMR shift increased as the electron-withdrawing character of the substituent increased, exhibiting shifts up to 14.60ppm.

Part II

A computational chemistry exercise intended for second-semester general chemistry students has been developed and used in the laboratory curriculum at a regional university. Students used the Avogadro software to build, optimize, and measure bond lengths and angles in simple organic molecules, focusing on the functional groups. The exercise was used as an out-of-class exercise for students to review VSEPR theory while simultaneously introducing them to organic functional groups and computational chemistry fundamentals. A pre-test and post-test were used to evaluate the educational efficacy of the exercise, and a survey was conducted to determine if students found the exercise helpful. Data from the student responses were also collected and evaluated to determine if the Avogadro software's default optimization parameters are adequate for this application.

CERTIFICATE OF APPROVAL OF THESIS
HAMMETT STUDY OF THE RESONANCE-ASSISTED HYDROGEN BOND IN
SUBSTITUTED *O*-ACYL NAPHTHOLS
AND
THE DEVELOPMENT OF A COMPUTATIONAL CHEMISTRY EXERCISE FOR
THE FRESHMAN-LEVEL GENERAL CHEMISTRY CURRICULUM

by

Jordan Anthony Jones

Graduate Advisory Committee:

David Crouse, Co-Chair

Date

Chad Rezsnyak, Co-Chair

Date

William Carroll

Date

Approved for the Faculty:

Mark Stephens, Dean
College of Graduate Studies

Date

DEDICATION

This thesis is the culmination of six years of overall research experience on my part, and much work from my predecessors. I dedicate it to everyone that has taught me to be a better person, a better leader, a better teacher, or a better scientist as I have grown up. That includes everyone from my parents, who let me be a little scientist and continue encouraging me to change the world even today. From them to the elementary school teachers that told me I would make a good science teacher someday, to my teachers and friends in the high school band that taught me many lessons about leadership and being a responsible person, and all the way up to my professors, supervisors, and friends at Tennessee Tech who have taught me more than I know how to put into words.

I would like to recognize a specific group of people that helped me realize how much I enjoyed teaching: my 150 friends of all sizes in the TTU Child Development Lab. The CDL served as my first job for five years, and working there taught me many things about communication, patience, and service. I always looked forward to going to work, and you all have my sincerest thanks for the role you played in helping me mature into a better teacher and a better person. Without all of you, I might not be where I am today.

ACKNOWLEDGEMENTS

The TTU Student Research Grant provided funding for my research. My sincere thanks are due to the chemistry department for providing these funds.

My foremost thanks go to Dr. Daniel Swartling and Dr. David Crouse, my primary research mentors during my time at Tennessee Tech. I have to thank Dr. Dan for letting me spend four years in his lab and putting up with the slow, sometimes painful process of teaching me the basics of being a good chemist. Thanks for everything, Dr. Dan.

Dr. Crouse has long been a mentor figure. In undergrad, if I asked his thoughts on a synthetic procedure for research, he was happy to give advice. It has been an honor to work for him in graduate school. Thanks for your guidance and for always having an open door!

Additional thanks go to Dr. Chad Rezsnyak, with whom I worked on the second part of this thesis. I learned a lot about teaching and administrating from Dr. Rezsnyak, and his guidance as I navigated my way through being a new Graduate Assistant was invaluable.

I would like to thank all of the faculty and staff of the chemistry department, all of whom have been a big help to me. My sincere thanks go to our support staff, Gene Mullins, Tina Norman, Lisa Norsworthy, and Tammie Hanchey, for keeping me on track. And to the other members of my graduate advisory committee, Drs. William Carroll and Corey Hawkins, thank you for serving on my committee. Thanks also go to Dr. Mike Allen in Mathematics for an incredibly useful discussion of statistics relating to this thesis.

To the other chemistry graduate students, thanks for supporting me and making this experience fun! I will miss you all as we part ways for now.

Finally, my thanks and my love go to my parents and family. They raised me and gave me the support I needed to make it this far. If not for you, I would not be here.

LIST OF FIGURES

Page 3	Figure 1.1: The D–H---A Hydrogen Bond Complex
Page 7	Figure 1.2: Tautomerization of a Ketone into an Enol
Page 8	Figure 1.3: Tautomerization of Acetylacetone
Page 8	Figure 1.4: Resonance Structures of Acetylacetone's Enol Isomer
Page 10	Figure 1.5: General Structures of the Enol and Keto Forms of an <i>ortho</i> -Ketophenol
Page 10	Figure 1.6: General Structure of <i>o</i> -Acyl-naphthols
Page 11	Figure 1.7: Tautomers of 2-Nitromalonamide
Page 12	Figure 1.8: The Suggested Resonance of the Acetylacetone System
Page 15	Figure 1.9: The Standard Reaction Chosen by Hammett to Define the Substituent Constant
Page 19	Figure 1.10: Structures of Series 1 and Series 2 <i>o</i> -Acyl-naphthols
Page 20	Figure 1.11: Hammett Diagrams for Series 1 Compounds
Page 21	Figure 1.12: Electronic Trend Observed by Mathis
Page 23	Figure 1.13: Proposed Synthetic Route; Reactions A and B
Page 23	Figure 1.14: Proposed Synthetic Route; Reaction C
Page 25	Figure 1.15: Proposed Synthetic Route; Reactions D, E, and F
Page 29	Figure 2.16 The Photochemical Reactor Setup Used
Page 52	Figure 3.17: Reaction Scheme While Producing 3-Methyl-1-naphthol
Page 54	Figure 3.18: Generic Reaction Equations for Attempted Naphthamine to Naphthol Syntheses

Page 54	Figure 3.19: Potential Reaction Scheme for an Azo Coupling
Page 55	Figure 3.20: Generic Esterification Equation and Series 1 and 2 Structures
Page 56	Figure 3.21: Generic Photo-Fries Equation and Series 1 and 2 Structures
Page 58	Figure 3.22: Mechanism of the Photo-Fries Equation
Page 62	Figure 3.23: Plot of Series 2 Enol ^1H NMR Shifts Versus Hammett Substituent Constants, σ_p
Page 62	Figure 3.24: Plot of Series 2 Carbonyl ^{13}C NMR Shifts Versus Hammett Substituent Constants, σ_m
Page 64	Figure 3.25: Plot of Series 1 Enol ^1H NMR Shifts Versus Hammett Substituent Constants, σ_p
Page 64	Figure 3.26: Plot of Series 1 Carbonyl ^{13}C NMR Shifts Versus Hammett Substituent Constants, σ_m
Page 71	Figure 4.27: Electronic Trend in Series 2 Compounds
Page 73	Figure 4.28: Proposed Structure of Series 3 Compounds
Page 77	Figure 5.29: VSEPR Model of Tetrachloroplatinate(II) Anion Versus Empirically Observed Structure
Page 92	Figure 7.30: The First Set of Molecules that Students have a Choice to Model
Page 94	Figure 7.31: Student Survey Results
Page 95	Figure 7.32: Student Responses on Question 1, Fall 2017 Versus Fall 2019
Page 96	Figure 7.33: Student Responses on Question 2, Fall 2017 Versus Fall 2019

LIST OF TABLES

Page 5	Table 1.1: The Six Chemical Leitmotifs
Page 27	Table 2.2: Information About Solvents, Reagents, and Other Chemicals
Page 56	Table 3.3: Yields of the Various Esters
Page 60	Table 3.4: Yields of the Various Ketones
Page 61	Table 3.5: ^1H NMR Shift Assignments for Series 2 Compounds
Page 61	Table 3.6: ^{13}C NMR Shift Assignments for Series 2 Compounds
Page 63	Table 3.7: ^1H and ^{13}C NMR Shift Assignments for Series 1 Compounds
Page 68	Table 3.8: Comparison of Enolic ^1H NMR Shifts for the Highest Shift Compound in Series 1, in Series 2, and the Hybrid Compound
Page 91	Table 7.9: Average Bond Angles Calculated by the Students and Expected Values
Page 92	Table 7.10: Results from the Pre-Quiz
Page 93	Table 7.11: Results from the Post-Quiz
Page 93	Table 7.12: Student Free-Responses from Survey
Page 97	Table 7.13: ANOVA test results from Question 1 (VSEPR) datasets
Page 97	Table 7.14: ANOVA test results from Question 2 (hybridization) datasets.
Page 97	Table 7.15: Descriptive statistics of the two datasets.

PART I:
HAMMETT STUDY OF THE RESONANCE-ASSISTED HYDROGEN BOND IN
SUBSTITUTED *O*-ACYL NAPHTHOLS

CHAPTER 1: INTRODUCTION

A. Hydrogen Bonds

1. The Hydrogen Bond and Methods of Study

A hydrogen bond (H-bond) is a phenomenon wherein a hydrogen atom with a sigma bond to a highly electronegative atom can experience a weak, mostly ionic interaction with nearby electronegative atoms (*I*). This interaction can be either intramolecular or intermolecular. In general, the H-bonded complex produced by such an interaction can be written as D–H•••A, wherein the D–H denotes the H-bond donor atom with hydrogen sigma bonded to it, A denotes the H-bond acceptor atom, and the ••• notation symbolizes the weak ionic interaction that is occurring. An H-bond type interaction is not limited to systems where a hydrogen atom is covalently bound to another atom in the donor-acceptor pair. However, this D–H•••A system denoted above is the most common form of H-bond that is encountered in nature; examples of alternative types of H-bonds will be discussed later in the text. For example, **Figure 1.1** shows an example using two water molecules, wherein the oxygen atom on the right serves as the H-bond acceptor, and the O–H pair on the left act as the H-bond donor. This occurs throughout molecular water in the liquid and solid phase, and the extensive network of hydrogen bonds accounts for many of the unique physical properties of water (*e.g.*, high boiling point, high melting point, wide range between melting and boiling, and ability to dissolve many compounds of varying solubility) (*I*).

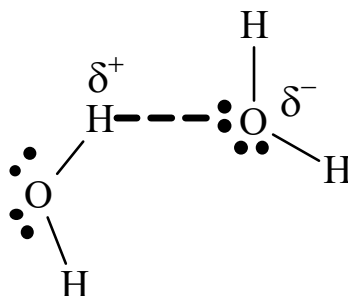


Figure 1.1. The D–H---A hydrogen bond complex (denoted with dashes here to avoid confusion with the lone pairs), demonstrated with two water molecules. In liquid water, each water molecule continually experiences many of these transient H-bonds with nearby water molecules.

A variety of methods can monitor hydrogen bonds. One of the earliest spectroscopic methods, utilized beginning in the early 1930s, was infrared (IR) spectroscopy, wherein the H-bonded complex, D–H•••A, induces a change in the vibrational stretching frequency of the D–H bond that can be observed when the H-bonded complex is not in place. Therefore, there can be defined an equation 1.1 where:

$$\Delta\nu = \nu^\circ - \nu \quad [1.1]$$

Wherein ν (nu) is the stretching frequency for D–H in the H-bonded state, ν° is the stretching frequency for D–H in the non-H-bonded state, and $\Delta\nu$ is the difference in the two stretching frequencies. This data can then be used to examine the strength of a hydrogen bond, as well as its spatial orientation, to a limited extent (*I*).

X-ray diffraction methods, or simply x-ray crystallography, have also been used to study H-bonds in crystals, with reviews of techniques beginning as early as the 1950s. These methods provided the first reliable means of determining the D•••A distances for common H-bonds in crystals. However, these methods are incapable of directly determining the position of the hydrogen atoms. There was a substantial growth of H-bond studies using x-ray diffraction in the 1970s when the development of computer-controlled x-ray diffractometers

and computational methods to solve most organic structures (1). This continued growth of the x-ray diffraction field has continued into recent times. For example, in 2002, researchers used variable-temperature x-ray crystallography to study a ketohydrazone–azoenol system (2). However, not being able to determine the exact location of the protons remains a barrier that fundamentally limits x-ray crystallography's usefulness (1).

In the 1950s, the advent of ^1H Nuclear Magnetic Resonance (NMR) brought about unprecedented sensitivity in the monitoring of H-bonds in solution in an effort spearheaded by Huggins, Pimentel, and Shoolery. They first studied ^1H -NMR of chloroform and determined its high chemical shift ($\delta=7.26\text{ppm}$) could be the result of H-bonding (3). The other methods of examining H-bonds are each important and useful. However, none have had an impact comparable with that of NMR, which makes the examination of weaker H-bond donors possible, provides more information about molecules as a whole, and can quickly identify the strength of a hydrogen bond based on the corresponding chemical shift of the proton. Gilli and Gilli report that N–H and O–H hydrogen bond donors can exhibit chemical shifts from “8 to 10ppm for weak up to 20-22 ppm for very strong H-bonds,” and that these high chemical shift signals “typically do not overlap with those of molecular protons, which rarely exceed shifts of 11-13ppm.” However, they also noted that the longer timescale of NMR measurements (10^{-1} to 10^{-8} s) compared to the vibrational spectroscopy methods (10^{-14} to 10^{-13} s) is a significant factor, and may result in difficulties when monitoring the tautomeric equilibrium $\text{D-H} + \text{A} \rightleftharpoons \text{D-H}\cdots\text{A}$ at room temperature. A variety of additional methods can be combined with NMR, including primary and secondary kinetic isotope effects (1).

2. The Hydrogen-Bond Chemical Leitmotifs

Gilli and Gilli divide H-bonds into six general categories, as seen in **Table 1.1**. The six chemical leitmotifs (CL) are discussed in the following paragraphs. An H-bond with A...D length of less than 2.60 Å is typically considered to be a strong H-bond (*I*).

Table 1.1 The six chemical leitmotifs. Adapted from the table on p. 32 of (*I*).

CL #	Name	Strength	Appx. Bond Length of A...D (Å)
1	Ordinary H-bond	Weak	2.60-3.00
2	Double Charge-Assisted H-bond	Strong	2.41
3	Negative charge-assisted H-bond	Strong	2.26-2.43
4	Positive charge-assisted H-bond	Strong	2.40-2.43
5	Resonance-assisted H-bond (π -bond cooperative H-bond)	Strong	2.38-2.55
6	Polarization-assisted H-bond (sigma bond cooperative H-bond)	Moderate	2.67

CL #1) The ordinary hydrogen bond is an H-bond that is neither “charge-assisted nor π -bond or sigma bond cooperative.” As mentioned earlier in chapter 1, these are simple, relatively weak electrostatic interactions that are usually transient by nature. This type of H-bond occurs widely in nature, vastly outnumbering the stronger H-bonds (*I*).

CL #2) The double charge-assisted H-bond is a strong H-bond between a donor and acceptor with similar pK_a values. An example of this leitmotif given by Gilli and Gilli would be the H-bonded complex between pyridine-N-oxide and trichloroacetic acid, which have pK_a values of 0.79 and 0.66, respectively (*I*).

CL #3) The negative charge-assisted H-bond is a strong H-bond between a donor and acceptor that correspond to the general formula, $[X...H...X]^-$, such as acid salts of carboxylic acids, those found in the bifluoride anion, $[F...H...F]^-$, or by salts of inorganic acids (*I*).

CL #4) The positive charge-assisted H-bond is a strong H-bond between two identical molecules bridged by the proton from a strong acid donor. They have the general formula $[X\cdots H\cdots X]^+$. An example is the bridged H-bond complex formed between the sulfoxide oxygen atoms of two dimethyl sulfoxide molecules in an acidic medium (*1*).

CL #5) The resonance-assisted H-bond (RAHB) is a strong H-bond wherein the donor or acceptor atoms are at the ends of a short molecular fragment with π -conjugation (*1*). This type of H-bond will be discussed in much greater detail in Section 3.

CL #6) The polarization-assisted H-bond was proposed by Jeffrey and Saenger in 1991, called the sigma bond cooperative H-bond (*4*). This type of H-bond is moderate in strength and occurs in chains, such as $\cdots O-H\cdots O-H\cdots$ in crystalline phenols (*1*).

3. Historical Background of the Resonance-Assisted Hydrogen Bond

The resonance-assisted hydrogen bond (RAHB) is the strongest type of H-bond. This type of H-bond is an example where a particular group of chemical bonds together assume a state that is more stable than the sum of the individual bond energies would imply, an effect called *cooperativity*. The most common examples of RAHBs are the result of resonance effects in π -conjugated chains or rings, such as those found in β -diketones. For example, many β -diketones are known to undergo keto-enol tautomerization (*1*). For well over a century, chemists have been studying keto-enol systems, which contain a form of RAHB, although they were not referred to as RAHBs until 1989. Early on, this even included Emil Erlenmeyer, who famously stated in the so-called Erlenmeyer Rule that “all alcohols in which the hydroxyl group [is] attached directly to a double-bonded carbon atom [will become] aldehydes or ketones” (*5*).

Generally, studies involve a system wherein a ketone exists in equilibrium with an enol isomer, as shown between **1** and **2** in **Figure 1.2**. This equilibrium relationship between isomers, called tautomerism, occurs via protonation of the oxygen by the loss of a proton on the α -carbon. In most cases, the enol, **2**, is the less stable isomer, and the equilibrium will favor the ketone (**1**).

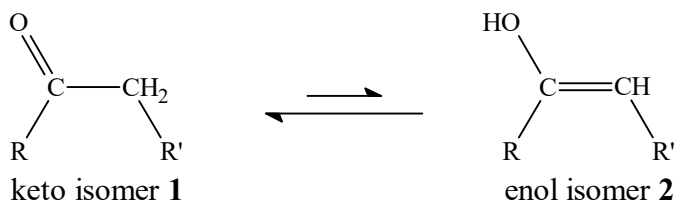


Figure 1.2. Tautomerization of a ketone into an enol. Often, the ketone is more favorable.

However, this is not always the case. In some molecules, an enol isomer can be more favorable under certain conditions. This is the case when an electron-withdrawing group (EWG) is present in the β position to the carbonyl. A classic example of a system with a favorable enol species would be acetylacetone, **3**, whose equilibrium with the enol form, **4**, is shown in **Figure 1.3**. The enol is stabilized by an intramolecular hydrogen bond with the adjacent carbonyl and the favorability of conjugation between the C=O and C=C bonds. Other systems with EWGs that have been observed to undergo similar enol stabilization include α -cyano, -nitro, and -sulfonyl ketones. Phenols are also stable enols (**1**).

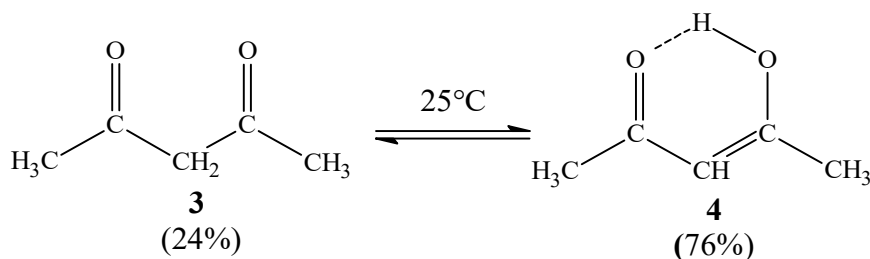


Figure 1.3. Tautomerization of acetylacetone into the more favorable enol. The dashed bond to the hydrogen atom is an intramolecular hydrogen bond. The enolic proton in **4** is reported in the literature to have a ^1H NMR shift of $\delta=14.7$ ppm (6).

The improved stability of the enol form of β -dicarbonyl compounds can be linked to resonance stabilization of the conjugated double bonds and the cyclic H-bond. In **Figure 1.4**, the enol tautomer of acetylacetone, **4**, has the resonance structures shown. Gilli and Gilli report that numerous studies have been performed on β -dicarbonyl compounds, attempting to learn more about the systems and what forces drive tautomerization (1).

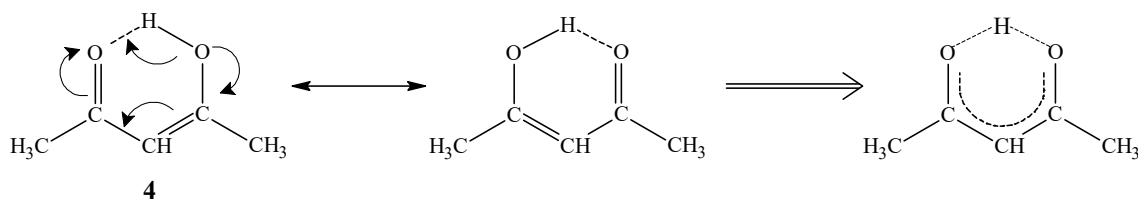


Figure 1.4. Resonance structures of acetylacetone's enol isomer, **4**. The dashed bond to hydrogen is the hydrogen bond. On the right, the net resonance form of **4**, showing that the proton is "suspended" between the two oxygen atoms (1).

As with H-bonds in general, keto-enol systems have also been extensively studied by a multitude of spectroscopic techniques, and specific enols have been selectively synthesized for study. For example, in 1970, Schmidt and colleagues monitored the decay of vinyl alcohol into acetaldehyde using variable temperature nuclear magnetic resonance spectroscopy to determine the half-life of the decay (7). High accuracy determinations of

keto/enol equilibrium constants have been a focus for research, as has the synthesis and study of “unusual” keto/enol systems (*e.g.*, systems where the enol predominates). Methods including NMR, IR, UV-Vis, and other physical investigations have been used to determine tautomeric equilibrium constants and further study the structure of enols (*1*).

Concerning NMR, a typical undergraduate organic chemistry text reports nominal chemical shifts of δ between 0.5 and 6.0 ppm for alcoholic protons. For phenolic protons, it reports δ between 4.5 and 7.7 ppm, and for carboxylic acids it reports δ between 10 and 13 ppm (*8*). However, Silverstein cites more comprehensive shift values for enolic protons of β -diketones (*e.g.*, compound **4**) and for intramolecularly bonded phenolic protons (*e.g.*, an *ortho*-ketophenol such as compound **5** in **Figure 1.5**), with typical shift ranges of δ 14.5 to 16.5 ppm and δ 5.5 to 12.5 ppm, respectively. For phenols with *ortho* ketones, the observed range of δ shifts to 10 to 12.5 ppm. (*9*).

Despite having an appearance similar to the enols discussed previously, a keto-phenol represents the opposite extreme. Specifically, the enol form is the far more desirable form in this case. Compound **5** in **Figure 1.5** below gives an example of the general structure of an intramolecularly hydrogen-bonded *ortho*-ketophenol. In this scenario, the enol, **5**, is the dominant species in solution because the C=C is part of the aromatic π cloud; formation of **6**, the keto form, breaks the aromaticity of the benzene ring, which is thermodynamically unfavorable. Thus, the keto form, **6**, is by far the less favorable form and is typically not observed (*1*).

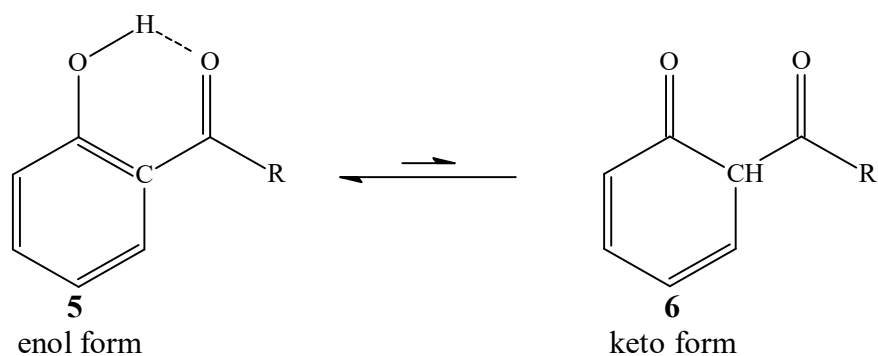


Figure 1.5. General structures of the enol and keto forms of an *ortho*-ketophenol. **5** maintains the aromaticity of benzene and will form the indicated intramolecular hydrogen bond.

Extreme proton chemical shifts have been detected in several types of compounds. They have been observed in studies of *o*-acylnaphthols, **7** (**10**), and substituted malonamides, **10** (**11**). In the 1981 study performed by Crouse *et al.*, a series of *o*-acylnaphthols, as in **Figure 1.6**, were synthesized by the photo-Fries rearrangement of various 1-naphthyl esters. The chemical shifts reported for the intramolecularly bonded phenols, **7**, ranged from δ 13.9 to 14.4 ppm (**10**).

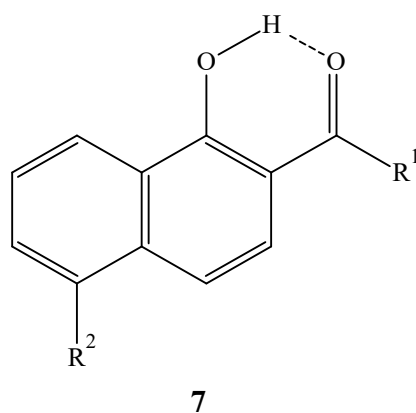


Figure 1.6. The general structure of *o*-acylnaphthols, **7**, studied by Crouse *et al.*, where $R^1 = -H, -COCH_3, -COC_6H_{11},$ or $-COC_6H_5$ and $R^2 = -H$ or $-OCH_3$.

In 2009, Basheer and colleagues synthesized and characterized 2-substituted malonamides, such as 2-nitromalonamide, **8**, and its tautomers **9**, enol, and **10**, *aci*-nitro, shown in **Figure 1.7**. Extremely high ^1H NMR shifts were recorded for the enols that formed from the synthesis. For the enolic tautomers, such as **9**, O–H protons of 2-nitromalonamide, 2-nitro-*N,N'*-dimethylmalonamide, and 2-acetyl-*N,N'*-diphenylmalonamide, chemical shifts of δ 18.93, 19.51, and 15.77 ppm were reported, respectively. The investigators used NMR integration to measure an equilibrium constant, K , for the various tautomers. They then used the information elucidated to compare with predictions generated using a density functional theory algorithm to determine how the compounds exist in various solvents and states (*11*).

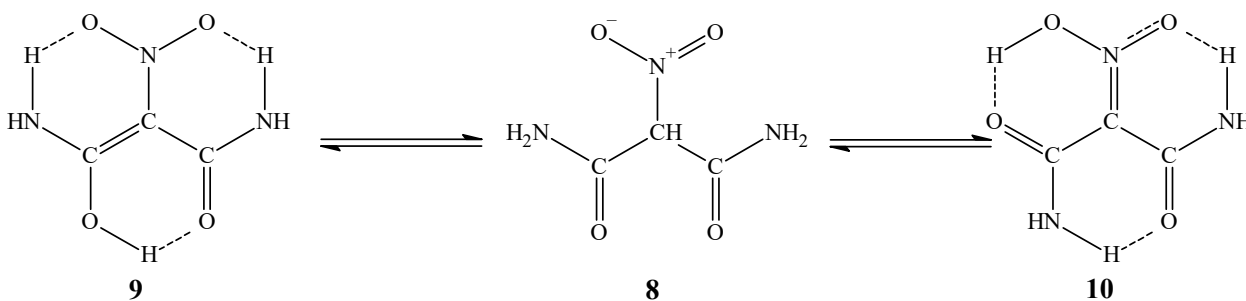


Figure 1.7. The tautomers of **8**, 2-nitromalonamide. **9** is the enol isomer, and **10** is the *aci*-nitro isomer.

4. The “Classification” of RAHBs and Some Contemporary Studies Thereof

As shown in the previous section, RAHBs have been known for quite some time, but were only classified as such in 1989 by Gilli *et al.* In his 1989 paper, Gilli and colleagues examined x-ray crystallographic data from many β -diketone systems, and used that data to form a semi-empirical model to estimate hydrogen bond energies in these systems. They suggested that this model further substantiated the case for a resonating bond wherein the hydrogen can experience a sigma bond with either oxygen in the acetylacetone systems, as shown in **Figure 1.8**. Because of this, they suggested that this system should be classified as

a discrete type of hydrogen bond, the resonance-assisted hydrogen bond (12).

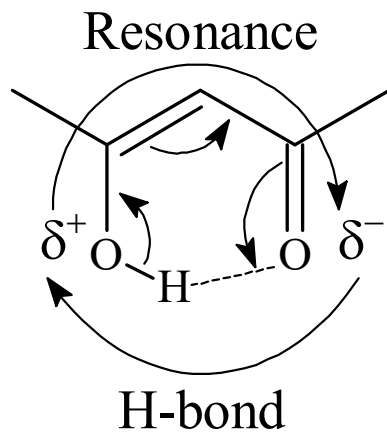


Figure 1.8. The suggested resonance of the acetylacetone system, wherein the sigma bond with the hydrogen atom resonates between the two oxygen atoms. Arrows representing the movement of resonance from δ^+ to δ^- and the movement of the H-bond from δ^- to δ^+ are depicted. This figure reproduced from (12) and (1).

In the following years, analysis of these β -diketones using neutron crystallography indicated another intriguing quirk of these systems. Neutron crystallography is a technique analogous to x-ray crystallography that uses a neutron beam instead of an x-ray source. The critical difference is that neutron crystallography can accurately detect the position of protons, but the technique is difficult and presents obvious barriers to use (e.g., neutron sources for use in crystallography are scarce). Combined analysis of the two types of crystallographic data showed that the enolic protons in the β -diketone systems reach a nearly-symmetric position, so close to symmetrical that the authors point out the proton being exactly centered is well within the range of experimental error. The authors noted there was a “remarkable lengthening of the O–H bond, and... the hydrogen bonds display more or less perfectly centered protons” that is atypical of normal H-bonds, which are usually asymmetrical. Typically, the D–H bond is shorter than the H...A interaction. It was

discovered that the hydrogen atom in the O–H•••O interaction displays a remarkable character of covalency in its interactions with both oxygen atoms and that this implies the bond energies in this system are much higher than a simple electrostatic interaction can explain. Finally, the authors concluded that this hydrogen atom displays a partial sigma bond character to both oxygen atoms in this system (13).

In a more recent review, Gilli and Gilli have determined two discrete ways to model the RAHBs. The first of those is the so-called *ionic model* and is essentially the model described by the 1989 paper referenced above. This simple model states that a RAHB can lead to a system, O•••H•••O, where the H-bond is driven by a “mechanism of generation and annihilation of charges,” which maintains no partial charges on the oxygen atoms by quenching the increase of charge by “resonating” between each oxygen atom possessing either a partial negative or partial positive charge, as previously demonstrated in **Figure 1.8** (12). The second, newer way of defining a RAHB is called the *resonant model*. In this model, quantum wave functions are considered for the four resonance forms of acetylacetone derivatives. This model builds upon the ionic model to produce more accurate predictions of H-bond energies but is significantly more complex (2,1). A further description of this newer model’s parameters is outside of the scope of this text.

B. Hammett Equation

A method used to examine the relationship between structure and reactivity of compounds is a so-called linear free energy relationship (LFER). In general, such a comparison between structure and reactivity is quantified using the electronic characteristics of a given structure and comparing the effects that different electronic characteristics have on

the rate constants or equilibrium constants for the reaction being studied. Various approaches to this have been proposed by, most notably, Hammett, Taft, and Brønsted (14).

Louis Hammett was one of the first chemists to propose such an LFER. In 1935, Hammett published a paper detailing some noticeable correlations between the basic hydrolysis rate constants of substituted ethyl benzoates and the ionization constants of the corresponding carboxylic acids. Under similar conditions (*i.e.*, in water at 25°C), plotting $\log k$ for the base-catalyzed ester hydrolysis versus the $\log K$ of acid ionization constants resulted in a linear relationship (15).

This correlation led Hammett, originally an analytical chemist, to three key conclusions. The first involved the mathematical relationship between the rate constants, k , and the equilibrium constants, K . Hammett asserted that both of these values were dependent on free energy changes, and a linear correlation indicated that the change in free energy of activation, ΔG^* , on the series of ethyl benzoates was proportional to the standard free energy change, ΔG° , of the corresponding acids in water. Secondly, Hammett noted that these linear relationships were discernable only when *ortho*-substituted benzene derivatives were left out of consideration. Similarly, it was also found that aliphatic analogs did not exhibit the linear relationships observed for aromatic compounds. In the case of *ortho* derivatives, Hammett reasoned that steric hindrance was likely affecting the relationship. However, with aliphatic compounds, Hammett reasoned that the lack of an aromatic π cloud made the transmission of any electronic effects much less reliable over the same distance, making them harder to compare than aromatic compounds. Finally, Hammett concluded that the correlations observed for the *meta*- and *para*-substituted benzene derivatives were due to the electronic properties of the substituent groups (15).

Over the next two years, Hammett developed his theories laid out in the 1935 paper, ultimately resulting in a quantitative determination of an equation that could describe the effects observed in these *meta*- and *para*-substituted benzene compounds by comparing them to an unsubstituted analog (**16**). With this equation, it became possible to predict what effect electron-donating groups (EDGs) and electron-withdrawing groups (EWGs) would have upon reactions. Using the so-called Hammett equation,

$$\log \frac{k_X}{k_H} = \rho \log \frac{K_X}{K_H} \quad [1.2]$$

a comparison of the rate and equilibrium constants was possible. In this equation, ρ (rho) is obtained as the slope of the resultant trendline, k_X or K_X represented the rate or equilibrium constant of the *m*- and *p*- substituted acid or ester, and k_H or K_H represented the rate or equilibrium constant of the unsubstituted acid or ester (**14**).

Next, Hammett studied the equilibrium constants for the ionization of benzoic acid and several *m*- and *p*- substituted derivatives in water at 25°C, as shown below in Figure 1.9. This reaction was chosen as the standard reference reaction because a wide array of K_X values were readily available in the literature at that time.

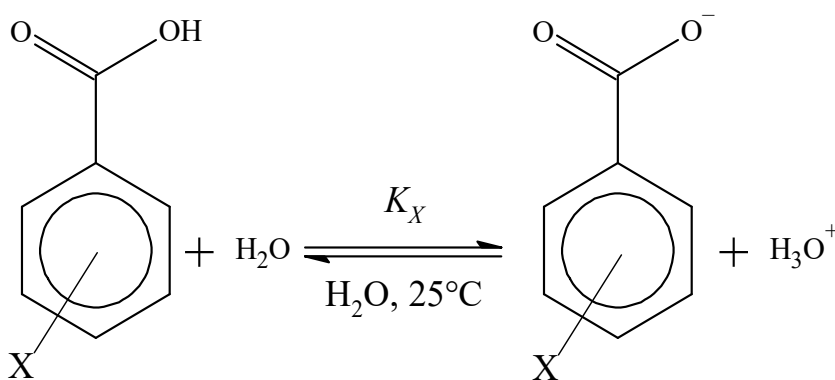


Figure 1.9. The standard reaction that was chosen by Hammett to define the substituent constant, σ . The X group denotes a substituent group on either the *meta* or *para* position (**16**).

Hammett set the value of ρ to 1.00 for the ionization of benzoic acid and its derivatives. He then defined the substituent constant, σ , as,

$$\sigma_X = \log \frac{K_X}{K_H} \quad [1.3]$$

where the constant K_H is specifically the equilibrium constant for benzoic acid. Equation [1.3] can also be rewritten simply as $\sigma = \text{p}K_{a(\text{H})} - \text{p}K_{a(\text{X})}$. Typically, Equation [1.3] is substituted into Equation [1.2], resulting in Equations [1.4] and [1.5], the most commonly used forms of the Hammett equation today (*14*).

$$\log \frac{k_X}{k_H} = \rho\sigma \quad [1.4]$$

$$\log \frac{K_X}{K_H} = \rho\sigma \quad [1.5]$$

The substituent constant, σ , is a quantitative estimate of the overall polar characteristics of a given substituent, and includes the sum of inductive effects and resonance effects. Values can be either positive or negative. A positive value correlates to a substituent that is electron-withdrawing (*i.e.*, the addition of the substituent caused a more acidic solution than benzoic acid). Conversely, a negative value correlates to a substituent that is electron-donating (*i.e.*, caused a less acidic solution than benzoic acid). Values of σ will vary, sometimes widely, depending on whether a substituent is in the *meta* or *para* position. In the case of *meta* substituents, this is due to the difference in distance from the reaction center. However, in the *para* position, resonance interactions with substituents such as alkoxy or nitro groups have contributing resonance forms that facilitate direct interaction with the aromatic π system in that position (*14*).

The reaction constant, ρ , is characteristic of a given reaction. Another name commonly used for ρ is the “sensitivity” constant. This is apt when considering that the value is a measure of how sensitive a reaction is to the electronic effects of *meta* and *para* substituents. As implied by equation [4], the value of ρ is typically obtained by determining the slope of a plot of $\log k_X/k_H$ versus σ_X for a reaction. The value of ρ , the slope of the plot, is indicative of a reaction’s transition or intermediate state. A positive value indicates the reaction is favored by EWGs, meaning the intermediate is likely anionic (carbanion). If the reverse is true, the intermediate is likely a cation (carbocation). The lower the magnitude of the slope, the more likely a reaction may proceed via a neutral or minimally polarized transition state or intermediate. The larger the absolute value of ρ , the more sensitive the reaction is to substituent change. Similar to reaction rates, ρ is also influenced by temperature and solvent; no broad generalizations can be made regarding those parameters (**14**).

1. The Intent of the Hammett Equation and Some Contemporary Uses Thereof

In general, the original intent of the Hammett function was to estimate the rates of reactions, to predict equilibrium behaviors of compounds, and to provide general information about the mechanisms of reactions analyzed in that manner (**16**). However, the equation has proven versatile enough to be used outside of its original intentions; it has been applied to many Hammett-like analyses of spectroscopic properties of compounds.

For example, in 2007, Spraul and colleagues conducted a study in which the synthesis of nineteen *para*-substituted aromatic trifluorovinyl ether compounds was accomplished. The compounds were then analyzed by ^{19}F NMR. Once the chemical shifts of the various fluorine signals were confirmed, the group made a plot of the various Hammett sigma constants

versus the ^{19}F chemical shifts. Plots of the chemical shifts observed for each given fluorine atom against the Hammett substituent constant, σ_p , showed a linear relationship (17).

Additionally, in 2001, Charton and Charton attempted to correlate the transmission of electronic effects on infrared stretching frequencies with the Hammett substituent constants. They found the Hammett analysis to be inferior to a more sophisticated treatment of the data. However, their attempt to apply the Hammett constants to the system was demonstrative of a modern attempt to expand its scope (18).

The sensitivity constant, ρ , can also be applied to these Hammett-like analyses. As with the standard Hammett analyses, there are two components of the sensitivity constant: sign and magnitude. A discussion as in the context of analyzing substituent constants versus NMR shifts, as in the Spraul paper described previously, is useful to consider. The sign of ρ is indicative of the effect substituents have in a given position. In the case of a positive sensitivity constant for the Hammett-like analysis with NMR data, which indicates that as the substituent's electron-withdrawing character increased, the NMR chemical shift increased. In the case of NMR, this means that the shift of the atom being observed has become more deshielded or electron-poor. In this same context, the numerical magnitude of the shift is a quantitative measure of how strong the effect of having a substituent in a given position is. In essence, the absolute magnitude of ρ can be used to compare the relative strength of the electronic effects of substituents in differing positions (17).

C. Prior Work on This Project

In 2009, T. Mathis completed a thesis on her works relating to the synthesis of a series of substituted *ortho*-acylnaphthols. Two series of *o*-acylnaphthols, **11** and **12**, were

proposed, shown in **Figure 1.10**. Mathis synthesized series 1, **11**, through the esterification of 1-naphthol by various *para*-substituted benzoic acids followed by photo-Fries rearrangements to give *o*-acylnaphthols (**19**).

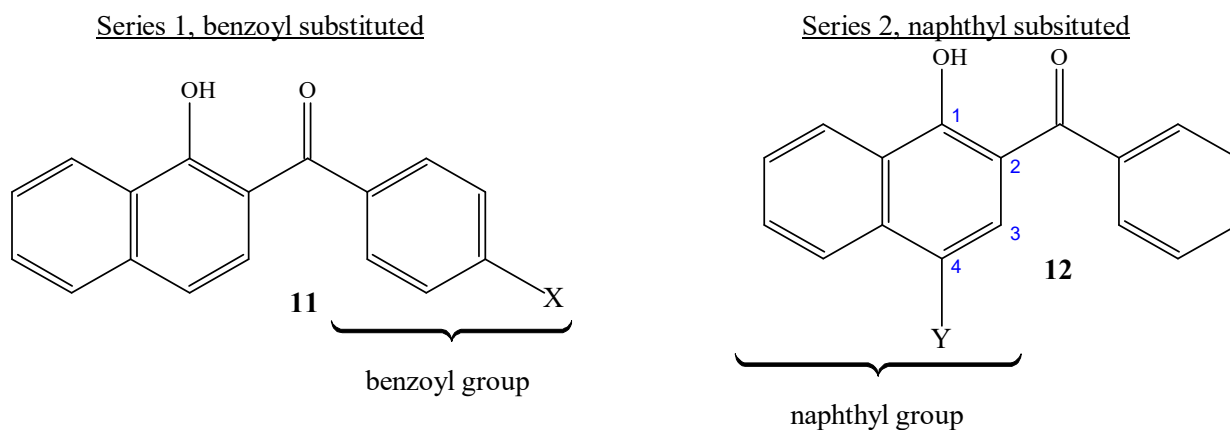


Figure 1.10. Structures of series 1, **11**, and series 2, **12**, *o*-acylnaphthol compounds. “X” or “Y” = -H, -OCH₃, -CH₃, -Cl, -Br, and -NO₂.

Mathis performed ¹H and ¹³C NMR to identify the compounds she synthesized in series 1, with attention given to the phenolic hydrogen and the carbonyl carbon. This is an enolic system; recall, the phenolic proton will undergo intramolecular hydrogen bonding, resulting in significantly downfield chemical shifts due to deshielding. She compared the chemical shifts of these positions to the Hammett substituent constants for the given -X groups. As seen in **Figure 1.11**, the Hammett diagram generated for the phenolic proton shifts produced a significant correlation at significance level 0.05. However, the correlation for the carbon shifts was not statistically significant at the same level.

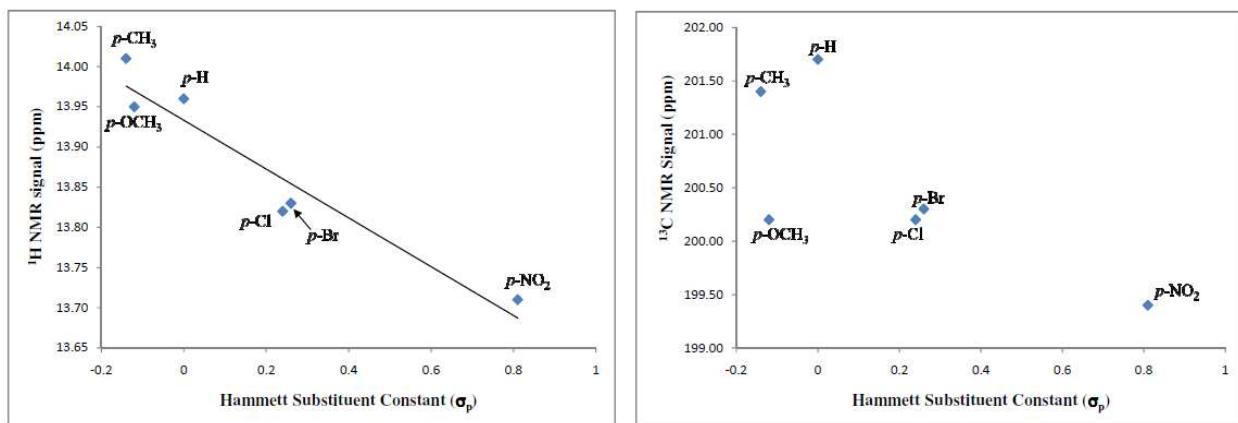


Figure 1.11. The Hammett diagrams generated for the series 1 compounds. On the left, the ¹H NMR shifts of the phenolic proton versus the Hammett substituent constant for the compound's substituent group, σ_p ($P=0.0024$, $R^2=0.9207$). On the right, the ¹³C NMR shifts of the carbonyl carbon versus the Hammett substituent constant, σ_p ($P=0.0869$, $R^2=0.560$) (19).

In general, it was observed that ¹H chemical shift was inversely correlated to the Hammett substituent constant; that is, the chemical shift of the phenolic proton shifted upfield as the electron-withdrawing character of the substituent on the benzene ring increased. To explain the observed trend in the ¹H chemical shifts, Mathis suggested that the carbonyl oxygen, the H-bond acceptor, was affected by the electronic characteristics of the substituents. In the case of electron-donating substituents, electron donation to the carbonyl oxygen resulted in increased strength of the H-bond. Mathis concluded that more available electron density on the benzene ring made the carbonyl oxygen a more effective H-bond acceptor (19). The trend observed by Mathis is further explained in **Figure 1.12**.

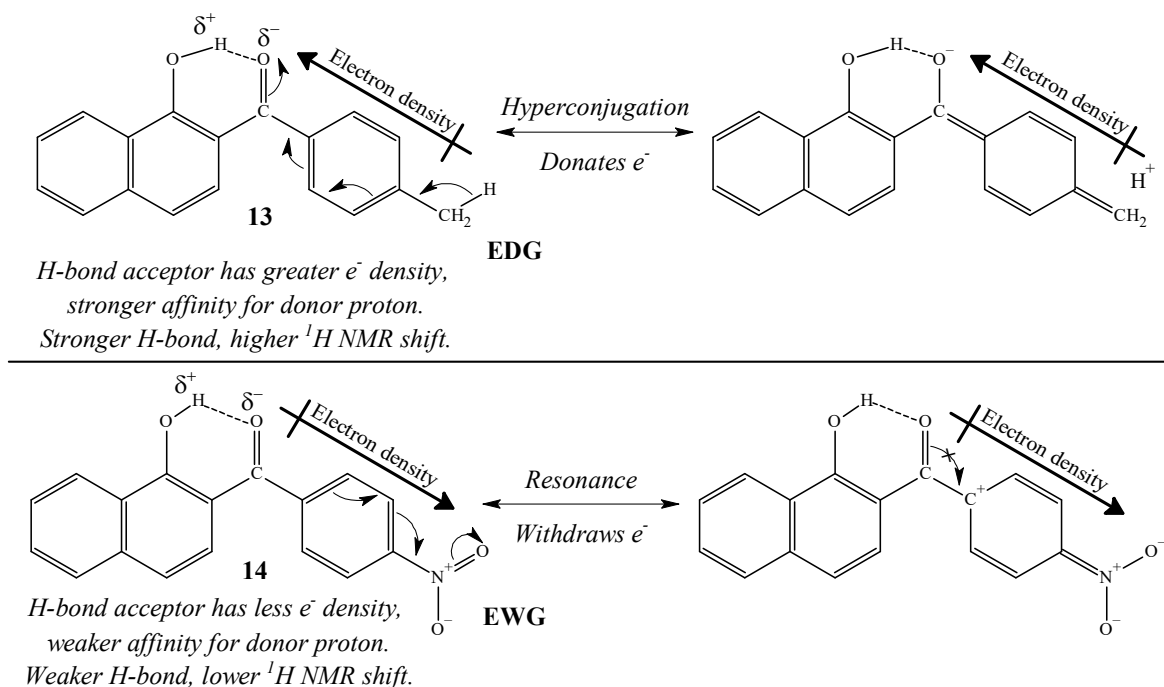


Figure 1.12. The trend observed by Mathis. In **13**, 2-(*p*-methylbenzoyl)-1-naphthol, the methyl substituent acts as an EDG, strengthening the capability of the carbonyl oxygen to act as an H-bond donor, resulting in a stronger H-bond and higher ^1H NMR shift of the enolic proton. The opposite is true for **14**, 2-(*p*-nitrobenzoyl)-1-naphthol. Hyperconjugation and resonance structures are shown for **13** and **14**.

D. Goals

It is hypothesized that electronic interactions within the substituted *o*-acylnaphthols can be shown to exhibit a significant trend according to the electronic properties of the substituents and lend support to the idea that the phenolic proton is in a resonance-assisted hydrogen bonding system. Three goals are proposed to support this hypothesis. The first goal is to continue the the work of Mathis by synthesizing the compounds proposed in Series 2, the 4-substituted-2-acylnaphthols, and characterize them.

The second goal of this work after the synthesis and characterization of the series 2 compounds, is to perform a Hammett analysis, as Mathis did, using ^1H -NMR to evaluate the effects of the EWG and EDG in the compounds on the enolic hydrogen. This will be used to

make inferences on the substituent effects on the intramolecular hydrogen bond. Studies will also be carried out using ^{13}C NMR and Fourier transform-infrared spectroscopy (FT-IR).

Finally, the third goal of this work is to evaluate the results of these studies and the ones initially performed by Mathis to characterize the *o*-acylnaphthol system and determine if its enolic system is consistent with a resonance-assisted hydrogen bond.

To accomplish these goals, the author proposes a synthetic route to prepare the second series of the *ortho*-acylnaphthols, **12**, as shown in the following paragraphs. The synthesis of the *o*-acylnaphthols will be accomplished as done by Mathis, shown in **Figure 1.13**, by first reacting 4-substituted-1-naphthols, **14**, with benzoyl chloride, **15**, to form the corresponding naphthyl esters, **16**. Next, the esters will be subjected to the photo-Fries rearrangement reaction to form the corresponding *o*-acylnaphthols, **12 (19)**.

However, not all the necessary naphthols are cheaply available commercially. Specifically, the author will attempt to synthesize 4-nitro-1-naphthol, 4-bromo-1-naphthol, and 4-methyl-1-naphthol. The bromo and nitro derivatives are available from Fisher Scientific, but they are priced somewhat high. The materials needed to attempt the synthesis of the nitro and bromo naphthols, 4-bromo- and 4-nitro-1-naphthamine, **16**, are both available in the laboratory. Furthermore, the synthetic route the author intends to follow for 4-nitro-1-naphthol and 4-bromo-1-naphthol, **19**, shown in **Figure 1.14**, is simple and should be relatively straightforward to test. As such, the author intends to attempt the conversion of the corresponding amines, **18**, to the phenols desired, **19**. They can be converted to phenols in modest yields by the reactions shown (**20**). If this synthesis is unsuccessful, the author will then investigate purchasing the materials.

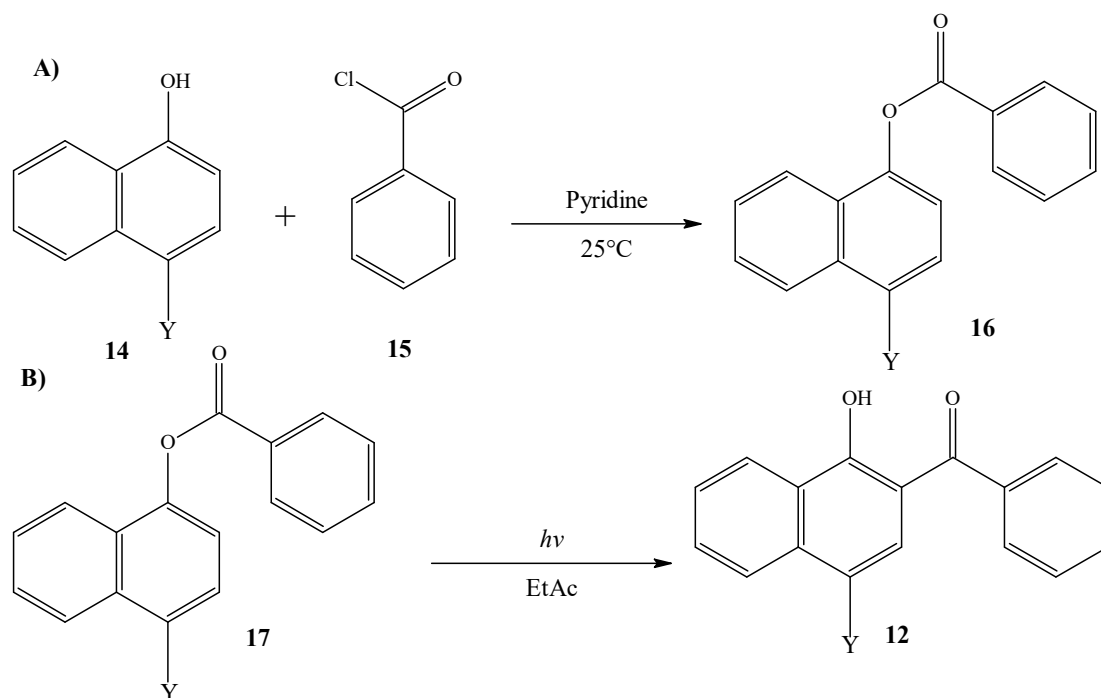


Figure 1.13. In reaction **A**, the esterification of a 4-substituted-1-naphthol, **14**, with benzoyl chloride, **15**, to form a 4-substituted naphthyl ester, **16**. In reaction **B**, the ester is subjected to the photo-Fries reaction, forming **12**, a 4-substituted-2-acylnaphthol. “Y” = -H, -OCH₃, -CH₃, -Cl, -Br, and -NO₂.

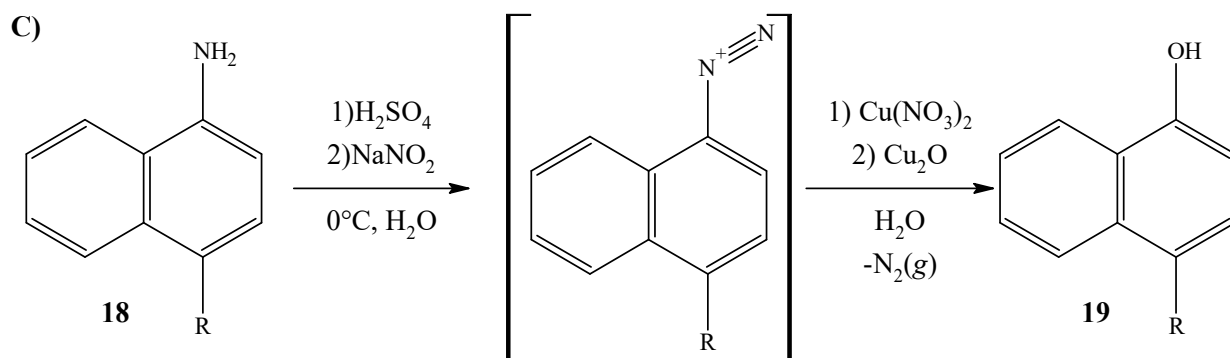


Figure 1.14. In reaction **C**, the diazotization and decomposition of 4-substituted 1-aminonaphthalenes, **18**, forms 4-substituted-1-naphthols, **19**. R = -Br and -NO₂.

Next, consideration must be given to the synthesis of 4-methyl-1-naphthol. It is available commercially but at high costs. It would be more cost-effective to attempt a synthesis before purchasing the material. **Figure 1.15** shows the synthetic route chosen. It is

worth noting that a more traditional route involves a Friedel-Crafts acylation using zinc cyanide to substitute a formyl group ($-\text{CHO}$) onto 1-naphthol, forming 4-hydroxy-1-naphthaldehyde (**21**). This is followed by a Clemmensen reduction of the resultant aldehyde using zinc-mercury amalgam and HCl, but that synthetic option is being considered a last resort due to the significant hazards involved (**22**).

Instead, in reaction **D**, anthranilic acid, **20**, is reacted with ethyl nitrite in dimethoxyethane (DME) to generate benzyne, **21**. Continuing, in reaction **E**, the benzyne generated *in situ* is reacted with 2-methylfuran, **22**, in the refluxing DME, resulting in a Diels-Alder reaction to form 1-methyl-1,4-dihydro-1,4-epoxynaphthalene, **23** (**23**). There are other possible methods of performing this reaction (**24**), but the one described is the most promising method.

In reaction **F**, a variety of conditions can be utilized to open the epoxy bridge, but the simplest of these is to reflux **23** in a solution of warm methanol and concentrated hydrochloric acid; near-quantitative yields were reported for the conversion to **24**, 4-methyl-1-naphthol (**25**). Another method used a ruthenium complex $[\text{RuCl}_2(\text{CO})_3]_2$ as a catalyst to open the epoxy bridge (**26**).

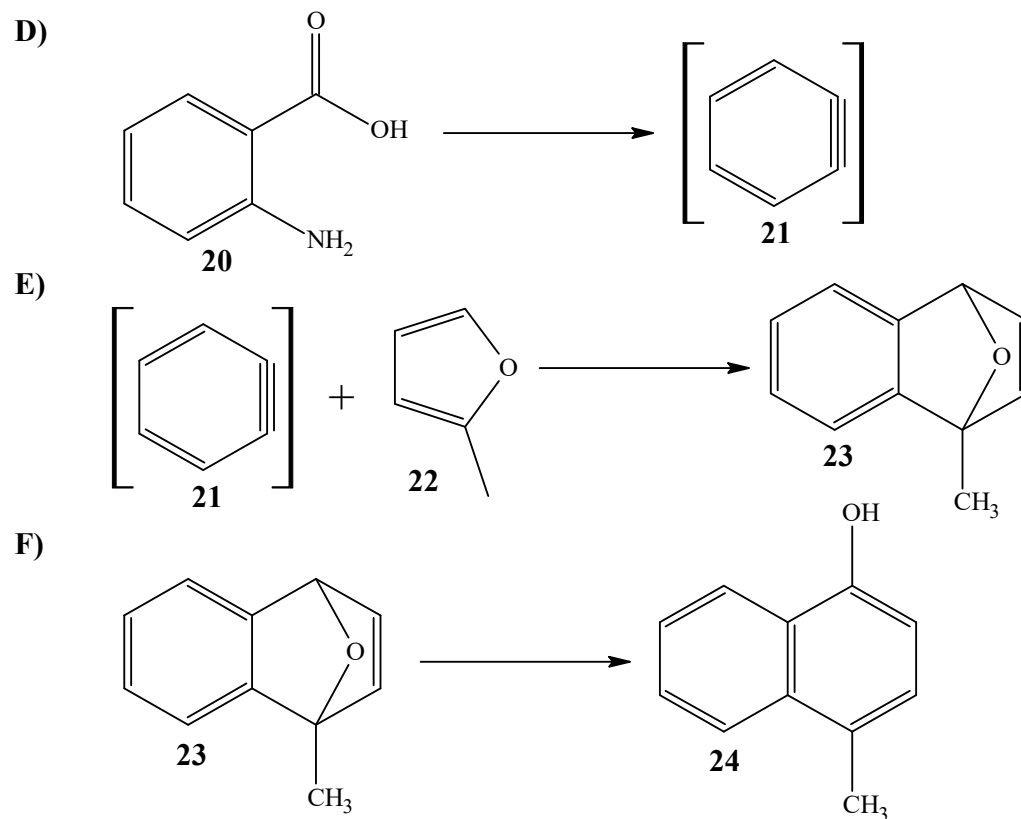


Figure 1.15. Synthesis of 4-methyl-1-naphthol, **24**. In reaction **D**, anthranilic acid, **20**, is diazotized and then decomposed, yielding benzyne, **21**. In reaction **E**, 1-methylfuran, **22**, reacts with benzyne in a Diels-Alder reaction to form 1,4-epoxy-1-methyl-1,2,3,4-tetrahydronaphthalene, **23**. Finally, in reaction **F**, the epoxy bridge on **23** is opened to produce 4-methyl-1-naphthol, **24**.

CHAPTER 2: EXPERIMENTAL

A. Materials

The majority of reagents and solvents used were obtained from commercial sources and used without any further purification. These reagents, their manufacturers, and lot numbers (if available) are listed in **Table 2.2**. However, some materials were pre-purified according to procedures from the literature. The materials which were purified or treated before use are not listed in **Table 2.2**, including anthranilic acid, deuteriochloroform. Ethyl acetate, molecular sieves, pyridine, silica gel, and thionyl chloride. Instead, purification procedures for these compounds are detailed in the following paragraphs. Further details for these purification procedures and alternative purification options can be obtained by consulting the references cited and looking for the CAS number of the chemical in question.

Anthranilic acid, or 2-aminobenzoic acid, (manufactured by Fisher Scientific Co.) was purified by recrystallizing it from boiling water with charcoal. The recrystallized material was air-dried thoroughly and stored in a dark place before use (27).

Deuteriochloroform (assayed at 99.8% deuterated material, manufactured by Acros Organics, lot number B0706565) with 0.02% tetramethylsilane for use in NMR spectroscopy was stored in the original bottle and treated as though it were ordinary chloroform. To ensure minimal contamination with water from the atmosphere, the solvent was dried over calcium chloride and stored over activated 3Å molecular sieves (27).

Table 2.2. Information about solvents, reagents, and other chemicals that were used without further purification. Lot numbers are provided if available, along with the manufacturer, assay, and chemical name. Some compounds did not have a specified assay. Note: ligroin and petroleum ether were both assayed as ‘pass’ or ‘fail’ and met the requirements as ACS Certified Reagents.

Chemical Name	Assay	Manufacturer	Lot Number
4-Bromo-1-naphthamine	97%	Aldrich Chemical Co. Inc.	BQ04713AN
4-Bromo-1-naphthol	95+%	Matrix Scientific Co.	T13T
4-Chloro-1-naphthol	99%	Acros Organics	A013819601
4-Methoxy-1-naphthol	98.0+%	Tokyo Chemical Industry Co.	DFZ7L-SA
4-Methyl-1-naphthol	97%	Ambeed Inc.	A645734-001
4-Nitro-1-naphthamine	n/a	Tokyo Chemical Industry Co.	FIM01
4-Nitro-1-naphthol	98.0+%	Tokyo Chemical Industry Co.	6EHWH-GQ
Ligroin	PASS	EMD Chemicals, Inc.	53074313
Petroleum ether	PASS	Fisher Scientific Co.	191808
Copper(I) oxide	97%	Acros Organics	A0283462
Copper(II) nitrate trihydrate	n/a	Acros Organics	A0224354
2-naphthol (β -naphthol)	n/a	Fisher Scientific Co.	734622
Diethyl ether	99.9%	Fisher Scientific Co.	193966
Tetrahydrofuran	95+%	Aldrich Chemical Co.	HS 14101HS
Isopentyl nitrite	97%	Alfa Aesar	10213662
2-Methylfuran	99%	Acros Organics	A0385653
Sodium nitrite	95%	Baker and Adamson	N/A
Dichloromethane	99.5+%	Honeywell International, Inc.	N/A
<i>N,N</i> -Dimethyl formamide	99%	Fisher Scientific Co.	704587
1,2-Dimethoxyethane	99%	Bean Town Chemical Co.	50029920
Benzoic Acid	99%	Alfa Aesar	10157941
<i>p</i> -Toluic Acid	n/a	Eastman Chemical Co.	A30

Ethyl acetate (assayed at 99.9+%, manufactured by Fisher Scientific Co.) was purified by drying and distilling from potassium carbonate and then stored over activated 5Å molecular sieves in a tightly sealed glass bottle, as indicated in the literature (27). Ethyl acetate for use in photoreactions was degassed by evacuation to approximately 100 torr and simultaneous sonication for 5 minutes. After sonication, the flask was agitated slightly before being refilled with nitrogen gas from a cylinder and agitated for several seconds. This process was repeated five times to ensure thorough degassing of the solvent (27).

Molecular sieve pellets of 3Å and 5Å pore size were activated according to a modified literature procedure (27). Sieves were heated to 250°C for 72 hours in an oven. The

sieves were cooled in a vacuum desiccator with anhydrous calcium chloride *in vacuo* (< 1 torr) to encourage the removal of any water remaining on the sieves. At the end of this period, the sieves were removed from the desiccator, quickly placed into a glass bottle, and tightly sealed. Sieves in the glass bottle were periodically reactivated according to this procedure to ensure consistent quality. A similar procedure was used for silica gel 60, 230-400 mesh (manufactured by L. D. McTomy Inc., lot number 20031115), which was used for flash column chromatography. This material was only heated to 120°C, as recommended in the literature (27).

Pyridine (manufactured by Alfa Aesar) was dried over potassium hydroxide pellets under nitrogen at ambient pressure and then distilled, as in the literature (27). This material was distilled into a glass bottle in small batches (ca. 75mL) and stored over an ample amount of 5Å molecular sieves to prevent the absorption of water.

Thionyl chloride, SOCl₂, (manufactured by Fisher Scientific Co.) was purified by distilling cautiously in a short-path distillation apparatus. Only material boiling at 75-76°C was collected, and it was used immediately. Thionyl chloride was purified on-demand in this manner when a procedure called for its use.

B. Methods

Melting points were determined using a DigiMelt MPA160 apparatus (serial number 139394) manufactured by Stanford Research Systems.

The thin-layer chromatography (TLC) plates used were aluminum-backed, 20 µm thick silica gel plates manufactured by SorbTech Mfg., Inc. The TLC plates were heated in an oven at 120°C for at least 15 minutes and allowed to cool just before use.

Flash chromatography separations were carried out on a 20 mm diameter column using silica gel according to the method described by Still (28). Column pressure was provided by nitrogen gas from a cylinder.

Photoreactions were run in an apparatus containing a 450 W Hanovia medium pressure mercury vapor lamp in a water-jacketed quartz immersion well. No other filters were used during irradiation. An example of the immersion well and photoreactor setup used is shown in **Figure 2.16**.

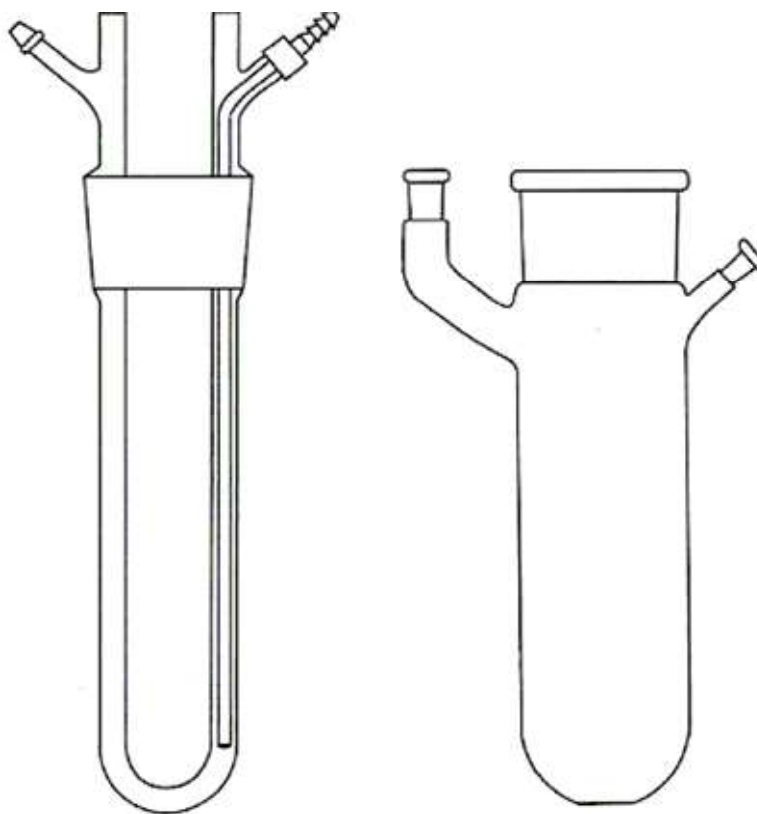


Figure 2.16. The photoreactor setup used. The quartz immersion well on the left houses the photochemical lamp and cools it with running water. The immersion well is inserted into the reactor vessel on the right, which contains the solution to be irradiated. The reactor vessel is equipped with a nitrogen gas line to bubble N_2 gas and a magnetic stir bar for mixing.

Nuclear magnetic resonance spectra were obtained on a Bruker AVANCE 500 FT-NMR spectrometer with a Prodigy cryoprobe. The spectrometer operated at 500 MHz for 1H

NMR and 126 MHz for ^{13}C NMR. Most NMR spectra were taken in deuteriochloroform (CDCl_3) with 0.02% tetramethylsilane (TMS), but some were erroneously taken with deuteriochloroform not containing TMS. The ^1H and ^{13}C spectra taken in CDCl_3 with TMS were corrected to have the TMS signal appear at exactly $\delta = 0.00\text{ppm}$. For spectra taken in CDCl_3 without TMS, referencing was done with the residual chloroform peak being corrected to $\delta = 7.26\text{ ppm}$ for ^1H spectra; for ^{13}C spectra, the center chloroform peak was corrected to $\delta = 77.36\text{ ppm}$ (**29**). The NMR spectra were processed using the Mestrelabs Mnova software. In processing, each spectrum had the default automatic phase correction performed, followed by automatic baseline correction using the Whittaker smoother algorithm. The ^1H spectra appear in Appendix A, and ^{13}C spectra appear in Appendix B. NMR signals are reported in parts per million (PPM).

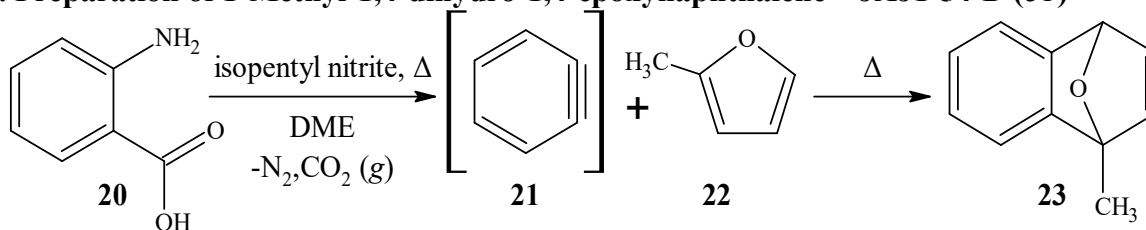
Infrared spectra were obtained on a Perkin-Elmer Spectrum Two FT-IR spectrometer with an attenuated total reflection (ATR) sampling apparatus, with the ATR set to a 1 cm pathlength. The FT-IR spectra were collected by accumulating eight scans at 4 cm^{-1} resolution with the samples compressed onto the ATR crystal under at least 100 Newtons of force using the anvil. Spectra were processed using the instrument's software to execute an ATR correction. Finally, using the freely available Spectragryph software, a baseline correction was performed and peaks were picked using the Spectragryph software (**30**). The FT-IR spectra appear in Appendix C. FT-IR signals are reported in cm^{-1} . The intensities were given as vw, w, m, s, and vs. Respectively, these stand for very weak ($>98\%T$), weak (98-95%T), medium (95-80%T), strong (80-70%T), and very strong ($<70\%T$). Peaks marked as br are broad.

All plots were prepared in Microsoft Excel. Statistical parameters were calculated using the “Regression” function from the Microsoft Excel Data Analysis Pack.

C. Naphthol Preparations

This section reports the experimental procedures for the attempted syntheses of the three naphthols discussed in Chapter 1, section D.

1. Preparation of 1-Methyl-1,4-dihydro-1,4-epoxynaphthalene – JAJ1-54-D (31)



A solution of 17.5 mL 2-methylfuran, **22**, (198 mmol) in an equal volume of 1,2-dimethoxyethane (DME) was heated to reflux in a three-necked 100 mL round-bottom flask equipped with a magnetic stir bar and a reflux condenser. One side neck was equipped with a rubber septum and the other was equipped with a sealed, pressure-equalizing addition funnel containing a solution of anthranilic acid, **20**, (3.426 g, 24.98 mmol) dissolved in 16 mL of DME. The reflux condenser was left open to the atmosphere at the top.

After the clear-colored solution in the flask was brought to steady reflux, the anthranilic acid solution was added dropwise concurrently with 4.20 mL (30.0 mmol) of isopentyl nitrite dispensed with a syringe needle through the rubber septum. Gas was observed to evolve from the system rapidly as the addition proceeded. The addition was maintained at a rate that kept the evolution of gases from becoming too vigorous.

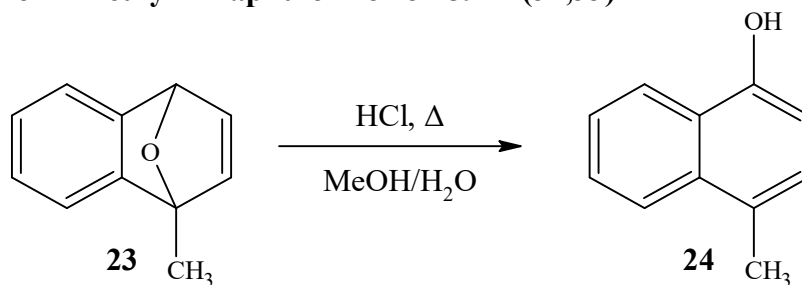
After addition, the solution had turned an amber-brown color and was allowed to continue refluxing for 30 minutes. At this point, excess 2-methylfuran and isopentyl nitrite

were removed from the solution *in vacuo*. The residue was then analyzed with TLC on silica gel (95% petroleum ether/ 5% EtAc), confirming the residue contained anthranilic acid starting material, DME, and an apparent crude product ($R_f = 0.58$). This residue was then vacuum distilled. A portion of the material boiled away into the vacuum trap before heat was applied. A small amount of DME was collected in the first fraction. NMR showed that the second fraction (64-70°C at 1.0 torr) and the third fraction (63°C at 1.0 torr) both contained the product, 1-methyl-1,4-dihydro-1,4-epoxynaphthalene, **23**, which was recovered as a viscous yellow oil with a foul odor (2.303 g, 58.3% yield).

$^1\text{H NMR}$ (500 MHz, CDCl_3): δ 7.17 (d, $J = 6.8$ Hz, 1H), 7.13 (d, $J = 6.8$ Hz, 1H), 7.00 – 6.89 (m, 3H), 6.73 (d, $J = 5.5$ Hz, 1H), 5.59 (s, 1H), 1.89 (s, 3H).

$^{13}\text{C NMR}$ (126 MHz, CDCl_3): δ 151.34, 150.55, 145.55, 144.32, 124.93, 124.71, 119.89, 118.75, 89.35, 81.75, 15.21.

2. Preparation of 4-Methyl-1-naphthol – JAJ2-39-A (32,33)



A solution was made by dissolving 0.805 g 1-methyl-1,4-dihydro-1,4-epoxynaphthalene, **23**, (5.09 mmol) in a warm mixture of 5 mL methanol and 1 mL water in a 50 mL round bottom flask, resulting in a light-yellow solution. This flask was equipped with a stir bar and a reflux condenser. With stirring, 3 mL of concentrated hydrochloric acid was added to the solution dropwise, and the solution was heated to reflux.

After thirty minutes at reflux, the mixture had turned murky white. Reflux was stopped, and methanol was removed *in vacuo*. The residue was diluted further with 15 mL water, and this aqueous material was extracted with dichloromethane (DCM) until the aqueous phase was colorless and transparent (3 x 15 mL). The dark-colored organic extracts were combined and then extracted with 10% NaOH (3 x 25 mL), producing a magenta-colored organic phase and a foggy-to-clear aqueous solution.

The base extracts were combined and poured into a beaker over about a dozen fresh ice cubes with a stir bar. With stirring, the solution was acidified cautiously with concentrated hydrochloric acid until it turned a persistent opaque milky color. Another 0.5 mL of acid was added to ensure adequate precipitation. Once the ice had melted, the solution was chilled in an ice bath and stirred until the milky appearance had wholly disappeared as clumps of crystals precipitated. This material was recovered by vacuum filtration with a Büchner funnel.

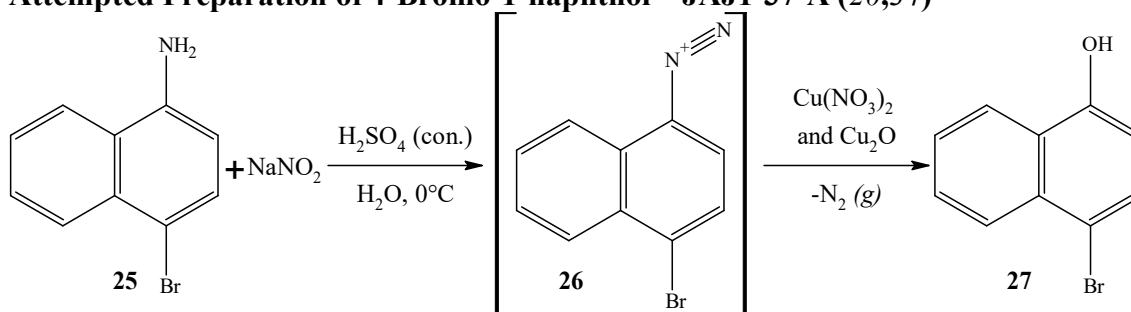
The crude product (0.7005 g) was tan to creamy brown in appearance and contained flecks of dark brown impurities. Once the material was dry, it was recrystallized with charcoal in 10 mL ligroin. Filtration of this material was especially difficult without losing product during removal of the charcoal, so some excess ligroin was required; there was still product lost. The purified product, 4-methyl-1-naphthol, **24**, was recovered as 0.2779 g (34.5%) of off-white powder melting at 83.0-84.0°C.

Average Yield: Over six trials of this reaction, there was an average yield of 28.8%.

¹H NMR (500 MHz, CDCl₃): δ 8.20 (dd, *J* = 8.1, 1.6 Hz, 1H), 7.94 (dd, *J* = 8.2, 1.5 Hz, 1H), 7.52 (dddd, *J* = 20.2, 8.1, 6.8, 1.4 Hz, 2H), 7.13 (d, *J* = 7.5 Hz, 1H), 6.72 (d, *J* = 7.5 Hz, 1H), 5.02 (s, 1H), 2.61 (s, 3H).

^{13}C NMR (126 MHz, CDCl_3): δ 149.81, 133.50, 126.69, 126.24, 126.06, 124.94, 124.50, 124.21, 122.02, 108.10, 18.85.

3. Attempted Preparation of 4-Bromo-1-naphthol – JAJ1-37-A (20,34)



This reaction was performed several times. The best of these attempts is presented in this experimental. The other attempts are further discussed in Chapter 3.

The 4-bromo-1-naphthamine, **25**, (439.7 mg, 1.980 mmol) was dissolved in 2 mL of warm 35% sulfuric acid solution in a large test tube with a triangular stir vane. This solution was cooled by adding a small cube of ice and then placing it in an ice bath. The temperature was monitored using a thermometer. Once the solution had reached 0°C , a solution of sodium nitrite (175.9 mg, 2.549 mmol) in 2.0 mL of water was slowly added dropwise, taking care to maintain the solution temperature below 5°C . The solution started creamy white and turned yellow-green as the sodium nitrite was added. The solution was maintained in an ice bath with stirring for 10 minutes, turning brown as the reaction proceeded.

To ensure the formation of the diazonium salt, **26**, had occurred, a qualitative test was performed using a solution of β -naphthol in aqueous sodium hydroxide (“the β -naphthol test”). A few drops of the reaction mixture were combined with a few drops of a basic solution of β -naphthol in a separate vial. This solution turned an intense red color, indicating

a diazo coupling reaction had taken place. This is a positive indicator for the presence of a diazonium ion, indicating that the 4-bromo-1-naphthamine had formed a diazonium salt (**34**).

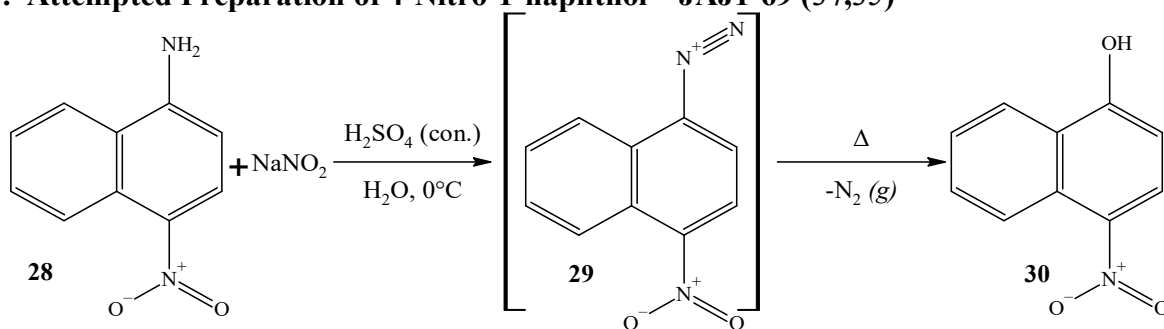
Next, a few crystals of urea were added to decompose any excess nitrous acid. The solution was allowed to stir for an additional 10 minutes, at which time another β -naphthol test was run. The test again indicated that the diazonium salt, **26**, was present. At that point, the reaction mixture was added to a beaker containing a premade solution of copper(II) nitrate trihydrate (7.51 g, 31.1 mmol) in 70.0 mL water. The copper(II) nitrate solution started blue but turned green-blue upon the addition of the reaction mixture. The stir vane was quickly replaced with a stir bar. With vigorous stirring, copper(I) oxide (268.1 mg, 1.873 mmol) was added into the solution, turning the solution brick red. This mixture was allowed to warm to room temperature with continued stirring. Gas evolved from the solution, presumably nitrogen.

After approximately 30 minutes of stirring, another β -naphthol test was run. The result was no color change, indicating there was no diazonium salt left over. This mixture was vacuum filtered to remove excess copper(I) oxide, leaving a green solution as the supernatant. This solution was extracted with DCM (4 x 15 mL). The DCM extracts were combined and back-extracted with 10% sodium hydroxide (2 x 50 mL) to recover any naphthol present in the extracts.

The sodium hydroxide extracts were combined and acidified with 10% sulfuric acid until the mixture was acidic to litmus. The acidified aqueous extracts were extracted with DCM (4 x 30 mL). The DCM extracts were dried over magnesium sulfate overnight. The next day, the solution was gravity filtered. The extracts were then evaporated *in vacuo*, leaving behind a residue of amorphous yellow particles.

The residue was dissolved in approximately 5 mL of warm 95% ethanol and heated to near-boiling. Heat was removed, and a large ice cube was added to this solution. Crystals formed. Once the ice cube melted, the mixture was vacuum filtered to recover crystals. The crystals were rinsed with water and then air-dried on a watch glass overnight. The 4-bromo-1-naphthol, **27**, was recovered as tan, needle-like crystals (81.5 mg, 14.4% yield). This product was not investigated spectroscopically due to the low yield.

4. Attempted Preparation of 4-Nitro-1-naphthol – JAJ1-69 (34,35)



This reaction was performed several times. The best of these attempts is presented in the following experimental. The other attempts are further discussed in Chapter 3.

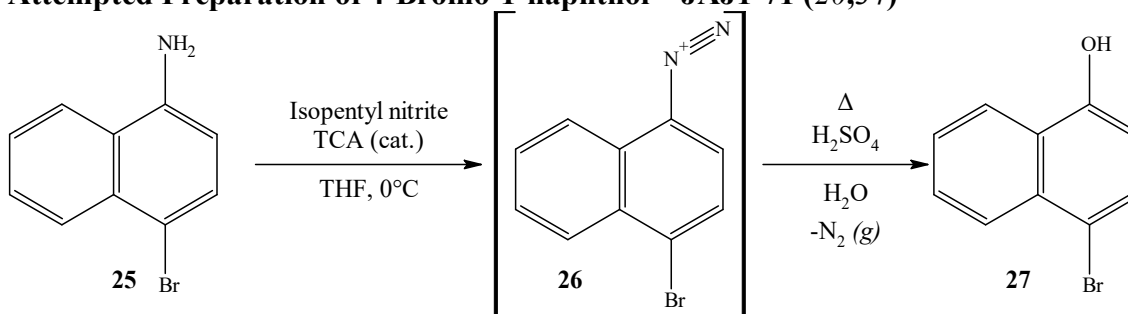
In a 100 mL beaker, a solution of 4-nitro-1-naphthamine, **28**, (776.5 mg, 4.126 mmol) was produced by dissolving the compound in the hot acidic solution formed by combining 3.6 mL of sulfuric acid and 10 mL of water. A stir bar was used to ensure adequate mixing. Once the compound was dissolved, it was cooled to 0°C by adding ice and placing it into an ice bath.

A solution of sodium nitrite (341.1 mg, 4.944 mmol) in 1 mL of water was added dropwise to the solution. After addition, the mixture was allowed to stir for 20 minutes before adding 5 mL of cold water and three cubes of ice. A few crystals of urea were added

to ensure any excess sodium nitrite decomposed. A β -naphthol test was run, giving a bright orange precipitate and confirming the presence of the diazonium salt, **29**.

A 250 mL three-necked flask was equipped with a thermometer and rubber septum on the side arms. To this flask was added a stir bar, 20.7 g of sodium sulfate, 13.5 mL of concentrated sulfuric acid, and 12.5 mL of water. A reflux condenser was connected to the middle neck, and the resulting solution was heated to reflux, with vigorous stirring. The reaction mixture was added slowly to the flask using a Teflon tube running through the rubber septum. Gas evolved aggressively throughout the addition. Once the addition was completed, the mixture was cooled in an ice bath and crystals precipitated. The light brown crystals were collected by vacuum filtration and air-dried. The crystals had a mass of 27.5 mg. NMR analysis of the sample yielded a complex spectrum that could not be correlated with the desired product.

5. Attempted Preparation of 4-Bromo-1-naphthol – JAJ1-71 (20,34)



This reaction was performed once as a final attempt to synthesize 4-bromo-1-naphthol, **27**, from the naphthamine. This procedure is hazardous, and anyone attempting to repeat it must read the warning in the referenced *Organic Syntheses* article carefully before proceeding (**20**).

In a smooth, brand new beaker, 4-bromo-1-naphthamine, **25**, (2.777 g, 12.50 mmol) was dissolved in 12.5 mL of THF and cooled in an ice bath to near 0°C. An additional 1.5 mL of THF containing 15.4 mg of trichloroacetic acid (TCA) was added to the solution to act as a catalyst. This mixture was a light brown color.

Next, 3.0 mL isopentyl nitrite was added to the mixture dropwise over the course of 3 minutes. The solution began to turn crimson red immediately and was warmed to 19°C over 20 minutes. The solution turned black as the diazonium salt, **26**, formed. At 25 minutes after addition, the temperature was 20°C and gas was evolving slowly. More ice was added to the ice bath. At 51 minutes after addition, the solution had lightened to crimson and remained that color. The temperature was maintained between 10°C and 20°C.

At 90 minutes after the addition of isopentyl nitrite, the solution was cooled to near 0°C. An extremely fine precipitate formed. The solution was allowed to stand at 0°C for 30 minutes. At this time, it was vacuum filtered to recover the precipitate, presumably 4-bromonaphthalene-1-diazonium, **26**. The precipitate was rinsed with 100 mL of ice-cold THF. The precipitate was kept wet with THF to prevent an explosion. It was then carefully added to a 400 mL beaker with 50 mL of 3 M sulfuric acid. With stirring, an additional 50 mL of 3 M sulfuric acid was added. This material was placed in an ice bath and stirred for 30 minutes. The solution was still crimson red. An additional 50 mL of 3M sulfuric acid was added and stirred for an additional 30 minutes. Any residual THF was removed *in vacuo*. This residue was placed in a beaker in the refrigerator at approximately 5°C.

Multiple attempts to retrieve crystals of the naphthol, **27**, from this solution were performed, to no avail. As such, the aqueous residue was extracted with DCM (2 x 50 mL)

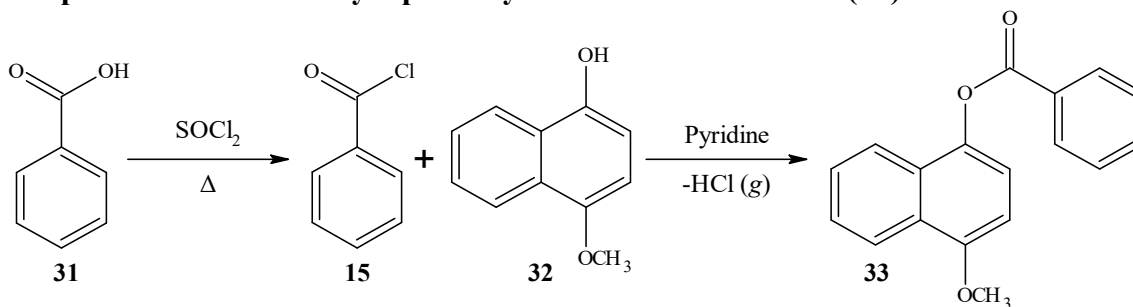
and with diethyl ether (2 x 50 mL). The extracts were dried separately over magnesium sulfate over the weekend.

The extracts were gravity filtered to remove the magnesium sulfate. Thin-layer chromatography was utilized to determine an adequate solvent mixture to separate crude products in the organic extracts. Petroleum ether was determined to be the best solvent. The solvent was removed *in vacuo*, and a flash column was run on the crude material left behind. Two distinct fractions were identified, and the eluent was removed *in vacuo*. A significant amount of material remained in the flash column and did not elute. The fractions contained 0.091g and 0.025g of a potential product. It was believed that, given the extreme danger of isolating the diazonium salt in this manner, a yield this poor was not worth investigating further. This result is discussed further in Chapter 3.

D. Esters

This section reports the experimental procedures for the synthesis of the series 2 substituted naphth-1-yl benzoate esters discussed in Chapter 1, section D.

1. Preparation of 4-Methoxynaphth-1-yl Benzoate – JAJ2-01-A (19)



All glassware used in this experiment was oven-dried. Benzoic acid, **31**, (2.887 g, 23.63 mmol) was placed into a 50 mL round-bottom flask. A magnetic stir bar was added to

the flask, along with a drop of dimethylformamide. This apparatus was placed into a heating mantle over a stir plate. The flask was briefly flushed with dry nitrogen gas from a cylinder, and 1.45 mL of freshly distilled thionyl chloride was added to the flask. The flask was then equipped with a reflux condenser and a calcium chloride drying tube. Stirring was started, and the mixture was heated gently until the benzoic acid dissolved. Gas evolved from the mixture during this period. At this point, the material was brought to reflux for 30 minutes, producing a yellow oil, presumed to be benzoyl chloride, **15**.

During the reflux period, the 4-methoxynaphthol (3.769 g, 21.54 mmol), **32**, was added to another 50mL round bottom flask. A magnetic stir bar was added, followed by 20 mL of dry pyridine. The flask was equipped with a pressure-equalizing addition funnel and a nitrogen gas inlet. The flask was then flushed thoroughly with nitrogen.

At the conclusion of the reflux period for the benzoyl chloride, the material was cooled in an ice bath for 10 minutes and then added into the addition funnel set up on the second flask. With positive pressure of nitrogen gas and magnetic stirring, the fresh benzoyl chloride was added dropwise to the solution of **32** over 30 minutes. Gas evolved as the addition proceeded. After the addition was complete, this solution was left to stir overnight.

The next morning, the solution had turned from a yellow color to darker amber, and white solid had precipitated from the solution. The mixture was poured into a 250 mL beaker with the acid resulting from dumping 25 mL of concentrated hydrochloric acid onto 50 grams of ice. This material was stirred until the ice melted. This resulting solution was then extracted with DCM (5 x 25 mL). The DCM extracts were then combined and rinsed with 3 M HCl (1 x 25 mL), 10% sodium hydroxide (2 x 50 mL), and with sodium chloride brine (2 x 50 mL). The DCM extracts were dried over magnesium sulfate for an hour.

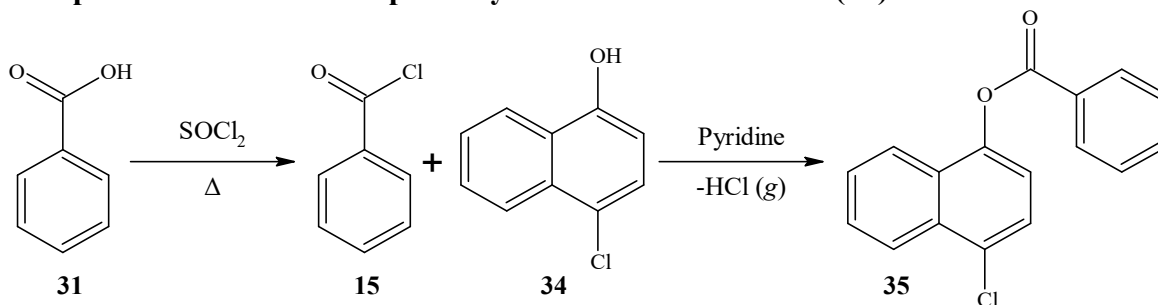
The extracts were gravity filtered, and the DCM was removed in-vacuo, giving crude product in the form of an amorphous, popcorn-like material. This material was recrystallized by dissolving the crude product in a few mL of fresh DCM and triturating with 95% ethanol. The solution was cooled in an ice bath until no more crystals precipitated. Vacuum filtration and air drying of the crystals gave the product, 4-methoxynaphth-1-yl benzoate **33**, as fine, off-white crystals (3.783 g, 63.9% yield, m.p. 118.1-118.9°C).

The remainder of the esterification reactions were carried out in this manner and at approximately the same scale. As such, their procedures will not be detailed. Instead, only notable exceptions during the procedure, the product appearance, and pertinent data such as yield, melting point, and NMR data will be reported for each reaction.

¹H NMR (500 MHz, CDCl₃): δ 8.33 (d, *J* = 7.7 Hz, 2H), 8.31 – 8.28 (m, 1H), 7.88 – 7.82 (m, 1H), 7.68 (t, *J* = 7.4 Hz, 1H), 7.57 (t, *J* = 7.7 Hz, 2H), 7.51 (dd, *J* = 6.4, 3.2 Hz, 2H), 7.27 (d, *J* = 8.3 Hz, 1H), 6.82 (d, *J* = 8.3 Hz, 1H), 4.03 (s, 3H).

¹³C NMR (126 MHz, CDCl₃): δ 165.71, 153.65, 140.27, 133.78, 130.38, 129.64, 128.80, 127.73, 127.12, 126.40, 125.88, 122.58, 121.11, 117.99, 103.06, 55.83.

2. Preparation of 4-Chloronaphth-1-yl Benzoate – JAJ1-19-A (19)

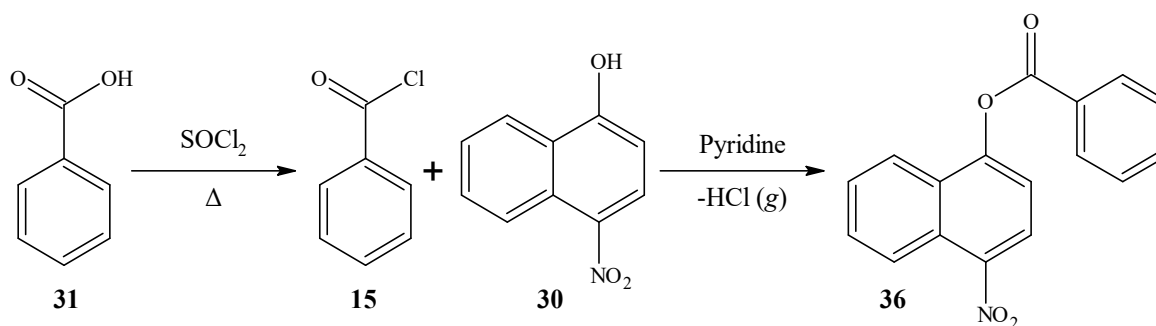


Result: carried out using 2.502 g (14.01 mmol) of the naphthol, **34**. The product, **35**, was obtained as fluffy white crystals (24.6% yield, m.p. 99.5-100.7°C). No recrystallization was necessary.

¹H NMR (500 MHz, CDCl₃): δ 8.31 (t, *J* = 8.9 Hz, 3H), 7.96 (d, *J* = 8.4 Hz, 1H), 7.69 (t, *J* = 7.4 Hz, 1H), 7.66 – 7.53 (m, 5H), 7.31 (d, *J* = 8.1 Hz, 1H).

¹³C NMR (126 MHz, CDCl₃): δ 165.17, 145.95, 134.12, 131.82, 130.50, 129.59, 129.23, 128.95, 128.16, 127.76, 127.43, 125.77, 125.08, 121.91, 118.49.

3. Preparation of 4-Nitronaphth-1-yl Benzoate – JAJ2-13-A (19)

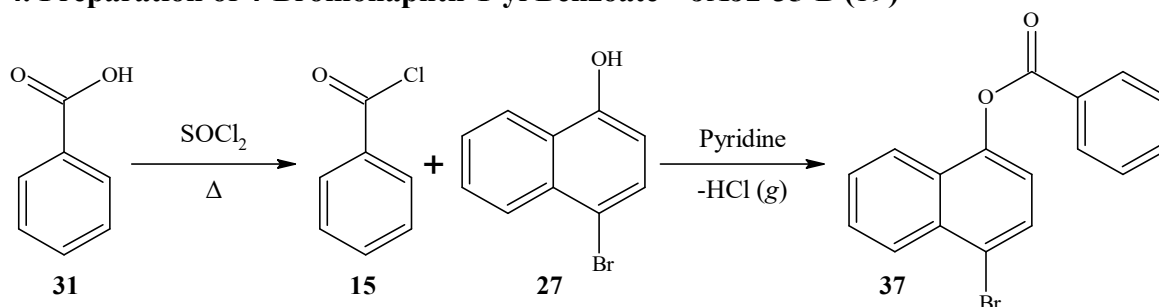


Result: carried out using 3.843 g (20.32 mmol) of the naphthol, **30**. Recrystallized by trituration with 95% ethanol from DCM. The product, **36**, was obtained as fine, light-yellow crystals (2.675 g, 44.90 % yield, m.p. 132.5-134.8°C).

¹H NMR (500 MHz, CDCl₃): δ 8.69 (d, *J* = 8.8 Hz, 1H), 8.39 – 8.31 (m, 3H), 8.13 (d, *J* = 8.5 Hz, 1H), 7.76 (dt, *J* = 22.1, 7.5 Hz, 2H), 7.69 – 7.58 (m, 3H), 7.51 (d, *J* = 8.4 Hz, 1H).

¹³C NMR (126 MHz, CDCl₃): δ 164.36, 151.31, 144.11, 134.40, 130.46, 130.04, 128.97, 128.53, 127.90, 127.75, 126.70, 124.66, 123.72, 122.09, 116.93.

4. Preparation of 4-Bromonaphth-1-yl Benzoate – JAJ2-35-B (19)

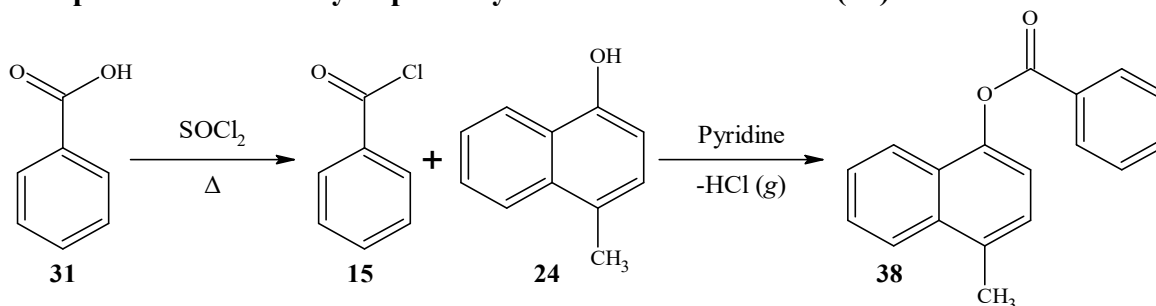


Result: carried out using 2.509 g (11.25 mmol) of the naphthol, **27**. Recrystallized by trituration with 95% ethanol from DCM. The product, **37**, was obtained as fine, light-yellow crystals (1.721 g, 46.8 % yield, m.p. 102.3-103.5°C).

$^1\text{H NMR}$ (500 MHz, CDCl_3): δ 8.33 (d, $J = 7.3$ Hz, 2H), 8.28 (d, $J = 8.5$ Hz, 1H), 7.96 (d, $J = 8.4$ Hz, 1H), 7.83 (d, $J = 8.1$ Hz, 1H), 7.71 (t, $J = 7.5$ Hz, 1H), 7.64 (t, $J = 7.2$ Hz, 1H), 7.59 (d, $J = 7.8$ Hz, 2H), 7.55 (d, $J = 7.8$ Hz, 1H), 7.27 (d, $J = 8.3$ Hz, 1H).

$^{13}\text{C NMR}$ (126 MHz, CDCl_3): δ 164.94, 146.55, 134.00, 132.92, 130.37, 129.33, 129.08, 128.81, 128.20, 127.93, 127.62, 127.32, 121.79, 119.94, 118.86.

5. Preparation of 4-Methylnaphth-1-yl Benzoate – JAJ2-56-A (19)

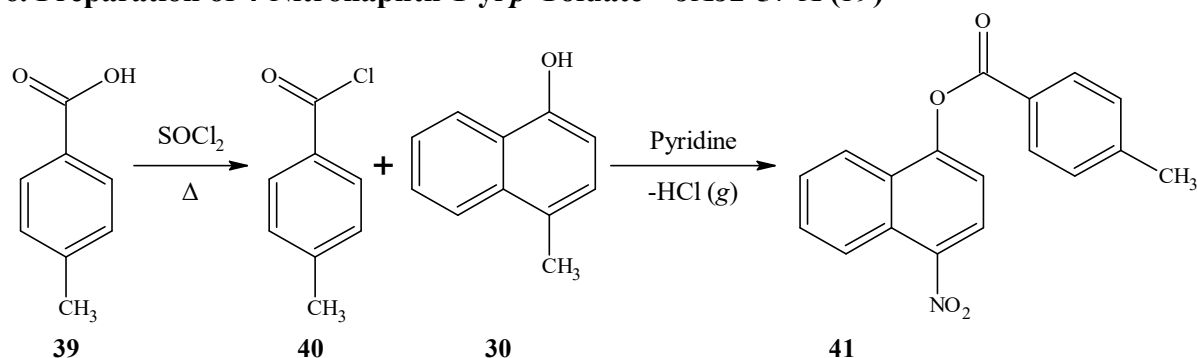


Result: carried out using 1.689 g (13.83 mmol) of the naphthol, **31**. Recrystallized from 95% ethanol. The product, **38**, was obtained as cubic, off-white crystals (1.066 g, 51.27% yield, m.p. 79.8-80.6°C).

$^1\text{H NMR}$ (500 MHz, CDCl_3): δ 8.34 (d, $J = 7.5$ Hz, 2H), 8.03 (d, $J = 8.4$ Hz, 1H), 7.95 (d, $J = 8.3$ Hz, 1H), 7.68 (t, $J = 7.4$ Hz, 1H), 7.61 – 7.52 (m, 3H), 7.52 – 7.46 (m, 1H), 7.35 (d, $J = 7.6$ Hz, 1H), 7.25 (d, $J = 3.6$ Hz, 1H), 2.71 (s, 3H).

$^{13}\text{C NMR}$ (126 MHz, CDCl_3): δ 165.37, 145.33, 133.71, 133.56, 132.54, 130.32, 129.51, 128.71, 126.95, 126.29, 126.13, 125.99, 124.59, 121.74, 117.78, 19.24.

6. Preparation of 4-Nitronaphth-1-yl *p*-Toluate – JAJ2-57-A (19)



Result: carried out using 1.401 g (7.406 mmol) of the naphthol, **30**, and 650 mg (4.78 mmol) of *p*-toluic acid, **39**. There was a calculation error, as this meant the limiting reagent was the acid, in this case. The crude material was recrystallized twice by trituration with 95% ethanol from DCM. The product, **41**, was obtained as fluffy, off-white crystals (482 mg, 36.5% yield, m.p. 177.0-178.1°C).

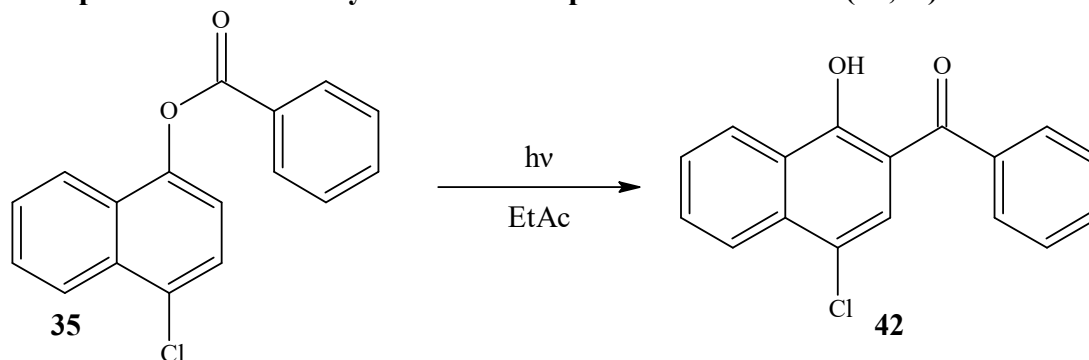
$^1\text{H NMR}$ (500 MHz, CDCl_3): δ 8.68 (d, $J = 8.8$ Hz, 1H), 8.36 (d, $J = 8.4$ Hz, 1H), 8.22 (d, $J = 8.1$ Hz, 2H), 8.12 (d, $J = 8.5$ Hz, 1H), 7.85 – 7.72 (m, 1H), 7.71 – 7.59 (m, 1H), 7.50 (d, $J = 8.4$ Hz, 1H), 7.40 (d, $J = 8.0$ Hz, 2H), 2.51 (s, 3H).

$^{13}\text{C NMR}$ (126 MHz, CDCl_3): δ 164.40, 151.44, 145.46, 144.00, 130.51, 130.00, 129.68, 127.83, 127.80, 126.70, 125.75, 124.71, 123.69, 122.15, 116.94, 21.89.

E. Photoreactions

This section reports the experimental procedures for the photo-Fries reactions performed upon the esters prepared in the previous section.

1. Preparation of 2-Benzoyl-4-chloro-1-naphthol – JAJ2-19-A (19,36)



A solution of the ester, **35**, (208 mg, 0.737 mmol) was prepared in 110 mL of thoroughly degassed ethyl acetate. The solution and a magnetic stir bar were placed into the photoreactor, and the lamp cooling jacket for the photoreactor was inserted. This solution then had nitrogen gas bubbled through it for 30 minutes, with stirring, before the medium pressure mercury lamp was inserted into the reactor with continued bubbling of N₂ gas.

The solution was then irradiated for 30 minutes, with a vigorous flow of cooling water through the cooling jacket. The temperature of the outflow water was monitored using a digital thermometer. When the outflow water temperature rose to approximately 30°C, the irradiation was terminated, and the setup was allowed to cool with continued water flow for 10 minutes before resuming the irradiation. This cycle was repeated until a total irradiation time of 30 minutes was achieved. After the beginning of each irradiation cycle, an extra minute was added at the beginning to allow the medium pressure mercury lamp to warm up and achieve its maximum output. This process required two cycles of irradiation of

approximately 16 minutes each. In this case, the solution started light yellow, and by the end of the photoreaction had achieved a color similar to an amber reagent bottle.

At the end of the irradiation cycle, the solution was removed from the reaction vessel, which was then rinsed with ethyl acetate. The rinse was added to the reaction mixture, and the solvent was removed *in vacuo*, leaving a dark brown oil. This crude product had a mass of 0.3000 g.

A series of solvent mixtures were tested using thin layer chromatography to determine an adequate solvent mixture for separation of the product on a flash column. In this case, a mixture of 99.5% petroleum ether and 0.5% ethyl acetate was found to achieve adequate separation. The crude product was then separated on a flash column. The fractions collected were left to evaporate overnight.

Fractions containing the product were combined, and the solvent was removed *in vacuo*. The product 4-chloro-2-benzoyl-1-naphthol, **42**, was recovered as an amorphous, bright yellow solid and required no recrystallization (86 mg, 41% yield, m.p. 132.5-134.8°C).

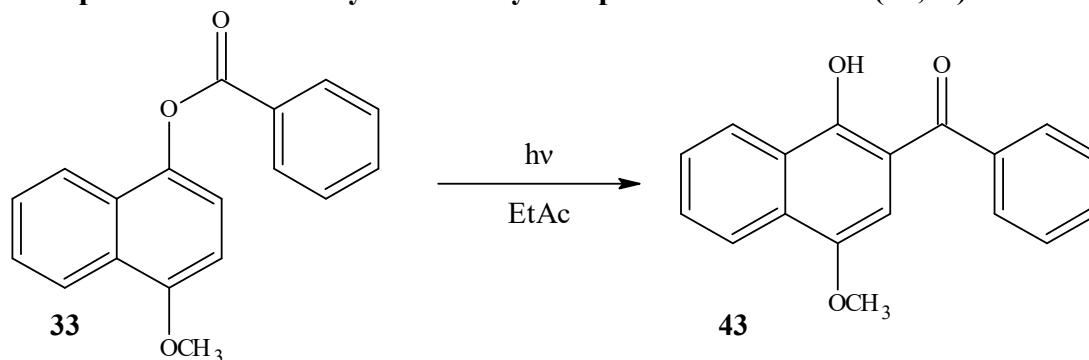
The remainder of the *o*-acylnaphthol photoreactions carried out in this manner and at approximately the same scale. As such, their procedures will not be detailed. Instead, only notable exceptions in the procedure, the chromatography solvent used, the product appearance, and pertinent data such as yield, melting point, and NMR data will be reported for each reaction.

¹H NMR (500 MHz, CDCl₃): δ 13.91 (s, 1H), 8.58 (d, *J* = 8.3 Hz, 1H), 8.20 (d, *J* = 8.4 Hz, 1H), 7.80 (ddd, *J* = 8.4, 7.0, 1.3 Hz, 1H), 7.75 – 7.69 (m, 2H), 7.69 – 7.60 (m, 3H), 7.60 – 7.53 (m, 2H).

^{13}C NMR (126 MHz, CDCl_3): δ 200.57, 162.93, 137.61, 134.33, 132.04, 131.38, 129.02, 128.60, 126.82, 126.51, 126.46, 124.95, 124.50, 121.04, 112.53.

FT-IR (ATR): 3083 (w), 3056 (w), 2955 (m), 2922 (m), 2852 (m), 1977 (w), 1752 (w), 1721 (vw), 1621 (vs), 1593 (vs), 1572 (vs), 1502 (m), 1446 (vs), 1375 (vs), 1334 (vs, br), 1247 (vs, br), 1206 (s), 1176 (s), 1107 (m), 1078 (m), 1036 (m), 996 (vs), 945 (s), 878 (m), 822 (vs), 761 (vs), 731 (vs), 697 (vs), 655 (s), 611 (m), 579 (s), 528 (m), 491 (s), 420 (s).

2. Preparation of 2-Benzoyl-4-methoxy-1-naphthol – JAJ2-53-B (19,36)



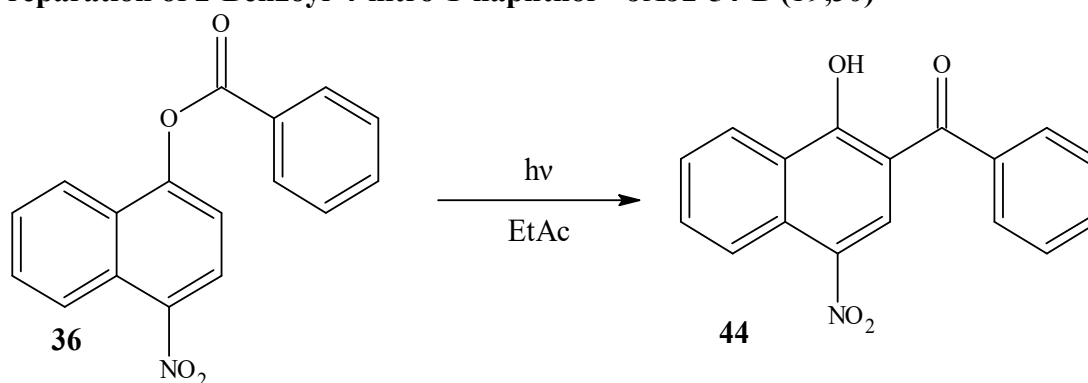
Result: the ester, **33**, (158 mg, 0.460 mmol) was irradiated for only 11 minutes due to an operator error. This reaction was run without any cooling water flow, causing much of the ethyl acetate to boil away before the reaction completed. The reaction appeared to have proceeded, so the crude product was flash chromatographed with 95% petroleum ether and 5% ethyl acetate (ketone $R_f = 0.306$ and ester $R_f = 0.213$ on TLC). Recrystallized from 95% ethanol. The product, **43**, was obtained as an amorphous, dull-yellow solid (19 mg, 12% yield, m.p. 106.1-108.5°C).

^1H NMR (500 MHz, CDCl_3): δ 13.66 (s, 1H), 8.52 (dt, $J = 8.4, 1.0$ Hz, 1H), 8.21 (dt, $J = 8.4, 0.9$ Hz, 1H), 7.80 – 7.72 (m, 3H), 7.70 (ddd, $J = 8.3, 6.9, 1.4$ Hz, 1H), 7.65 – 7.57 (m, 2H), 7.54 (t, $J = 7.4$ Hz, 2H), 3.84 (s, 3H).

^{13}C NMR (126 MHz, CDCl_3): δ 200.92, 158.82, 146.98, 138.46, 131.61, 130.06, 128.95, 128.38, 126.66, 126.01, 124.45, 121.95, 111.40, 103.53, 55.67, 29.71.

FT-IR (ATR): 3099 (vw), 3052 (vw), 2959 (m), 2919 (m, br), 2849 (m), 1592 (m), 1571 (m), 1506 (w), 1446 (m), 1385 (m), 1335 (m), 1255 (m), 1183 (w), 1098 (m), 1025 (m), 856 (w), 773 (m), 732 (m), 699 (m), 636 (w), 591 (w), 550 (w), 466 (w), 430 (vw).

3. Preparation of 2-Benzoyl-4-nitro-1-naphthol – JAJ2-54-B (19,36)



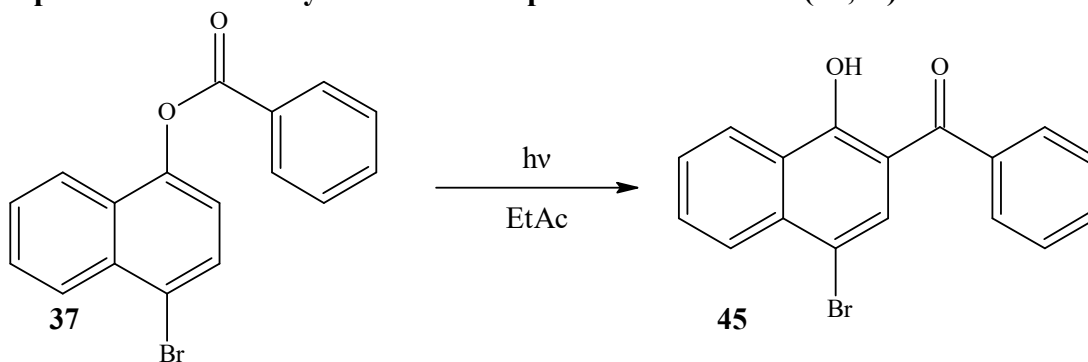
Result: the ester, **36**, (194 mg, 0.660 mmol) was irradiated for 30 minutes. The crude product was flash chromatographed with 85% petroleum ether and 15% ethyl acetate (ketone $R_f = 0.479$ and ester $R_f = 0.422$ on TLC). The product was recovered *in vacuo* and then recrystallized from 95% ethanol. The product, **44**, was obtained as an amorphous, dull-yellow solid (10 mg, 5.4% yield, m.p. 118.8-120.5°C). NMR suggests some ester co-eluted with the product. Further separation was not possible.

^1H NMR (500 MHz, CDCl_3): δ 14.60 (s, 1H), 8.79 (d, $J = 8.7$ Hz, 1H), 8.37 (d, $J = 8.4$ Hz, 1H), 8.34 (d, $J = 7.6$ Hz, 1H), 7.92 (t, $J = 7.8$ Hz, 1H), 7.72 – 7.58 (m, 5H), 7.51 (d, $J = 8.4$ Hz, 1H).

^{13}C NMR (126 MHz, CDCl_3): δ 200.64, 168.12, 134.41, 133.53, 132.88, 130.47, 129.20, 128.98, 128.95, 128.35, 127.50, 125.22, 123.89, 116.94, 110.27.

FT-IR (ATR): 3103 (w), 3075 (w), 3005 (w), 2921 (vw), 2849 (vw), 2323 (vw, br), 2100 (vw, br), 1964 (vw), 1890 (vw), 1823 (vw), 1740 (vs), 1598 (s), 1573 (s), 1517 (vs), 1450 (m), 1345 (s), 1312 (s), 1256 (vs), 1224 (vs), 1159 (s), 1086 (vs), 1021 (m), 922 (w), 861 (m), 827 (s), 762 (vs), 697 (vs), 568 (m).

4. Preparation of 2-Benzoyl-4-bromo-1-naphthol – JAJ2-58-A (19,36)



Result: the ester, **37**, (234 mg, 0.716 mmol) was irradiated for 30 minutes. The crude product was flash chromatographed with 97.5% petroleum ether and 2.5% ethyl acetate (ketone $R_f = 0.47$ and ester $R_f = 0.33$ on TLC). The product was recovered *in vacuo* and required no recrystallization. The product, **45**, was obtained as a crystalline yellow solid (63 mg, 27% yield, m.p. 129.6-131.1°C).

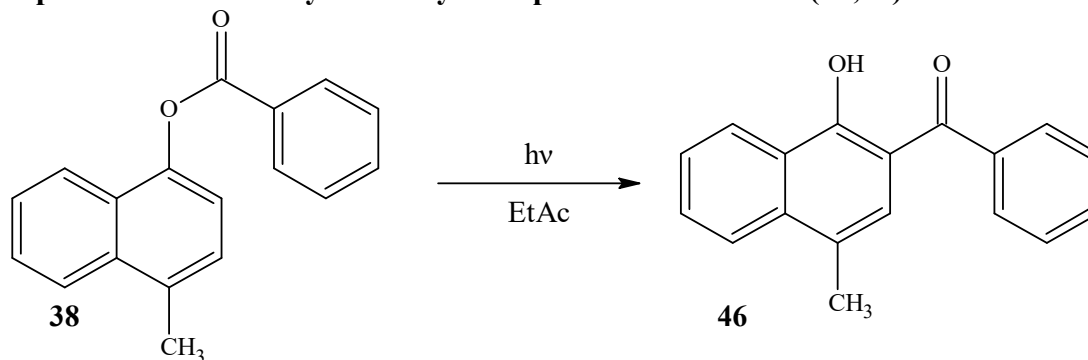
$^1\text{H NMR}$ (500 MHz, CDCl_3): δ 13.92 (s, 1H), 8.57 (d, $J = 8.3$ Hz, 1H), 8.16 (d, $J = 8.4$ Hz, 1H), 7.86 (s, 1H), 7.79 (t, $J = 7.7$ Hz, 1H), 7.72 (d, $J = 7.5$ Hz, 2H), 7.63 (t, $J = 7.7$ Hz, 2H), 7.56 (t, $J = 7.6$ Hz, 2H).

$^{13}\text{C NMR}$ (126 MHz, CDCl_3): δ 200.45, 163.49, 137.56, 135.39, 132.07, 131.61, 130.20, 129.04, 128.61, 127.16, 126.83, 126.58, 124.93, 113.28, 110.82.

FT-IR (ATR): 3055 (w), 2923 (m, br), 2853 (w), 2568 (vw, br), 2510 (vw, br), 2323 (vw, br), 2164 (vw), 2050 (vw), 1978 (w), 1911 (vw, br), 1819 (w), 1732 (w, br), 1593 (s),

1501 (m), 1444 (s), 1372 (s), 1246 (s), 1076 (m), 995 (s), 922 (m), 880 (m), 822 (s), 759 (vs), 696 (vs), 606 (s), 489 (m), 420 (s).

5. Preparation of 2-Benzoyl-4-methyl-1-naphthol – JAJ2-59-A (19,36)



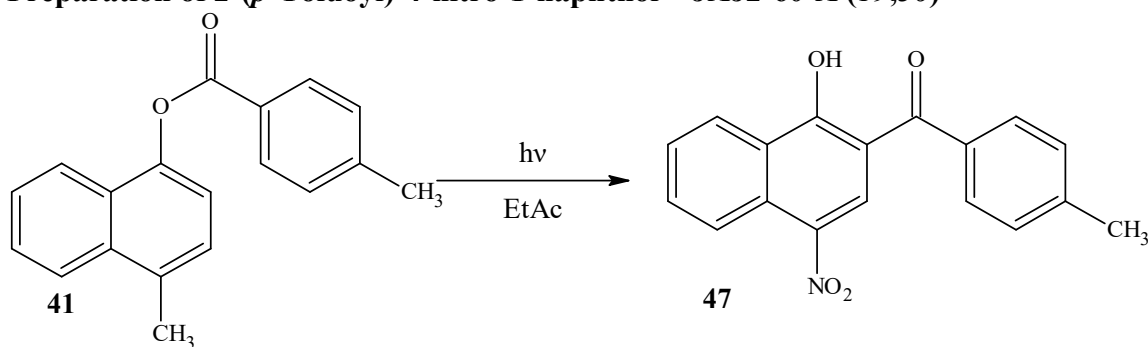
Result: the ester, **38**, (213 mg, 0.812 mmol) was irradiated for 30 minutes. The crude product was flash chromatographed with 97.5% petroleum ether and 2.5% ethyl acetate (ketone $R_f = 0.74$ and ester $R_f = 0.53$ on TLC). The product was recovered *in vacuo* and required no recrystallization. The product, **46**, was obtained as a crystalline yellow solid (75 mg, 35% yield, m.p. 88.9-90.9°C).

$^1\text{H NMR}$ (500 MHz, CDCl_3): δ 13.82 (s, 1H), 8.57 (d, $J = 8.3$ Hz, 1H), 7.91 (d, $J = 8.4$ Hz, 1H), 7.72 (t, $J = 7.4$ Hz, 3H), 7.63 – 7.50 (m, 5H), 7.37 (s, 1H), 2.53 (s, 3H).

$^{13}\text{C NMR}$ (126 MHz, CDCl_3): δ 201.31, 162.73, 138.35, 136.66, 131.55, 130.30, 129.05, 128.35, 126.78, 125.68, 125.42, 124.98, 124.09, 123.73, 112.16, 18.95.

FT-IR (ATR): 3192 (vw), 3066 (w, br), 3034 (w), 2967 (w), 2923 (m, br), 2852 (w), 1741 (w), 1630 (m), 1595 (m), 1571 (m), 1506 (m), 1444 (m), 1391 (m), 1334 (m), 1249 (m), 1111 (m), 1003 (m), 888 (m), 755 (m), 703 (m), 578 (m), 466 (w).

6. Preparation of 2-(*p*-Toluoyl)-4-nitro-1-naphthol – JAJ2-60-A (19,36)



Result: the ester, **41**, (231 mg, 0.752 mmol) was irradiated for 30 minutes. The crude product was flash chromatographed with 95% petroleum ether and 5% ethyl acetate (ketone $R_f = 0.55$ and ester $R_f = 0.44$ on TLC). The product was recovered *in vacuo* and recrystallized by triturating from DCM with 95% ethanol. The product, **47**, was obtained as an amorphous, pale-yellow solid (41.3 mg, 18% yield, m.p. 150.2-154.1°C). NMR suggests some ester co-eluted with the product. Further separation was not possible.

^1H NMR (500 MHz, CDCl_3): δ 14.64 (s, 1H), 8.79 (d, $J = 8.7$ Hz, 1H), 8.71 (s, 1H), 8.66 (d, $J = 8.5$ Hz, 1H), 7.91 (t, $J = 7.8$ Hz, 1H), 7.73 – 7.61 (m, 5H), 2.50 (s, 3H).

^{13}C NMR (126 MHz, CDCl_3): δ 200.30, 168.04, 143.91, 137.15, 133.89, 133.40, 130.00, 129.62, 129.46, 129.11, 127.40, 125.83, 125.16, 123.86, 110.38, 29.71.

FT-IR (ATR): 3467 (vw), 3107 (w), 3080 (vw), 3066 (vw), 2921 (w, br), 2851 (w, br), 1935 (vw), 1743 (vs), 1602 (m), 1568 (m), 1518 (s), 1424 (m), 1352 (m), 1223 (s), 1181 (s), 1082 (s), 1017 (m), 873 (m), 825 (m), 757 (m), 683 (w), 618 (w), 532 (vw), 472 (w), 413 (w).

CHAPTER 3:

DISCUSSION

A. Analysis of Synthetic Methods

1. Synthesis of Naphthols

The preparation of the naphthols was a difficult process. Of the three naphthols that the author attempted to synthesize, only 4-methyl-1-naphthol, **24**, was formed in any appreciable quantity. As mentioned in Chapter 1, there were several methods of preparing this compound available. The route attempted, shown in **Figure 3.17**, was the easiest accomplished one of these, and should have had appreciable yields. In the first step, benzyne, **21**, afforded by the reaction of anthranilic acid, **20**, with isopentyl nitrite undergoes a Diels-Alder reaction with 2-methylfuran, **22**, to form 1-methyl-1,4-dihydro-1,4-epoxynaphthalene, **23**. This step was not difficult, and yields consistent with those found in the literature were obtained (**23**). In the next step, the epoxy bond in **23** is cleaved, resulting in the formation of 4-methyl-1-naphthol, **24**.

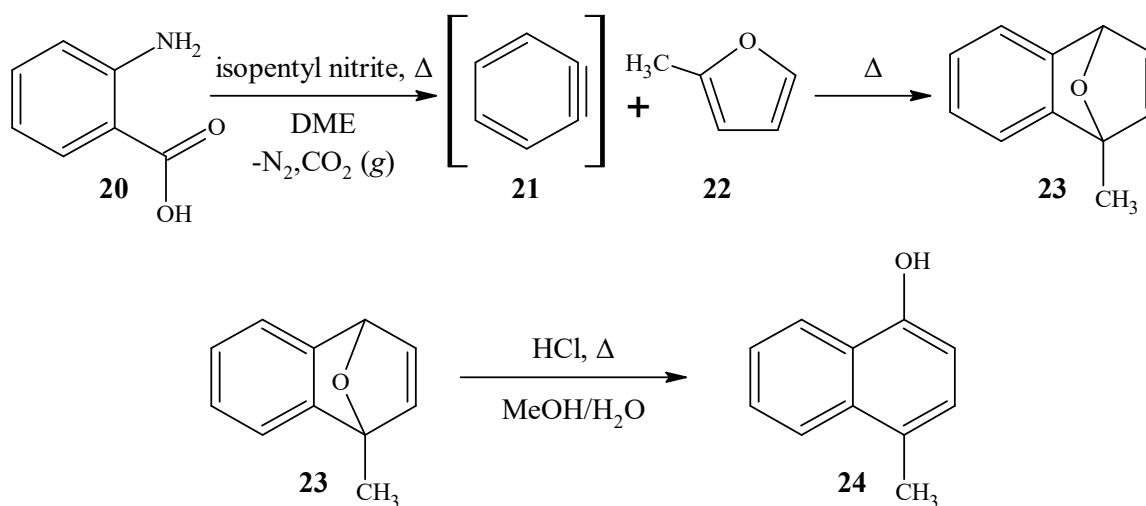


Figure 3.17. The reaction scheme followed to obtain 4-methyl-1-naphthol, **24**.

As noted in Chapter 2, the average yield for the desired 4-methyl-1-naphthol, **24**, was not on par with literature values. The yield reported by Wolthuis *et al.* was 86%, while this study could only obtain an average of 26% (37).

As for the 4-bromo- and 4-nitro-1-naphthols, **27** and **30**, all synthetic attempts essentially failed. A generic reaction scheme is shown in **Figure 3.18**. Nowhere in the literature was the author able to find a reference synthesizing a naphthol from the corresponding naphthamine. However, as stated in Chapter 1, the reactivity of aniline and its conversion into phenols is well-known, and it seemed logical that this reactivity would be analogous in naphthamine systems. Thus, assuming that the reactivity of naphthamines would be comparable, literature procedures intended for aniline derivatives were used. For each of the two naphthamines, nearly a dozen variations of the methods described in Chapter 2 sections C.3 and C.4 were attempted.

In each, reaction step 1 involved the generation of nitrous acid to form the diazonium salt. The second step was generally varied between the use of copper salts in a Sandmeyer-type reaction or merely trying to decompose the diazonium salt in warm-to-boiling water. As described in Chapter 2, section C.5, an attempt was even made to isolate the diazonium salt in step 1. A month was spent trying to get these conversions to work. Repeatedly, when the diazonium ion was formed, it produced a deep, darkly colored product that was hardly soluble in all solvents and did not appear to be the product of interest.

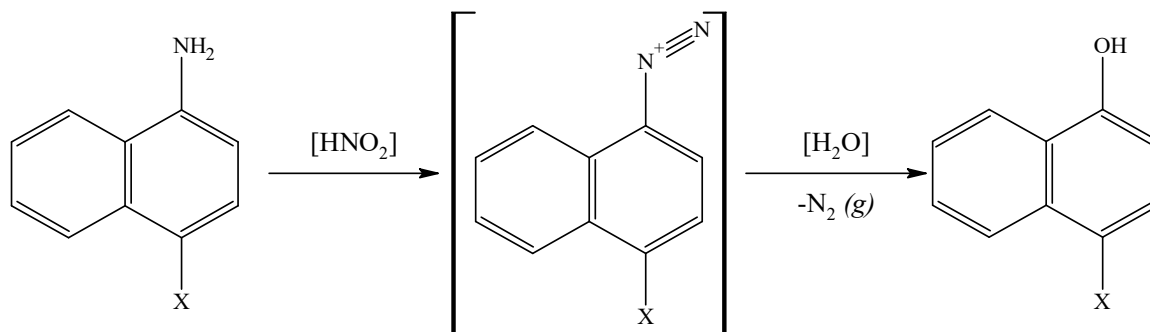


Figure 3.18. The generic equation for the reactions attempted for the synthesis of naphthols from naphthamines. X = “Br” or “NO₂.”

However, these products do fit the general description of an azo dye. Therefore, it is believed that an azo coupling reaction may have been outcompeting the decomposition reaction that was being attempted. This would not be expected in systems on a benzene ring. However, even on a naphthalene ring with an electron-withdrawing group deactivating the ring, the highly electrophilic diazonium salt may still have been able to attack readily in an electrophilic aromatic substitution reaction, as seen in **Figure 3.19**. This was not proven due to no isolation of the azo dyes, but this is a reasonable explanation for the observed results.

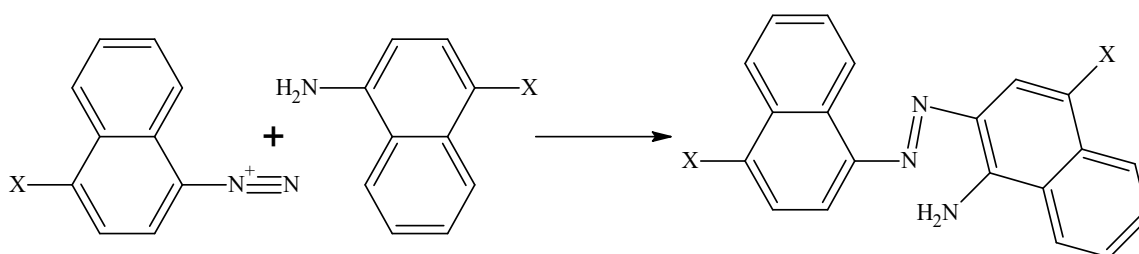


Figure 3.19. A potential reaction scheme for the observed reaction if an azo coupling took place. X = -NO₂ or -Br.

The ultimate conclusion of these experiments was that the synthesis of the needed naphthols was not going to be a fruitful endeavor. However, adequate quantities of the necessary starting materials were available commercially at moderate prices.

2. Esterification Reactions

The esterification reactions went as expected, with the general reaction scheme seen in **Figure 3.20**. The figure shows the reaction for both series 1 and series 2 compounds.

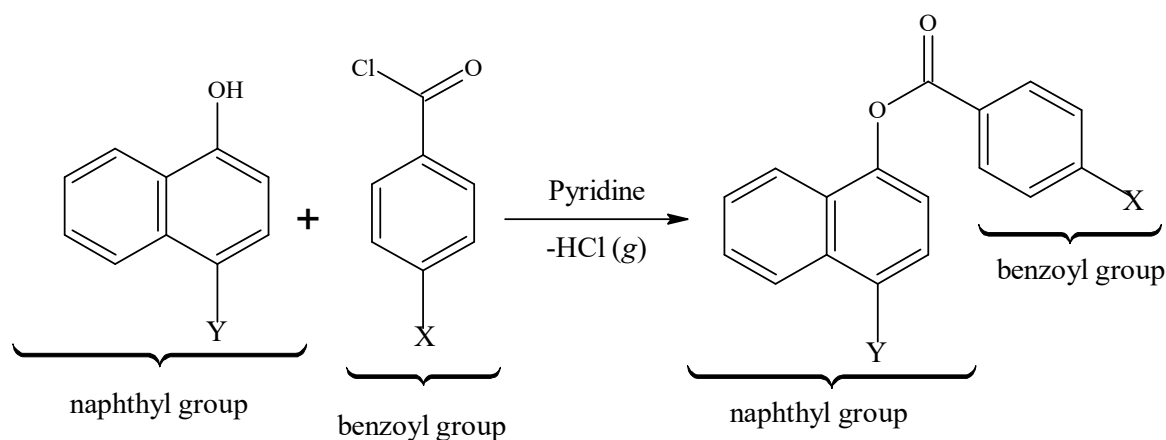


Figure 3.20. The generic form of the esterification reaction equation and the structures of series 1 and series 2 ester compounds. For series 1, “Y” = H and “X” = -H, -OCH₃, -CH₃, -Cl, -Br, and -NO₂. For series 2, “X” = H and “Y” = -H, -OCH₃, -CH₃, -Cl, -Br, and -NO₂.

Some difficulty was encountered when recrystallizing these compounds. Due to basic structural theory, it is conceivable that in some esters, the functional groups may disrupt the crystal packing of the system, hindering recrystallization (**38**). An unusual effect was noticed when comparing yields of the series 1 (X-substituted) and series 2 (Y-substituted) compounds. See **Figure 3.20** for the structures of the series 1 and series 2 esters.

As seen in **Table 3.5**, the compounds in series 2 generally had lower yields than those seen by Mathis in series 1, and were generally more difficult to work with; naphth-1-yl

benzoate had 54% yield. While Mathis was able to recrystallize most of her compounds in 95% ethanol or methanol, half of the series 2 analogs had to be triturated from DCM with 95% ethanol. This trend of difficulty was also evident in the photoreactions (19).

Table 3.3. Yields of the various esters. Series 1 yields reported by Mathis. *The series 1 *p*-nitro compound was synthesized using a different method (19).

Substituent	Series 1, X- (%)	Series 2, Y- (%)
Bromo	20	46.8
Chloro	66.4	24.6
Methoxy	53.6	63.9
Methyl	63.7	51.3
Nitro	N/A*	44.9

3. Photo-Fries Reactions

The photo-Fries reaction was discovered initially by Anderson and Reese in 1960 (39). Examples of the photoreaction for series 1 and 2 compounds are given in **Figure 3.21**.

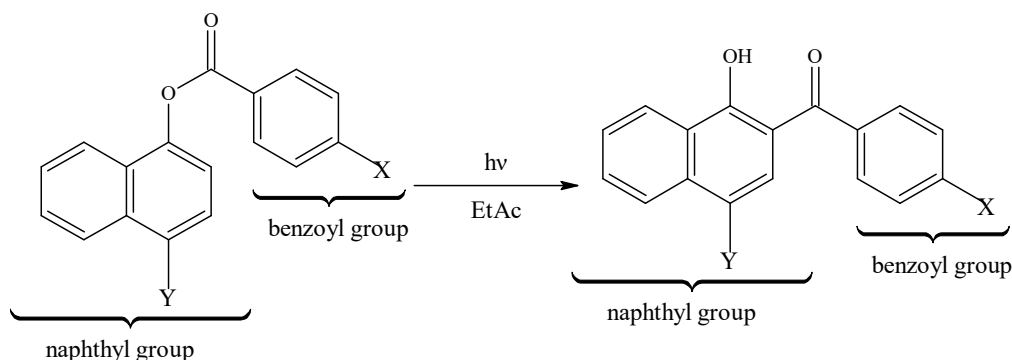


Figure 3.21. Generic form of the photo-Fries rearrangements underwent by the esters, along with the generic structures of the series 1 and 2 compounds. For series 1, “Y” = H and “X” = –H, –OCH₃, –CH₃, –Cl, –Br, and –NO₂. For series 2, “X” = H and “Y” = –H, –OCH₃, –CH₃, –Cl, –Br, and –NO₂.

A mechanism for this reaction was later proposed by Kobsa and is detailed in **Figure 3.22**. According to Kobsa, the rearrangement starts with photoinduced dissociation of the ester into a pair of acyl and phenoxy radicals in a solvent cage. Cleavage occurs as a result of UV-induced excitation of the ester carbonyl group to the singlet state, followed by homolytic

cleavage of the C–O bond. These radicals then lead to the formation of the three known major photoproducts: phenol, and 2- and 4-acyl-phenols. The *ortho*- and *para*-isomers, in the middle and on the right, respectively, are formed in the solvent cage. This is the result of the recombination of the acyl radical with the phenoxy radical at the sites of the highest radical density, as indicated by the contributing resonance structures. However, as seen on the left-hand side, phenols are formed by the phenoxy radical dissociating or escaping the solvent cage and abstracting a hydrogen from the solvent (40).

During the irradiation period, whenever the lamp is shut off, it is obvious the reaction has proceeded. Besides spectroscopic techniques, the easiest way to monitor the reaction is by the drastic color changes in the solution. The esters used are all white or off-white crystals, but the ketones produced are all light to bright yellow crystals, with the exception of the 4-nitro ketone, which was isolated as off-white crystals.

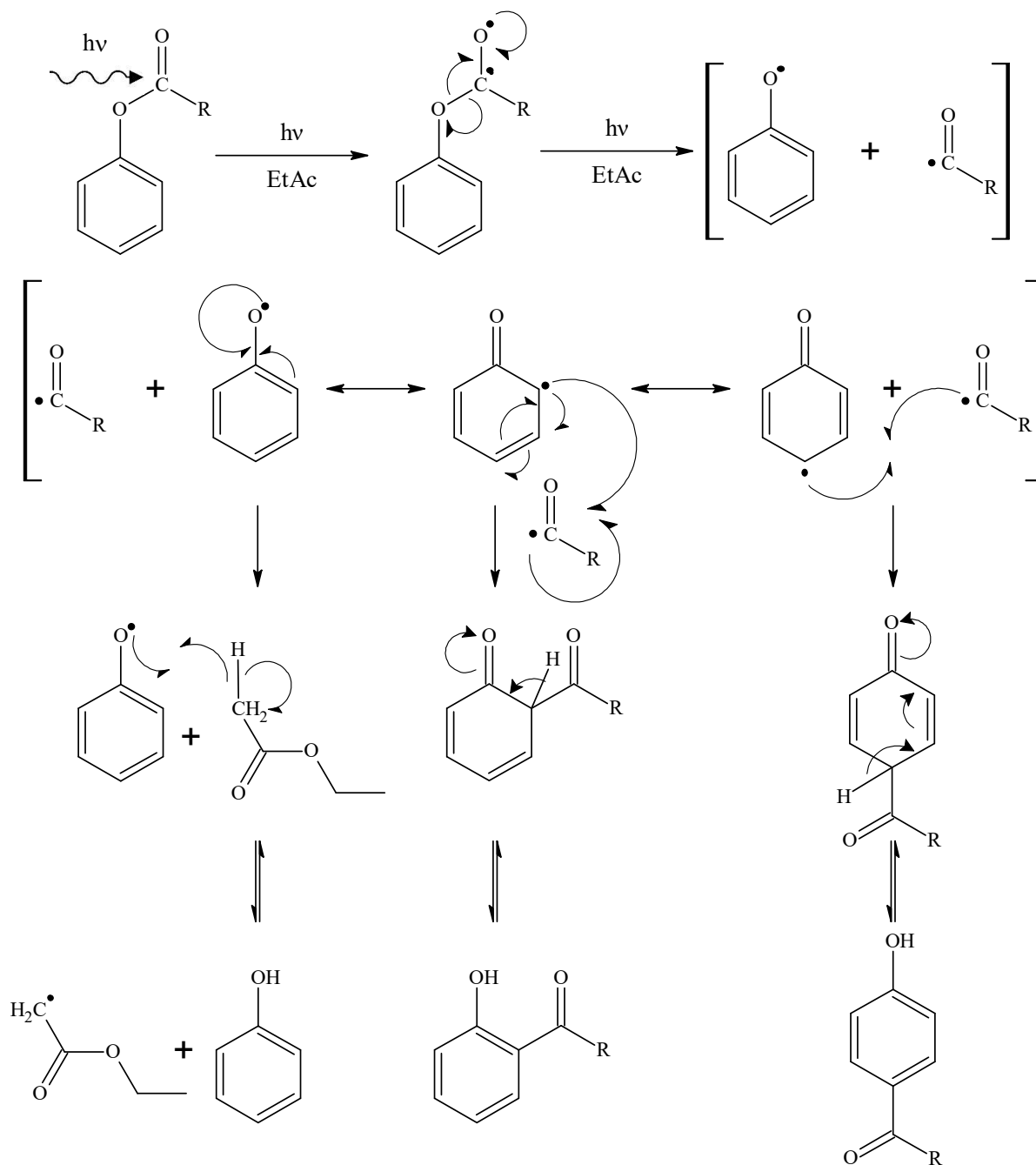


Figure 3.22. Mechanism of the photo-Fries rearrangement reaction (40).

The principal difficulty in these reactions was the chromatographic separations. There was great difficulty in selecting chromatography solvents that afforded adequate separation. For 4-nitro-2-benzoyl-1-naphthol and 4-nitro-2-(*p*-methylbenzoyl)-1-naphthol, a solvent mixture was not found that achieved complete separation of the ester and ketone. Both of

those materials were contaminated with the corresponding ester after chromatography. In the series 1 compounds, no ester was co-eluted with the photoproducts. As a result, a comparatively thorough characterization using NMR was required to ensure the desired compound was present in these cases of ester co-eluting. Fortunately, because the 4-position was blocked on the naphthalene ring, there was no evidence of the *para* rearrangement taking place for any of the compounds.

Aside from the major products of the photo-Fries reaction, there is an additional reaction that occurs in small amounts. If the solvent has any atmospheric oxygen dissolved in it, the diatomic oxygen will intercept radicals and cause a variety of oxidation reactions. These side products in the reaction tend to be minor to none depending on how well a solution was degassed and purged. Indeed, when Crouse *et al.* performed the photo-Fries reaction to form 2-benzoyl-1-naphthol and other substituted naphthols, the only compounds determined to be present after the reaction were the naphthol, photo-product, and unreacted ester (**10**).

However, the yields were rather low for both the series 1 (X-substituted) and series 2 (Y-substituted) compounds (refer to **Figure 3.22**), as seen in **Table 3.4**. This can be explained by considering a few factors in the reactions. During the reaction, a discrete wavelength or range of wavelengths of UV radiation from the medium pressure mercury lamp is required to excite the ester to the singlet state and cause the ensuing homolytic cleavage of the ester. As the reaction proceeds, this leads to the formation of the *ortho*-substituted ketone and the corresponding naphthol. The ketone produced absorbs UV radiation at the same wavelength(s) required to excite the ester. After a certain length of time, the amount of UV radiation being absorbed by the product becomes so high that it effectively

halts the reaction of additional ester. This situation appears to occur more rapidly with specific functional groups. For example, in the reactions for both series 1 and series 2 compounds, poor yields were observed for the nitro-substituted compound (19).

Table 3.4. Yields of the various ketones. Series 1 yields reported by Mathis (19).

Substituent	Series 1, X- (%)	Series 2, Y- (%)
Bromo	38.6	27
Chloro	39	41
Methoxy	39.6	12
Methyl	38	35
Nitro	6.3	5.4

In addition to the photoreactions proposed in Chapter 1, one additional experiment was carried out to form 4-nitro-2-(*p*-methylbenzoyl)-1-naphthol. This was intended to be a hybrid made by combining an X and Y group and was synthesized in order to test if the combination of the two created a combined effect and markedly affected the NMR shift of the enolic proton. The combined groups were both the ones that produced the most downfield shifts for the enolic proton for their corresponding series (*p*-methyl for series 1, 4-nitro for series 2). The results of this experiment are discussed in the following section.

B. Hammett Study

1. Results from Series 2 Compounds

The results of spectroscopic studies of the series 2 ketones are presented in **Table 3.4** and **Table 3.5**. Following the tables is **Figure 3.23**, depicting a plot of the *para* substituent constant (σ_p) versus enol ^1H NMR shifts, and **Figure 3.24** depicting a plot of the *meta* substituent constant (σ_m) versus carbonyl ^{13}C NMR shifts.

A plot of the carbonyl ^{13}C NMR shift versus the *para* substituent constant did not give results that fit as well as those from plotting the shifts against the *meta* substituent

constant. This is logical, considering the substituent group is in a *meta*-position relative to the acyl group. Therefore, a plot of that information was not prepared ($P > 0.25$ and $R^2 < 0.30$). Additionally, for both series 1 and 2, plots of the C–O ^{13}C NMR shifts versus either substituent constant had large P values ($P > 0.50$) and very low R^2 values ($R^2 < 0.1$). Based on these statistical values, it can be assumed that there is no significant correlation for the three situations described.

Table 3.5. ^1H NMR shift assignments for the Series 2 compounds with corresponding Hammett substituent constants from (41). *The 4-H compound was synthesized by Mathis (19). They are sorted in order of ascending σ_p .

		Hammett Substituent Constants	^1H NMR Chemical Shifts (PPM)
Compound #	4-substituent	σ_p	Enol Proton (OH)
43	OCH_3	-0.27	13.66
46	CH_3	-0.17	13.82
--*	H	0.00	13.96
42	Cl	0.23	13.91
45	Br	0.23	13.92
44	NO_2	0.78	14.60

Table 3.6. ^{13}C NMR shift assignments for the Series 2 compounds with corresponding Hammett substituent constants from (41). *The 4-H compound was synthesized by Mathis (19). They are sorted in order of ascending σ_m .

		Hammett Substituent Constants	^{13}C NMR Chemical Shifts (PPM)	
Compound #	4-substituent	σ_m	C=O (carbonyl)	C–O (Enol)
46	CH_3	-0.07	201.31	162.73
--*	H	0.00	201.70	164.20
43	OCH_3	0.12	200.92	158.82
42	Cl	0.37	200.57	162.93
45	Br	0.39	200.45	163.49
44	NO_2	0.71	200.64	160.12

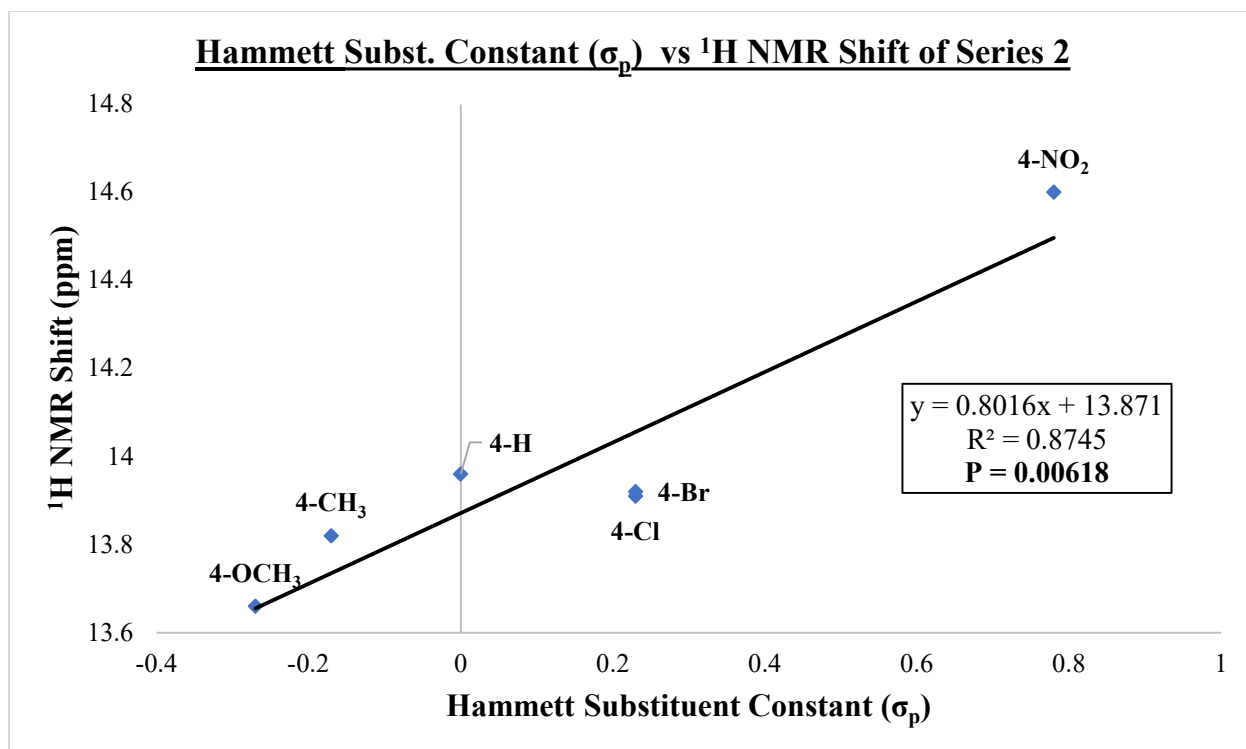


Figure 3.23. Plot of the Series 2 enol ^1H NMR shift vs. Hammett substituent constants, σ_p .

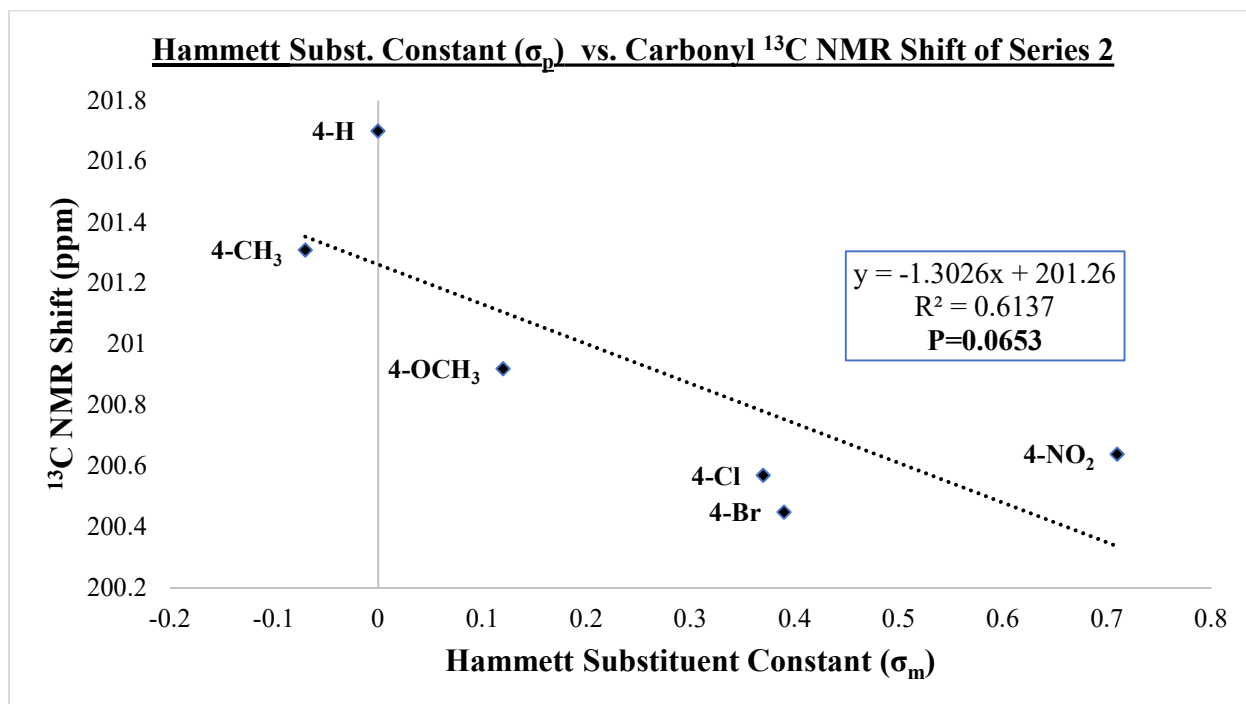


Figure 3.24. Plot of the series 2 carbonyl ^{13}C NMR shift versus Hammett substituent constants, σ_m . A dotted line is used because the trend is not statistically significant.

2. Revision of Previous Results

A small error has been found in the work previously reported by Mathis in her thesis. In her analysis, she assigned $\sigma_p = -0.12$ for a methoxy group. However, the accepted literature value for this substituent constant should have been $\sigma_p = -0.27$. It is believed that Mathis mistakenly entered the negative value of the meta substituent constant for the methoxy group, which has the literature value of $\sigma_m = +0.12$ (41). As such, the plots and statistical data in the Mathis thesis contained errors. Therefore, the data was re-calculated; the updated results are listed in

Table 3.7. The series 1 compounds can only interact with the carbonyl from the *para* position; therefore, there is no need for a table with *meta* substituent constant values. Plots of the enol ^1H NMR shifts versus σ_p and the carbonyl ^{13}C NMR shifts versus σ_p are given as **Figure 3.25** and **Figure 3.26**, respectively (19).

Table 3.7. The corrected version of the table from p. 47 of the Mathis thesis (19). They are sorted in order of ascending σ_p .

<i>p</i> -substituent	Hammett Substituent Constants σ_p	^{13}C NMR Chemical Shifts (ppm)		^1H NMR Chemical Shifts (PPM)
		C=O	C-O	Enol Proton (OH)
OCH ₃	-0.27	200.2	162.9	13.95
CH ₃	-0.17	201.4	164.0	14.01
H	0.00	201.7	164.2	13.96
Cl	0.23	200.2	164.2	13.82
Br	0.23	200.3	164.3	13.83
NO ₂	0.78	199.4	164.8	13.71

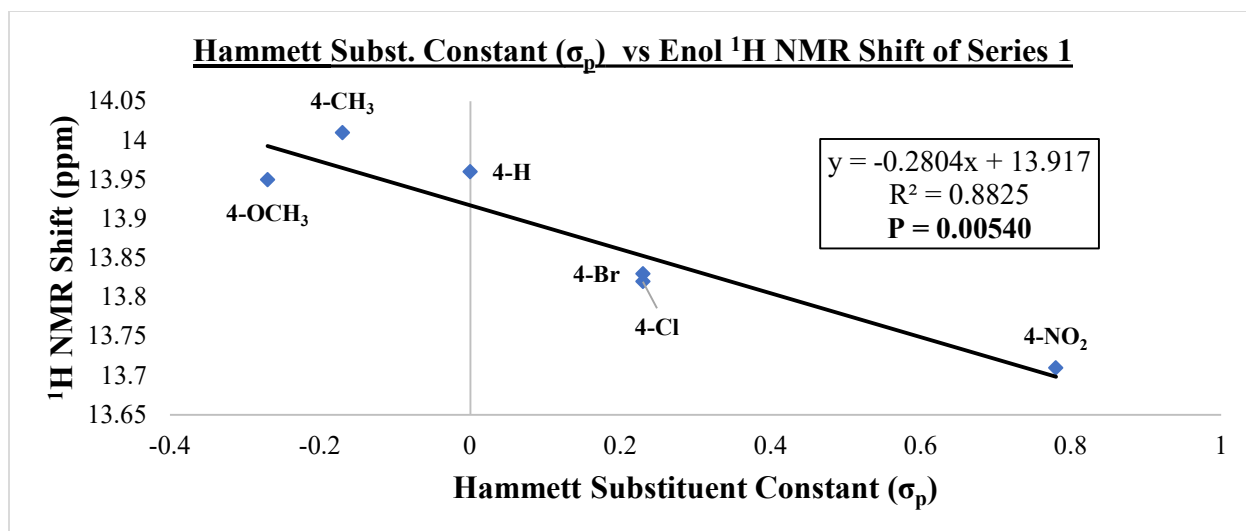


Figure 3.25. Plot of the Series 1 enol ^1H NMR shift versus Hammett substituent constants, σ_p .

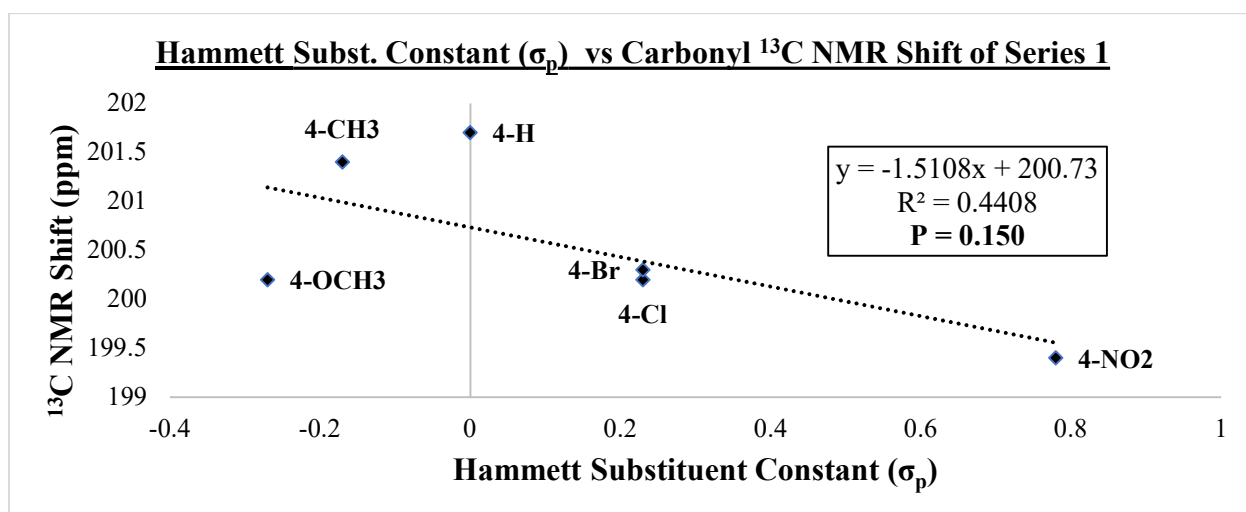


Figure 3.26. Plot of the Series 1 carbonyl ^{13}C NMR shift versus Hammett substituent constants, σ_p . A dotted line is used because the trend is not statistically significant.

3. Discussion of Hammett Study Data for Series 1 and 2 Compounds

When looking at each dataset, it is necessary to discuss the statistical parameters involved. The null hypothesis (or default conclusion) for this study is that the slope of the plot is zero (i.e., there is no correlation between the NMR shifts and the Hammett substituent constants). The alternate hypothesis is that the slope is not zero, meaning there is a linear

correlation (i.e., there is a correlation between the two variables). In order to reject the null hypothesis at the significance level $\alpha = 0.05$, the linear regression trendline between the two variables must yield a p-value of less than 0.05. This p-value is the probability of observing the trend in question if the null hypothesis were true; thus, a lower p-value corresponds to a lower chance of the correlation observed being the result of random chance. At this significance level 0.05, if the condition $p < 0.05$ is met, the null hypothesis is rejected, and the alternate hypothesis that there is a statistically significant linear correlation is accepted (42). No test for normalcy was performed for this dataset.

The R^2 parameter measures the percentage of how well a linear model explains the variability of a dependent variable; for example, $R^2 = 0.60$ indicates that 60% of the variability in the trend being modeled is explained by the linear equation calculated using the ordinary least-squares method. The R^2 value is not as crucial as the p-value, but it is nonetheless a useful statistic to consider when modeling a trend (42). Using these two parameters, an examination of the electronic effects of the substituents can be performed.

In **Figure 3.23**, the plot of the Series 2 enol ^1H NMR shifts versus Hammett *para*-substituent constants, σ_p , gives $R^2 = 0.87$ and $p = 0.0062$, which indicates a statistically significant correlation. The plot has a positive slope, indicating that analogs in Series 2 containing electron-withdrawing groups (Cl, Br, NO_2) had higher enol ^1H NMR shifts. Conversely, those containing electron donor groups had lower shifts, with the 4-methoxy analog representing the extreme.

Regarding the sensitivity constant (i.e., the slope of trendline) observed for the series 2 enol NMR shifts versus the substituent constants, there are two essential groups of information to be seen from these. The first of those is the signs of the trendline. For series 2,

ρ was positive, indicating that as the electron-withdrawing character of the *para*-substituents increased, the enolic hydrogen's NMR shift went up. This means that higher electron-withdrawing character of substituents in that position resulted in greater shielding of the enolic proton for series 1 compounds, which Mathis attributed to the fact that the carbonyl oxygen was becoming a less effective H-bond acceptor (*i.e.*, a less effective Lewis base). As mentioned previously in chapter 1, the magnitude of the slope can be used to compare the two substitution positions. This will be done after the discussion of other data.

In **Figure 3.24**, the plot of the Series 2 carbonyl ^1H NMR shifts versus Hammett *meta*-substituent constants, σ_m , gives $R^2 = 0.61$ and $p = 0.065$, which does not indicate a statistically significant correlation at significance level $\alpha = 0.05$. However, this correlation is very narrowly insignificant at this significance level.

Thus, the trend in **Figure 3.24** shows that the substituent groups in the series 2 compounds do have some effect on the electronic properties of the carbonyl carbon, though not nearly as strong of a correlation as was observed between the enolic proton and the Hammett *para*-substituent parameters. The plot has a negative slope, indicating that analogs in series 2 containing substituents that are electron-withdrawing groups (OCH_3 , Cl , Br , NO_2) had lower carbonyl ^{13}C NMR shifts. The methoxy group is an EWG in this situation because the oxygen can only undergo the inductive withdrawal of electrons with groups in the *meta* position. Conversely, those groups containing electron donor groups had higher shifts, with the 4-methyl analog representing the extreme. The correlation is weak, but this result seems to suggest that a carbonyl in this system with more electron density donated to it is further upfield.

Moving on to the Series 1 compounds made by Mathis, it would appear that her original conclusions, discussed in Chapter 1 of this thesis, stand intact, despite the data error. In **Figure 3.25**, the plot of the enol ^1H NMR shifts versus Hammett *para*-substituent constants is still a significant trend with $R^2 = 0.88$ and $p = 0.0054$, indicating that her initial analysis stating that, “these results indicate that the electronic character of the substituent group, as represented by the Hammett [*para*-substituent constant], is significant in determining the electronic environment of the enolic proton” was correct. Likewise, in **Figure 3.26**, the plot of the carbonyl ^{13}C NMR shifts versus Hammett *para*-substituent constants trend is still insignificant. Indeed, the trend became worse with the updated data, with $R^2 = 0.44$ and $p = 0.15$, indicating that there may be a vague trend, but that it cannot be explained by a simple application of the Hammett parameters.

Regarding the slope of the series 1 enol shifts versus Hammett substituent constants trendline, ρ (the slope) was negative, indicating that as the electron-withdrawing character of the *para*-substituents increased, the enolic hydrogen's NMR shift went down. This means that higher electron-withdrawing character of substituents in that position resulted in greater shielding of the enolic proton for series 1 compounds, which Mathis attributed to the fact that the carbonyl oxygen was becoming a less effective H-bond acceptor (*i.e.*, a less effective Lewis base).

Regarding the second part of the sensitivity constant data mentioned previously, the magnitude of the slopes can be compared. This is simply accomplished by comparison of the slopes of the series 1 and 2 trendlines. The elucidated trendlines of the enolic NMR chemical shifts reveal that the trendlines for the series 2 compounds ($m = 0.80$) and the series 1 compounds ($m = -0.28$) are not equal in slope. Indeed, the absolute value of the series 1

trendline is nearly one third less intense than the series 2 trendline. This evidence shows that the electronic effect of substituents in the 4-naphthyl position was three times stronger than those of substituents in the *p*-benzoyl position, and suggests that the effect of the 4-naphthyl substituent is more directly affecting the enolic proton.

Combining the trends in both series 1 and series 2 suggested that a higher value for the ¹H NMR shift of the enol hydrogen could be obtained by synthesizing 4-nitro-2-(*p*-toluoyl)-1-naphthol, **47**. A comparison of the series 1 analog, the series 2 analog, and the hybrid compound is shown in **Table 3.8**. The small increase from the series 2 4-nitro compound to that of the hybrid compound (only .04 ppm) was a relatively small change, but a dramatic increase of nearly an entire ppm was observed between the series 1 *p*-toluoyl compound and the series 2 4-nitro compound.

Table 3.8. Comparison of the enolic shifts of the three compounds with the highest enolic ¹H NMR shift in series 1, series 2, and the hybrid compound. The compounds are sorted in ascending order of the enolic proton ¹H NMR shift. *The first compound was synthesized by Mathis (19).

Compound, #	Enolic Proton ¹ H NMR shift (ppm)
2-(<i>p</i> -toluoyl)-1-naphthol*	14.01
2-benzoyl-4-nitro-1-naphthol, 44	14.60
4-nitro-2-(<i>p</i> -methylbenzoyl)-1-naphthol, 47	14.64

Overall, these results imply that a substituent group at the 4-position on the naphthol ring is a much more effective transmitter of electronic effects to the enolic proton than the *para*-position on the benzoyl group. Combined with the small increase afforded by having the *p*-toluoyl group on the 4-nitro-1-naphthol system, this data presents evidence supporting the conclusion that the electronic effects of substituents on the naphthalene ring will more directly affect the enolic proton's relative-acidity. From this, it can be concluded that

substituents on the naphthalene ring also exhibit a more substantial effect on the RAHB system, causing more considerable changes to its properties depending on the substituent in question.

CHAPTER 4: CONCLUSIONS

The five 4-substituted analogs of naphthyl benzoate and the corresponding *o*-acylnaphthols have been successfully synthesized. In addition, a sixth disubstituted analog has also been synthesized, one (nitro) on the 4-naphthyl position and the other (methyl) on the *p*-benzoyl position. A study involving the synthesis of some of the parent naphthols was conducted and was unsuccessful.

Similar to Mathis in 2008, the photo-Fries reaction, which requires no particularly harsh reaction conditions, was found to be a suitable method for converting the esters into the *o*-acylnaphthol analogs. Though this reaction does form a mixture of products and unreacted ester, total separation by flash chromatography was typically possible. Despite the problematic separations sometimes encountered, the relative ease of conducting the photo-Fries rearrangement reaction when compared to the thermal Fries rearrangement reaction made it suitable for small-scale synthesis in these situations.

In both the new Hammett study and the one done by Mathis, a high-significance correlation was observed between the enolic ^1H NMR shifts and the Hammett para-substituent constants (σ_p). For the series 1 compounds made by Mathis, there was a correlation observed wherein substituents with electron-donating character exhibited higher chemical shifts. Mathis concluded that more available electron density on the benzene ring made the carbonyl oxygen a more effective H-bond acceptor. The effect on the enolic hydrogen is indirect. This was further explained visually in **Figure 1.12 (19)**.

In contrast, the opposite trend has been observed in the series 2 compounds. As expected, substituents with higher electron-withdrawing character resulted in higher chemical

shifts for the enolic proton. As seen in **Figure 4.27**, withdrawal of electron density from the naphthol oxygen results in that oxygen atom withdrawing more electron density from the enolic proton, which in turn strengthens the resonance-assisted hydrogen bond found between that proton and the carbonyl.

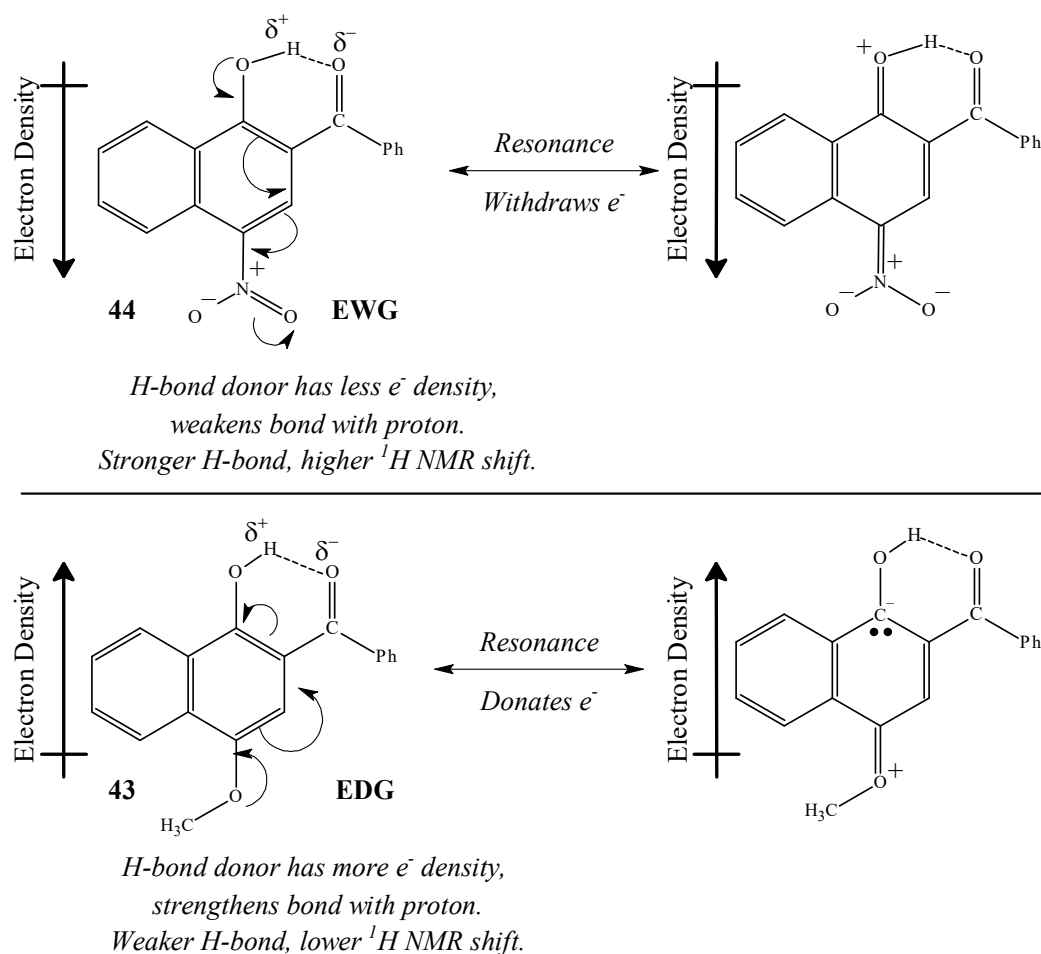


Figure 4.27. The electronic trend observed for the analogs of 2-benzoyl-1-naphthol in the series two compounds. In **44**, 2-benzoyl-4-nitro-1-naphthol, the nitro substituent acts as an EWG, strengthening the RAHB by decreasing the donor oxygen's electron density and weakening the covalent O–H bond. The opposite is true for **43**, 2-benzoyl-4-methyl-1-naphthol. Resonance structures are shown for **44** and **43**. The benzene ring is abbreviated as Ph.

0020

Based on the higher range of ^1H NMR shifts observed, the electronic effect from substituents in the 4-naphthyl position appears to be transmitted more effectively to the

RAHB. Indeed, the results from the 2-(*p*-toluoyl)-4-nitro-1-naphthol seemed to support this. The series 2 analog with the highest NMR shift, the 4-nitro compound, had the enolic proton at 14.60 ppm; for the series 1 analogs, the *p*-methyl analog had the highest shift at 14.01 ppm. The hybrid compound had a shift of 14.64 ppm (**19**). This is a substantial increase from the 14.01 in the *p*-methyl compound but is only a tiny increase from the 4-nitro compound. This also suggests the effect of substituents at the 4-benzoyl position is weaker than those in the 4-naphthyl position.

Additionally, evidence was shown that the ^{13}C NMR shifts for the carbonyls in the series 2 analogs exhibited a weaker correlation, showing that the chemical shift of the carbonyl tended to go down as the Hammett *meta*-substituent constant increased. This could add to the explanation of why the series 2 enol ^1H NMR shifts were so much higher than those recorded with the series 1 shifts. The effect of the *meta*-interactions with the H-bond acceptor carbonyl may not be contributing much. Instead, the *para*-interactions with the H-bond donor oxygen may be primarily causing the changes in the carbonyl oxygen, resulting in the observed effects on the carbonyl chemical shifts.

A. FUTURE WORK

The immediate need for future research is to undertake the computational modeling of these compounds, which may present more insights into the data currently in hand. As mentioned in Chapter 1, literature precedence has been established for the study of RAHB systems using density functional theory (DFT) methods (**2,13,12**).

Any future experimenters may wish to spend more time determining optimal recrystallization solvents for the series 2 compounds. Also, future research on this complex

system may stand to benefit from the acquisition of x-ray crystallographic structures of all of the series 1 and series 2 compounds. If possible, neutron crystallography would be even better, because of its power to resolve the position of hydrogen atoms. Finally, future researchers with adequate resources may even synthesize hybrid compounds from a third series, proposed in **Figure 4.28**.

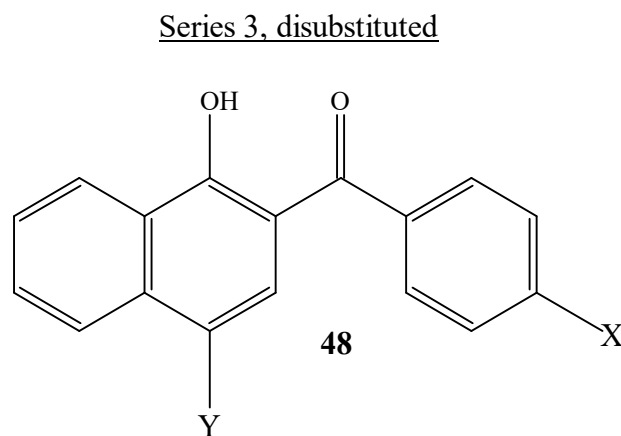


Figure 4.28. The proposed structure of series 3 *o*-acylnaphthol compounds. “X” and “Y” are any combinations of $-\text{OCH}_3$, $-\text{CH}_3$, $-\text{Cl}$, $-\text{Br}$, and $-\text{NO}_2$.

PART II:
THE DEVELOPMENT OF A COMPUTATIONAL CHEMISTRY EXERCISE FOR
THE FRESHMAN-LEVEL GENERAL CHEMISTRY CURRICULUM

CHAPTER 5: INTRODUCTION

A. The Valence Shell Electron Pair Repulsion Model

1. History of the Model

In 1957, Gillespie and Nyholm introduced the idea that the valence bond theory was influenced by valence electron-pair repulsion and applied several rules utilizing their premise for determining inorganic and organic stereochemistry (43). In a 2008 review paper, Gillespie states that he was dissatisfied with the previous methods of understanding molecular theory that he had been teaching and decided to work together with his colleague, Nyholm, to develop a new theory with logical methods of reasoning out molecular geometries. The phrase Valence Shell Electron Pair Repulsion (VSEPR) theory was proposed in a 1963 paper and has been the term used for the theory ever since (44).

Using a series of predictions published by other chemists in the community, Gillespie and Nyholm were able to use available data in the literature to correlate the arrangements of atoms in molecules to correspond to the predictions and extend them to encompass more situations. Citing the Pauli Exclusion Principle, Gillespie also "...emphasized in the original 1957 paper that electron pairs in a valence shell behave as if they repel each other and that this behavior is a consequence of the Pauli principle and not of electrostatic repulsion." This is a common error made when describing the model in contemporary settings (44).

The model can be broken down to three simple rules.

- i) Repulsions between electron pairs in a valence shell decrease in the order:
lone pair–lone pair > lone pair–bond pair > bond pair–bond pair. Lone pairs tend to

occupy as much angular space as possible in the valence shell of the atom to which they are associated.

ii) Bonds of a different order (*e.g.*, single, double, triple) differ in repulsion strength, decreasing in the order: triple–double > double–double > double–single > single–single. This effect can be rationalized by the fact that higher-order bonds possess multiple electron pairs, which in turn must take up more angular space than single electron pairs.

iii) The strength of repulsion between single bonds decreases with increasing electronegativity of the ligand atom and vice-versa. For increasing electronegativity of the central atom, the strength of repulsion between single bonds also decreases (*e.g.*, stronger repulsion in H₂O than in H₂S due to the highly electronegative oxygen). These trends are observed due to the effect an electronegative atom has to effectively sequester electron density across a polar covalent bond (44).

2. Modern Day Classroom Significance

In contemporary introductory chemistry courses worldwide, the VSEPR model holds an essential place as the initial step for introducing students to molecular geometry. Although the VSEPR model has been effectively succeeded by superior theoretical treatments such as the molecular orbital theory, VSEPR is still the most widely taught method of conceptualizing molecular geometry at the introductory level (44).

When taught in combination with Lewis structures, the VSEPR model makes for a compelling method of introducing the challenging concept of molecular geometry to students without needing them to bring orbitals into consideration (44). However, teaching VSEPR in

a traditional way is increasingly seen as an ineffective way to accurately impart the concept of molecular and electronic structure to students. One paper argues not for abandoning VSEPR, but rather aggressively augmenting it in classes beyond the introductory level. For example, the paper demonstrates using the VSEPR model for the tetrachloroplatinate(II) anion. According to the VSEPR theory, it would have the tetrahedral structure suggested in **Figure 5.29**. However, empirical observations establish that the second structure, with a square planar metal center, is the correct one (45).

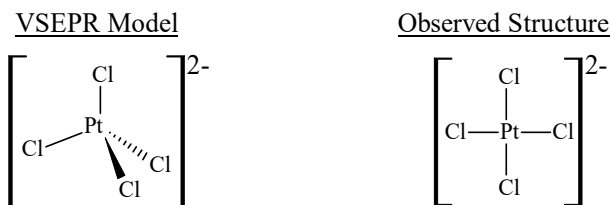


Figure 5.29 On the left, the VSEPR model's proposed tetrahedral structure of the tetrachloroplatinate(II) anion juxtaposed with the correct square planar structure on the right. This figure was adapted from (45).

However, the VSEPR model has withstood the test of time as a theoretical model, but not without some challenges. It has been generally superseded in the field by models taking into account quantum effects, such as molecular orbital theory. Gillespie points out that there are many examples of molecules in the literature that defy the rules for the original model, but points out that while the VSEPR model may not be the cutting edge understanding of molecular geometry anymore, it is still a useful “back of the envelope” method for researchers to roughly determine molecular geometries (44).

In a 2008 review, Gillespie himself recommends that VSEPR being taught for introductory purposes should include a disclaimer regarding transition metal compounds and have some discussion of ligand-ligand interactions and the ligand close packing model at

some point, but not necessarily in the first course of an introductory sequence. He even asserts there is an opportunity to use cases where VSEPR theory is inaccurate as teaching cases for the orbital models (e.g., molecular orbital theory or crystal field theory) in later organic and inorganic chemistry courses (44). A paper in the *Journal of Chemical Education* is pushing the idea that any approach to augmenting the VSEPR model is going to need to include some amount of computational chemistry, in part because of the ease of access to it with software available for free and the remarkable accuracy afforded by even the simplest computational models (45).

B. Computational Chemistry

1. The Basics of Computational Chemistry

Modern computational chemistry is partly founded on the use of a Density Functional Theory (DFT) quantum mechanical modeling algorithm to investigate the electronic structure of molecules. This can be done reasonably well using modern computers for small systems. For larger systems, more and more powerful computers are needed to run a simulation in a reasonable amount of time (46).

A DFT calculation is based on using the Schrödinger equation to model a system directly by modeling only one electron at a time, slowly modeling an entire system in this manner. The mathematics of the Schrödinger equation is outside the scope of this text and will not be discussed at any appreciable level. What is important is that, at the quantum level (*i.e.*, subatomic level), the Schrödinger equation can be used to describe the behavior of a quantum system as a wave function. Whereas Newton's second law is the ultimate descriptor of the behavior of any physical system, the Schrödinger equation is the ultimate descriptor

for a quantum mechanical system. The Schrödinger equation can be used to model things above the subatomic level as well (*e.g.*, atoms and molecules), but this is an incredibly complex task that requires a great deal of computational power as more nucleons and electrons are added to a system being modeled (**46**).

Another popular fundamental approach in computational chemistry is based on using known empirical parameters of the atoms and bonds in a system to model it. By varying parameters in the system in some predefined way, a computational chemistry method can optimize the geometry of a system over a series of steps. Many other things can be accomplished from this approach, but the most crucial part is that these optimizations are intended to reveal properties of the system(s) being studied, such as structure (*e.g.*, in protein modeling) (**46**).

These algorithms are commonly referred to as forcefields and include empirical parameters relating to the atoms and bonds found in the structures being modeled. Many forcefields, such as the Amber forcefield, are intended for studying large biomolecules, while others are intended for simulating smaller molecules. The use of a forcefield to model a system over a period of time is referred to as a molecular dynamics simulation. Using DFT or an equation based empirical parameters, the energy of a given system (*e.g.*, a molecule) can be calculated after each optimization step, allowing for the program to gauge the effectiveness of the changes, and continue optimizing it toward a lower energy state. Given enough optimization steps, this can eventually result in the program arriving at a reasonable facsimile of the true structure of a compound in the conditions specified by the forcefield's parameters (**46,47**).

2. Uses of Computational Chemistry in Research and Industry

Computational chemistry is a very widely applicable field of chemistry and can be used in a great variety of situations. The examples given in this section are not intended to be exhaustive. Two of the more prominent uses for computational modeling include protein structure elucidation and drug discovery.

For protein structure elucidation, it is necessary to note that some proteins are difficult to isolate as crystals suitable for analysis by x-ray crystallography (XRC). This can be because the protein is simply hard to isolate with acceptable purity or because the protein is naturally embedded in a membrane or other location that makes an XRC experiment not representative of the actual structure of the protein *in vitro*. In these situations, it might be preferable to attempt to model the protein *in silico* and determine a reasonable facsimile of its structure based on computational simulation of the chain of amino acids that make up the protein. In some cases, nuclear magnetic resonance spectroscopy is a useful tool for determining solution structures of proteins and is often combined with computational modeling. Likewise, protein structures obtained by XRC can be simulated under the solution conditions the protein would experience *in vitro*, which can give more insight into its behaviors in solution (48).

Drug discovery is one of the central thrusts of contemporary computational chemistry research (49). For drug discovery, a previously determined protein structure is used along with a molecular dynamics simulation. The protein in question is one of therapeutic interest. By feeding a database of small organic molecules into the program, one can perform so-called docking simulations to determine which of the small molecules might be candidates for pharmaceuticals that would interact with the active site of a protein. Using this method,

researchers can test many molecules against a protein without having to run physical experiments with the compounds and the protein in question. This type of method can test millions of different compounds in a matter of days or weeks. By running these simulations, computational chemists can save experimental chemists in labs a significant amount of time by telling them which small molecules among those tested are most likely to be good drug candidates (50).

3. Computational Chemistry in the Classroom

In the last decade, many educators have published examples of exercises developed for the laboratory setting that utilize computational chemistry. In this section, a survey of several of these articles is presented.

In 2015, a group from the Imperial College in London, UK, published an article wherein they describe a laboratory experiment for upper-level organic chemistry students. In this experiment, students are introduced to computational modeling of organic structures and given a background on how a semi-empirical quantum mechanical approach can be used to calculate NMR, IR, and optical properties of a molecule. Afterward, the students complete an experimental laboratory in which they synthesize a chiral epoxide compound in one of two methods offered to them. Next, using the “quantum mechanical toolbox” given to them in the earlier portion of the lab, which includes the Gaussian 09 program, they must establish which of the absolute stereochemical configurations of their epoxide they synthesized. The students accomplished this by using Gaussian 09 to predict properties of the different products that could have been formed and determining which one matches their empirically observed properties of the compound they formed (51).

In 2016, O'Brien published an article describing a method of using 3-dimensional (3D) models as a tool to help students visualize reaction pathways. The method in the article is intended for use in upper-division undergraduate classes. Acknowledging that stereochemistry is difficult for many students to grasp, the author goes on to make a case for using 3D models, either virtual or physical, to help students visualize stereochemistry. Utilizing both virtual and physical models, O'Brien describes a method by which he was able to make detailed videos depicting stereospecific reaction pathways by chaining together images of virtually modeled structures and annotating them using virtual transparency programs. Reactions he utilized this methodology for include the Diels-Alder cycloaddition, Zimmerman-Traxler transition states, and stereoselective reductions (52).

In early 2019, another group of researchers from the University of California at Davis published an article about computer-aided drug design exercises meant for upper-division undergraduates. In this article, several experiments are described, ranging from merely viewing a protein-ligand complex up to the complex task of performing automated docking of drug candidates with a protein of interest to examine potential drug candidates. This course was the second one in a sequence about pharmaceutical chemistry, and these laboratory exercises are modularized, meant to be run once weekly in 3-hour laboratory periods. The authors reported that student feedback indicated that students grew in their appreciation for the roles of chemists in the drug discovery process (53).

Another 2019 article published by a group from the State University of New York at Buffalo describes an experiment using computational methods to model 2-dimensional (2D) materials intended for upper-division undergraduates. The experiment used the Avogadro program, which will be discussed in more detail later, for molecular editing and the WebMO

interface for the computational work. The experiment used computational simulations to show how the properties of 2D materials can be finely manipulated by varying chemical structures (54).

Finally, in 2020, another group published an article about a computer-aided drug-design activity intended for second-year undergraduates in organic chemistry courses. Their publication of an activity for this group is in response to a lack of computational chemistry exercises for second-year students in the literature. The authors detail a weeks-long, research-like exercise for second-semester organic chemistry students, where the students use freely-available web sources to evaluate a protein (acetylcholinesterase). The students were educated on the background and function of the protein and introduced to the idea of inhibitors. Next, in small groups, they proceed with the project, working on docking a known inhibitor to familiarize themselves with which protein residues interact with the inhibitor. From there, the groups design a novel ligand by using docking simulations and then evaluate their new ligand with other studies. This activity is also intended as a gateway to perhaps interest students in undergraduate research (49).

4. The Avogadro Software

As mentioned earlier, the Avogadro software package is a freely-available program available for download on the internet. It is named after Amadeo Avogadro, the famed originator of the Avogadro Law and a widely acknowledged founder of modern atomic molecular theory, for whom the Avogadro constant, N_A , was also named. The software allows users to build and manipulate chemical structures freely, as well as providing simple forcefields suitable for the optimization of structures. The software's user interface makes it

remarkably easy to use, it gives users a simple way to visualize chemical structures, and it is also extensible for use with many non-free programs, such as Gaussian. It was intended not only for molecular modeling research but also for educational use (55).

C. Goals

It is hypothesized that the computational chemistry exercise previously in place in the CHEM-1120 laboratory curriculum at Tennessee Technological University can be improved by changing from the Hyperchem software platform previously used to conduct the exercise and instead using the Avogadro software due to its superior interface. From this change, we seek to answer the question of whether a computational chemistry exercise can be an effective method of reviewing VSEPR model concepts while at the same time facilitating a simple introduction of computational chemistry and a fundamental organic chemistry concept, functional groups. To support this effort, the author assisted the laboratory coordinator in laying the framework for an exercise suitable for students and has conducted several methods of analysis of the newly developed “Avogadro exercise.” The laboratory coordinator developed the “pre-lab” material for the exercise, including the background information about computational chemistry, organic functional groups, and the VSEPR concepts review.

The goals of this thesis are to implement this new Avogadro exercise, to evaluate student performance and outcomes qualitatively and quantitatively, and finally to publish this material for the scientific community at large.

CHAPTER 6:

METHODS

A. The Avogadro Exercise

The CHEM-1120 course is split into two distinct portions: the lecture and laboratory. The lecture is intended to be the students' primary source of chemistry knowledge, and the laboratory curriculum is intended to augment and reinforce the lecture material. The Avogadro Exercise has been implemented as a laboratory exercise for students to do outside of the classroom during their first week of labs, where they traditionally do not have an in-lab activity.

This research studied the results of introducing a new out-of-class exercise utilizing the Avogadro software. The Avogadro Exercise was designed to introduce students to organic chemistry functional groups, computationally modeling structures, and also to review VSEPR concepts. Students were introduced to the exercise with a section about computational chemistry and its uses in research and industry, a section reviewing VSEPR, and a section introducing the various organic functional groups. They were provided with a written tutorial and a video tutorial on how to use the Avogadro software, as well as another written tutorial instructing them how to install the software on their personal computer if they wished. The text of the Avogadro Exercise can be found in Appendix D.

In the worksheet portion of the exercise, students were asked to use the VSEPR theory to predict electron domain geometry (EDG), molecular geometry (MG), and the hybridization for several organic molecules. The students were then asked to use Avogadro to construct a set of molecules and measure their bond lengths and angles pre-optimization

using the measurement tool in the software. They report these measurements on the worksheet. Finally, they were to optimize the molecule using Avogadro's built-in geometry optimization procedure and record the new bond lengths and angles post-optimization.

The students use the default forcefield parameters in Avogadro, which utilizes the MMFF94 forcefield for optimization. The optimization is limited to 500 steps and uses the Steepest Descent algorithm with a convergence limit of 10^{-7} kJ/mol. For each step of the optimization, the algorithm calculates the energy difference after changing the bond lengths and angles of the molecule slightly. It continues the optimization until either the energy difference is 10^{-7} (or less) or until it reaches 500 steps.

The written and video Avogadro tutorials showed students how to do these operations with a simple model system. After that, students were asked to use their knowledge of VSEPR theory to predict the EDG, MG, and the hybridization of the nitrogen atom in formamide (CH_3NO). They then constructed and optimized formamide in Avogadro as they did in the previous section and reported its pre- and post-optimization parameters. Students were then asked if the observed structure from Avogadro matched their predictions and to defend their answers.

The last question was meant to see if students were paying attention to the bond geometries they predicted and the angles that Avogadro calculated. The correct molecular geometry for the nitrogen in formamide is trigonal planar. However, many students will predict a tetrahedral EDG and trigonal pyramidal MG, as they are unaware of the resonance effect that causes partial-double bond character around amide nitrogen atoms. If students responded with the appropriate response based on their original prediction, they were awarded points. For example, a student predicts the compound to have a tetrahedral EDG and

trigonal pyramidal MDG, but Avogadro returned a bond angle inconsistent with that prediction. If that student recognized that their prediction did not match and offered a reasonable explanation for why that could be (*e.g.*, Avogadro was wrong or the nitrogen being near the carbonyl affects the system in an unexpected way or that a process they did not understand might be occurring), they would be given full points for that question.

B. Data Collection

The data collection methods utilizing data from human subjects described in this chapter were reviewed by the Tennessee Technological University (TTU) Institutional Review Board (IRB) before their implementation. The TTU IRB authorized these procedures as IRB #2170.

Several methods were used to collect data about the efficacy of the exercise as a VSEPR review, including collecting student data from the completed worksheets, administering of student surveys, pre- and post-quizzes, and collecting aggregate data from final exams. Each method is described in further detail throughout the following sections.

1. Secondary Worksheet Data

As previously reported in section A of this chapter, in their worksheet submissions, students were asked to record pre- and post-optimization data for the molecules they modeled in Avogadro. This data was recorded during grading by the laboratory teaching assistants and provided to the laboratory coordinator in the form of an Excel spreadsheet as totally anonymized data. The data was collected by the molecule modeled. This data was collected

to determine if the default settings on Avogadro were sufficient to produce reasonable geometries compared to what the VSEPR model predicts.

2. Pre-Quizzes and Post-Quizzes

In the first week of the laboratory curriculum, second-semester general chemistry students were given a pre-quiz to gauge their understanding of VSEPR concepts. On this pre-quiz, students were assigned a non-traceable code on their pre-test to maintain anonymity, which they were instructed to remember by any means necessary (*e.g.*, writing it down in their notebook). This code was then used to identify which students were taking the post-test so that the efficacy of the exercise in teaching the VSEPR and functional group content could be evaluated. The code was later used to identify whether students consented for researchers to use the results of their quizzes in the study.

The post-quiz was given the next week when students turned in their Avogadro Exercises. The quizzes both tested the students over similar material. On the pre-quiz, students were asked a series of questions regarding the hybridization, molecular geometry, and the bond angles found in methanol and formaldehyde. In the post-quiz, students were asked the same questions regarding dimethyl ether and acetonitrile. The purpose was to determine if the students performed better on the post-quiz, in particular the first question set, as methanol and dimethyl ether are very similar in their geometry for the questions being asked. Students only had their quiz results included in the research if they consented by providing their test code in the surveys described in the following section.

The pre- and post-quizzes are provided in Appendix E and Appendix F, respectively.

3. Student Survey

Later in the semester, after they had completed the Avogadro Exercise, students were asked via email from the lab coordinator on behalf of the author to participate in an anonymous survey regarding the Avogadro Exercise. The students were surveyed electronically using the Qualtrics software. They were first informed of what the information they would be providing would be used for and then asked for their consent to be surveyed. If they consented, they were asked to provide their pre- and post-quiz code if they agreed to let the researchers use the results. If a student did not consent during the survey or did not respond, their papers were not scored and will be destroyed at the end of two years.

The remainder of the survey asked students to share their thoughts regarding the Avogadro Exercise by responding to a series of student-satisfaction questions and rating their experience. They were also allowed to leave any additional comments they may have had. The full content of the survey is provided in Appendix G.

4. Final Exam Aggregate Data

For internal evaluation purposes, the CHEM-1120 lecture faculty retain aggregate data regarding student answers on the final exams; in essence, how many students marked which answer choice for each question. Using aggregate data from Fall 2017 and Fall 2019, the author has performed a time-based comparison of the number of students correctly answering relevant questions on the final exam relating to the Avogadro Exercise content. These questions relate to VSEPR and hybridization. The questions do not change year to year; thus, using this data, the authors believe they can demonstrate the educational utility of

the exercise. Due to confidentiality concerns, the text of these questions is not able to be included in this thesis.

The collection of this data was left to the faculty supervisor, who anonymized it and used Excel to categorize the responses from students into ranked data from best to worst answer. An analysis of variance (ANOVA) test was run on the data from the two semesters in question using the Data Analysis Pack in Microsoft Excel. The ANOVA test is similar to the student's t-test; it compares the means of two sets of data using the F-distribution. In contrast to the student's t-test, ANOVA works with unequal sample sizes. The null hypothesis is that the two means are equal; the alternate hypothesis is that the two means are not equal. If an ANOVA test gives significant results ($p < 0.05$), the null hypothesis is rejected, and the alternate hypothesis is accepted (42).

There were plans to use data from the May 2020 final exams, but due to the CoViD-19 pandemic causing a drastic shift in classroom delivery methods, it is believed that this data would be invalid. Therefore, the researchers have chosen not to use that data.

CHAPTER 7: RESULTS

All numerical data in this study was processed using Microsoft Excel.

A. Secondary Worksheet Data

Average post-optimization values reported by the students for each molecule is found in **Table 7.9** and includes a listing of the expected bond angles. Also included in the table is the standard deviation of each average bond angle and the number of students' responses included in the average. The emphasis of this analysis is on the bond angles given by the students because VSEPR has no bearing on bond lengths. Thus, no predicted bond lengths are given. In **Figure 7.30**, some of the molecules that students had the option to model are shown, along with an indication of each bond angle examined by the students. Students had others they could model in this way; refer to Appendix D for the other structures. Any outliers detected using the Grubbs' test (95% confidence level) were excluded (42).

Table 7.9. A listing of the average bond angles simulated by students. The approximate expected bond angles are those predicted using the VSEPR theory and consider only the central atom's hybridization (44).

Molecule	Count	Average Optimized Bond Angle (°)	Approximate Expected Bond Angle (°)	Average Bond Length (Å)
Butanone	15	108.1 ± 30.6	120	1.4 ± 0.3
Acetone	15	120.5 ± 1.2	120	1.6 ± 0.6
Acetaldehyde	16	121.4 ± 2.8	120	1.2 ± 0.1
Propanal	10	117.7 ± 6.4	120	1.2 ± 0.1
Tetrahydrofuran	5	108.7 ± 1.0	109.5	1.4 ± 0.0
Diethyl ether	12	111.4 ± 1.3	109.5	1.4 ± 0.0
Allyl alcohol	7	108.7 ± 2.2	109.5	1.3 ± 0.2
Propargyl alcohol	20	110.2 ± 1.3	109.5	1.4 ± 0.4
<i>trans</i> -2-Butene	8	116.2 ± 0.1	120	1.8 ± 0.7
1-Butene	36	102.6 ± 34.1	120	1.2 ± 0.2
Formamide	51	108.2 ± 29.0	120	1.4 ± 0.1

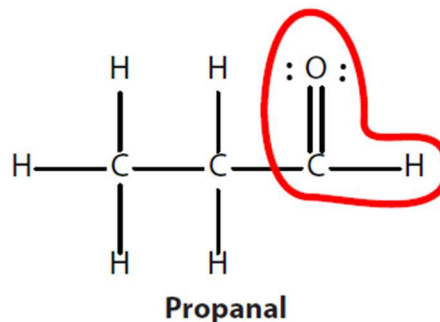
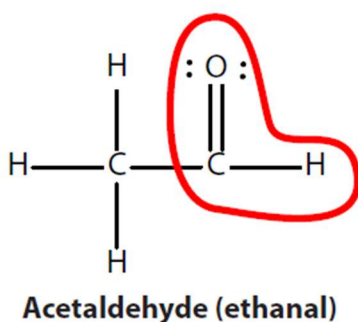
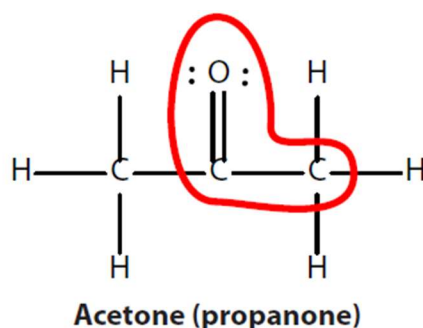
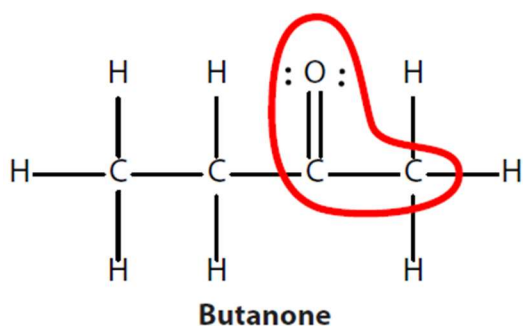


Figure 7.30. The first set of molecules that students have a choice to model. For only one of these, students modeled the structure in Avogadro and used the measurement tool to measure the C=O bond length and the bond angle between the three circled atoms, both pre- and post-optimization.

B. Pre-Quizzes and Post-Quizzes

A total of seven students gave the author permission to use their pre- and post-quiz data. The pre-quiz responses are shown in **Table 7.10** and the post-quiz responses in **Table 7.11**. The two quizzes were different but covered similar concepts in a similar order. Questions 1 and 4 on each quiz were related to hybridization. Questions 2, 3, 5, and 6 on each quiz are related to molecular geometry. The pre- and post-quizzes can be found in Appendix E and Appendix F, respectively.

Table 7.10. The results from the pre-quiz. N = 7.

Question	Q1	Q2	Q3	Q4	Q5	Q6	Average Score
Success Rate	0%	43%	0%	43%	57%	43%	31%

Table 7.11. The results from the post-quiz. N = 7.

Question	Q1	Q2	Q3	Q4	Q5	Q6	Average Score
Success Rate	86%	43%	0%	71%	71%	86%	60%

C. Student Survey

A total of 13 students responded to the survey. The survey asked students several questions about their experience with the Avogadro Exercise and allowed them to respond with their own comments. A listing of individual student comments is given in **Table 7.12**. Students were asked to indicate their level of agreement with several statements. These statements and student responses are displayed in **Figure 7.31**.

Table 7.12. Student responses from the free-response section of the survey. Responses are given verbatim.

Response #	Student Response
1	This exercise was sweet! It introduced concepts related to bond angles, geometry, and functional groups in a simple and logical manner. The computer building portion was also very user-friendly.
2	The software was a little tricky to understand. I had a lot of trial and error before I understood how to answer the questions.
3	The system itself was hard to work with on the computer
4	I seen as work that just need to be done and less of a learning opportunity
5	I think this would be a great review for future students.

STUDENT SURVEY RESULTS

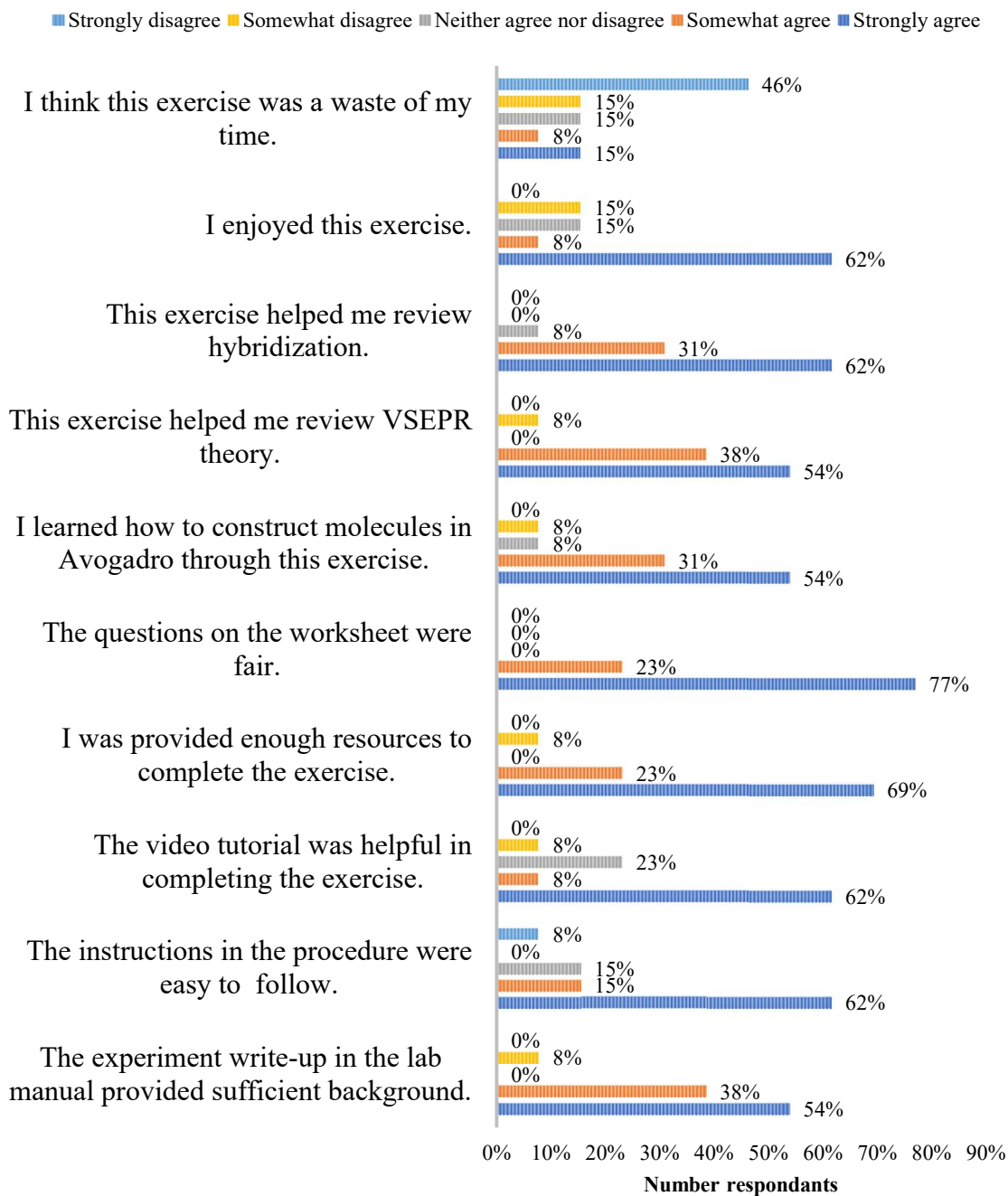


Figure 7.31. The results of the Fall 2019 student survey (N = 13).

D. Final Exam Aggregate Data

Data was collected from two questions on the lecture final exams for two semesters, Fall 2017 and Fall 2019. Both semesters had the same instructor and the same laboratory curriculum except for the addition of the Avogadro Exercise in 2019. Two multiple-choice final exam questions were studied from this test. Question 1 tested students on their knowledge of VSEPR, and Question 2 tested students on their knowledge of hybridization. For this study, the responses were ranked from best to worst in terms of learning achievement by the lecture instructor, with 1 being the worst answer and 5 being the correct/best answer. The lecture instructor is a faculty member with seven years of experience teaching general chemistry at the collegiate level. A Shapiro-Wilk test for normality gave negative results for all datasets, meaning the data was not normally distributed.

An analysis of variance (ANOVA) test was run on the data sets from the two semesters in question using the Data Analysis Pack in Microsoft Excel. Data from Question 1 is presented in **Figure 7.32** and data from Question 2 in **Figure 7.33**.

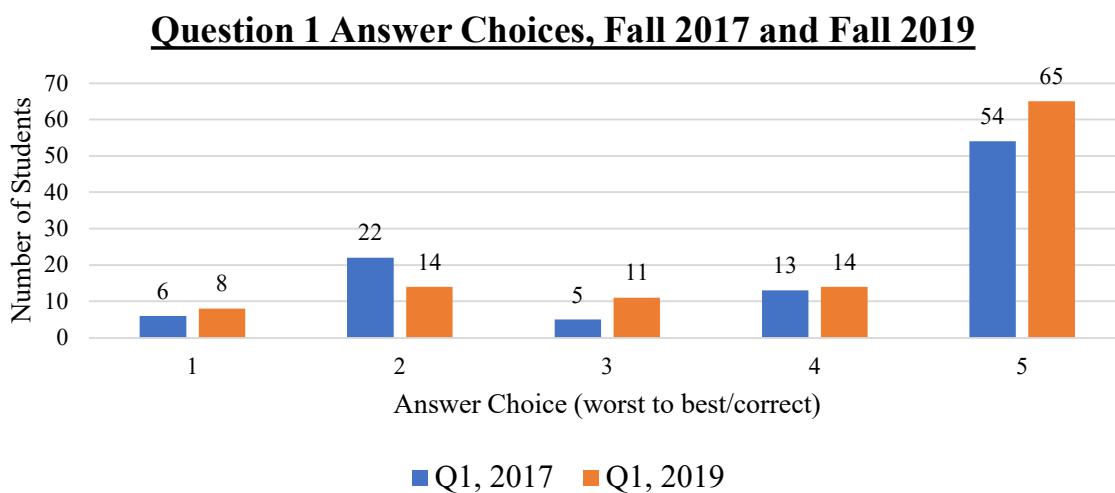


Figure 7.32. A bar chart representing student answers for the VSEPR question. In Fall 2017, N = 100 and in 2019, N = 110.

Question 2 Answers, Fall 2017 and Fall 2019

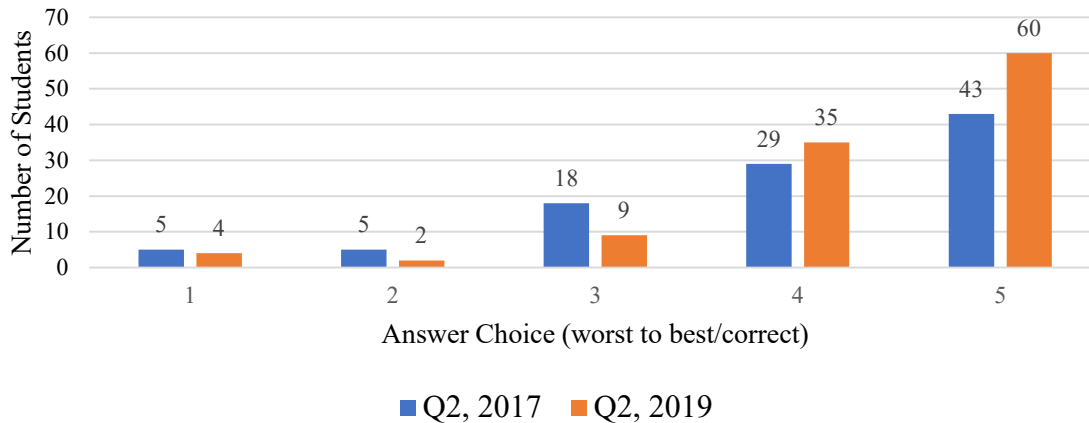


Figure 7.33. A bar chart representing student answers for the hybridization question. In Fall 2017, N = 100 and in 2019, N = 110.

The results of the ANOVA test between Fall 2017 and Fall 2019 for Question 1 are presented in **Table 7.13**. The results of the ANOVA test between Fall 2017 and Fall 2019 for Question 2 are presented in **Table 7.14**. According to the ANOVA test, the two datasets of Question 1 ($p = 0.442$) were not statistically different at the 95% confidence level ($\alpha = 0.05$), but the results of the Question 2 ANOVA test ($p = 0.0289$) reveal that there is a significant difference between the two datasets at the 95% confidence level (**42**). In **Table 7.15**, further information on Question 1 and Question 2 datasets is given. Overall, the scores on question 2 in Fall 2019 were higher than those in Fall 2017, indicating there was a factor affecting Fall 2019 or Fall 2017 significantly.

Table 7.13. ANOVA test results from Question 1 (VSEPR) datasets.

ANOVA – Q1F17 vs. Q1F19						
<i>Source of Variation</i>	<i>SS</i>	<i>df</i>	<i>MS</i>	<i>F</i>	<i>P-value</i>	<i>F crit</i>
Between Groups	1.15017316	1	1.150173	0.593235	0.442045	3.886555
Within Groups	403.2736364	208	1.938816			
Total	404.424	209				

Table 7.14. ANOVA test results from Question 2 (hybridization) datasets.

ANOVA – Q2F17 vs. Q2F19						
<i>Source of Variation</i>	<i>SS</i>	<i>df</i>	<i>MS</i>	<i>F</i>	<i>P-value</i>	<i>F crit</i>
Between Groups	5.303	1	5.303	4.840	0.0289	3.887
Within Groups	227.864	208	1.095			
Total	233.167	209				

Table 7.15. Descriptive statistics of the two datasets.

Question	Fall 2017 Question 1	Fall 2019 Question 1	Fall 2017 Question 2	Fall 2019 Question 2
Number Students	100	110	100	110
Mean Response	4.0	4.3	3.9	4.0
Standard Deviation	1.1	0.9	1.41	1.36
Median Response	4	5	5	5
Mode	5	5	5	5
Correct Responses (%)	54	43	54	59

CHAPTER 8:

DISCUSSION

A. The Performance of the Avogadro Software

As seen in Chapter 7, section A, **Table 7.9**, students often achieved nearly optimum bond angles in the molecules they modeled. However, some molecules in the exercise gave large standard deviations. This includes 1-butene and formamide. Given the large numbers of students choosing to attempt these, it is reasonable to assume that many of them may have followed the procedure incorrectly or otherwise drawn the molecule so poorly in the first place that the program could not compensate in the short optimization period. It is worth considering an addition to the instructions that students should edit their forcefield parameters to utilize greater computational power.

As mentioned in Chapter 6, the students use the default forcefield parameters in Avogadro. In many cases, it is reasonable to assume students are likely reaching the 500 step limits because their structures are not drawn in a manner that gives the program a good starting point, resulting in the outlier and mediocre bond angles observed.

It appears that smaller molecules are easier for Avogadro to optimize using the default parameters. This includes acetaldehyde, acetone, allyl alcohol, diethyl ether, propanal, propargyl alcohol, tetrahydrofuran, and *trans*-2-butene, whose average bond angles were close to the optimal bond angles, and all had low standard deviations (less than 5°).

According to the Avogadro software website, the default MMFF94 forcefield is suitable for organic-type molecules (55). Instead of discarding any of the molecules in use now, it may be prudent to have students edit the forcefield parameters. According to the literature, the optimum algorithm for this activity would be Conjugate Gradients instead of

Steepest Descent, both of which are options in Avogadro. The Conjugate Gradients algorithm utilizes an algorithm that attempts to find all energy minima of the molecule being optimized in order to detect the lowest energy configuration. The Steepest Descent algorithm merely follows the first energy minima it finds, limiting it based on the starting configuration of the molecule (56). Thus, swapping to the Conjugate Gradients algorithm and adding additional optimization steps (e.g., 1000 or 2000) may allow for students to get more consistent values in their optimizations and expose them to another computational chemistry concept.

B. Student Satisfaction and Learning Outcomes

The results from the various data collected in all this study are compelling. Of the seven students that gave the author permission to use their pre- and post-quiz scores, there was an improvement on all questions except question 3. However, the sample size is quite small, and these quizzes were not the same material, so these results are more of a qualitative test.

The student satisfaction survey results (**Figure 7.31**) indicated that the 13 students surveyed mostly found the exercise to be a useful expenditure of their time, enjoyed it, and found it to be a useful review of VSEPR theory and hybridization. Students overwhelmingly found the worksheet questions to be fair and felt they were provided adequate resources to complete the exercise. The majority of them also found the tutorial helpful and the procedure easy to follow, and 12 of them agreed with the statement that the experiment write-up provided sufficient background.

For the student free-response comments (**Table 7.12**), two of the five indicated that they had a positive experience with the exercise. Two of the others found the exercise

difficult and commented they had trouble with the Avogadro software. Finally, one student felt negatively about the exercise, commenting that it was "...work that just need [sic] to be done and less of a learning opportunity."

Most of these responses were in keeping with the objective of the Avogadro Exercise. The objective was to deliver a review exercise that introduced second-semester students to new concepts, such as computational chemistry and organic functional groups, while at the same time serving as a review of first-semester concepts, including Lewis structures, VSEPR theory, and hybridization. The exercise is intended to be relatively easy and serves as a gentle introduction to the new concepts. If students do the work and ask questions of their instructors via email, it is believed that most of them will receive high scores. The author and faculty coordinator believe that this approach to the exercise is optimal. Instead of introducing students to a paid, complicated software, such as Hyperchem, that they have to figure out on their own, the students are given access to an easy-to-learn, free-to-use software in order to complete a series of relatively simple tasks.

Finally, student learning outcomes must be assessed. As mentioned in Chapter 7, two questions on Final Exams were analyzed. Question 1 had to do with VSEPR theory, and Question 2 had to do with hybridization. After ANOVA analysis, it was found there was no significant difference between the average student performance in the Fall 2017 and Fall 2019 semesters with regards to Question 1 (**Figure 7.32** and **Table 7.13**). However, a comparison of the Fall 2017 and Fall 2019 responses to Question 2 (**Figure 7.33** and **Table 7.14**) showed a statistically significant difference in performance between the two semesters. The students in Fall 2019 performed better than the students in Fall 2017 on the VSEPR question.

The central limit theorem supports the idea that these two classes are comparable. Both have relatively large samples ($n \leq 100$), and both had the same instructor and lab curriculum, aside from the addition of the Avogadro Exercise in 2019. However, this cannot be attributed solely to the introduction of the Avogadro Exercise and the students' increased performance on Question 2. It could also be that the instructor was particularly adept at teaching these students hybridization or that the students were otherwise pre-dispositioned to perform better on hybridization. Despite this, it is reasonable to assume that even if the Avogadro Exercise was not the only influential factor in this observed difference, it almost certainly contributed to overall student success with the concept.

CHAPTER 9: CONCLUSION

The introduction of the new Avogadro Exercise has been a success. Responses from the student survey give high confidence that the exercise is serving adequately as a gentle introduction for students to computational chemistry and organic functional groups while also serving as a relatively easy review of VSEPR theory and hybridization. Some updates may be necessary for the exercise in the future. Additionally, one aspect not analyzed is whether students that went on to take organic chemistry found their experiences with the Avogadro Exercise to have been useful in preparing them to learn about organic functional groups.

An important point with this exercise is that it fills an apparent gap that introductory chemistry students face in computational chemistry concepts. Similar to Acuna *et al.*, the author has observed a distinct lack of any computational chemistry integration in curricula for lower-division undergraduates (49). Indeed, the author has failed to observe anything intended for first-year undergraduates. The Avogadro Exercise is intended to fill this gap. As efforts continue towards publishing this research in a peer-reviewed journal, the author intends to encourage other educators to develop computational chemistry exercises for freshman-level undergraduates and increase the recognition of this critical area of modern chemistry.

A. Future Work

The Avogadro Exercise may need to have the students make changes to the forcefield parameters to ensure they consistently achieve optimum bond angles. This includes changing

the algorithm to Conjugate Gradients and increasing the number of optimization steps to 1000. In addition, future efforts to improve the exercise might involve the development of new sets of molecules for the students to model. Finally, future researchers may consider giving a pre- and post-test for the Avogadro Exercise that tests students over more concepts and the same material on the pre- and post-tests.

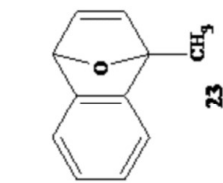
APPENDIX A: ¹H NMR DATA

Spectra taken in CDCl₃ with TMS were corrected (if needed) to have the TMS signal appear at exactly $\delta = 0.00$ ppm. For spectra taken without TMS, referencing was done with the residual chloroform peak being corrected to $\delta = 7.26$ ppm for ¹H spectra (**29**). The NMR spectra were processed using the Mestrelabs Mnova software. In processing, each spectrum had the default automatic phase correction performed, followed by automatic baseline correction using the Whittaker smoother algorithm.

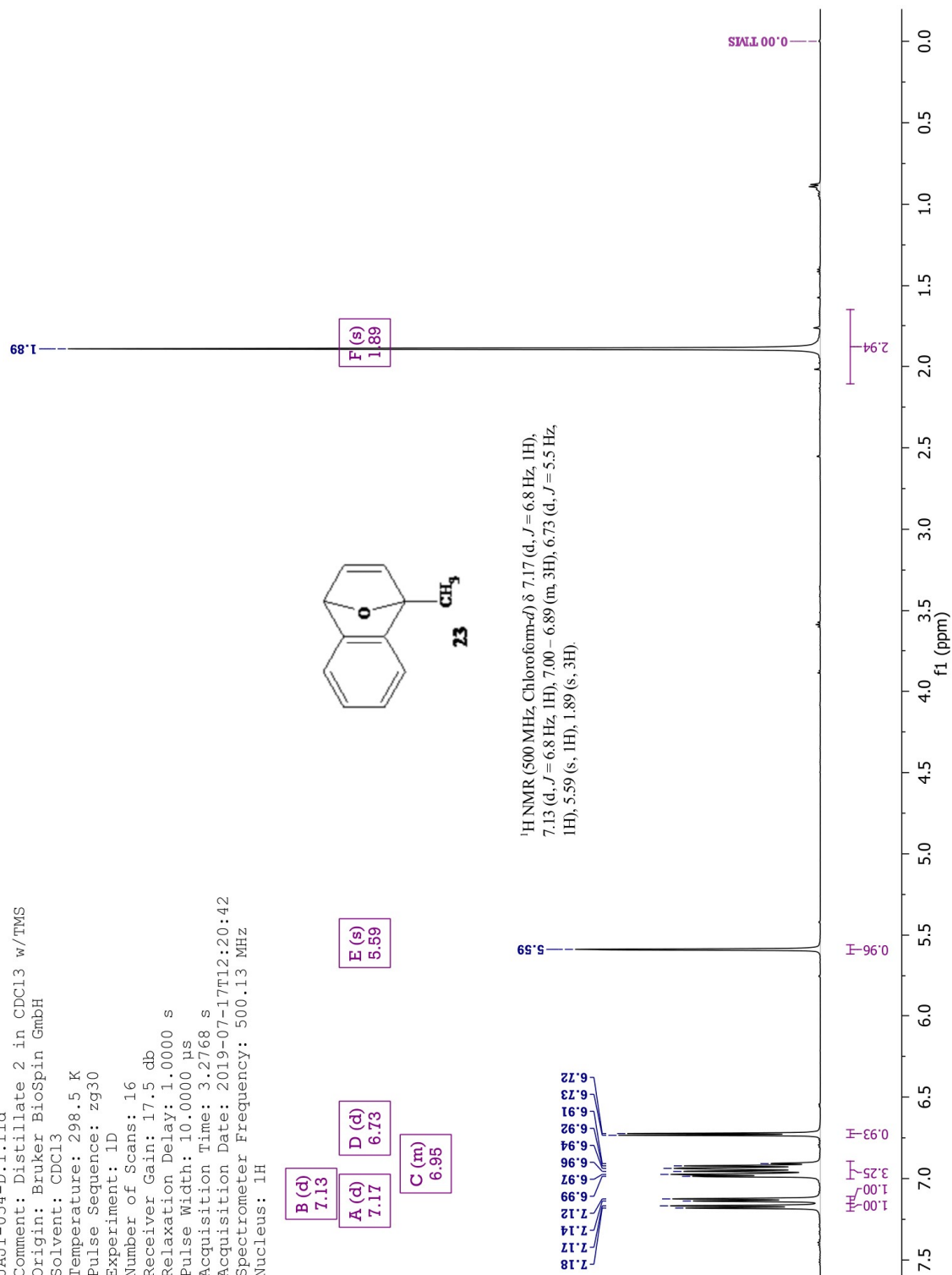
List of ¹H Spectra in Appendix A

Page 105	1-Methyl-1,4-dihydro-1,4-epoxynaphthalene – JAJ1-54-D
Page 106	4-Methyl-1-naphthol – JAJ2-39-A
Page 107	4-Methoxynaphth-1-yl Benzoate – JAJ2-01-A
Page 108	4-Chloronaphth-1-yl Benzoate – JAJ1-19-A
Page 109	4-Nitronaphth-1-yl Benzoate – JAJ2-13-A
Page 110	4-Bromonaphth-1-yl Benzoate – JAJ2-35-B
Page 111	4-Methylnaphth-1-yl Benzoate – JAJ2-56-A
Page 112	4-Nitronaphth-1-yl p-Toluate – JAJ2-57-A
Page 113	2-Benzoyl-4-chloro-1-naphthol – JAJ2-19-A
Page 114	2-Benzoyl-4-methoxy-1-naphthol – JAJ2-53-B
Page 115	2-Benzoyl-4-nitro-1-naphthol – JAJ2-54-B
Page 116	2-Benzoyl-4-bromo-1-naphthol – JAJ2-58-A
Page 117	2-Benzoyl-4-methyl-1-naphthol – JAJ2-59-A
Page 118	2-(p-Toluoyl)-4-nitro-1-naphthol – JAJ2-60-A

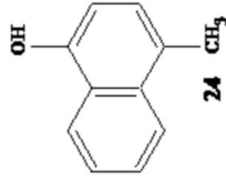
JAJ1-054-D-1.1.fid
 Comment: Distillate 2 in CDCl3 w/TMS
 Origin: Bruker Biospin GmbH
 Solvent: CDCl3
 Temperature: 298.5 K
 Pulse Sequence: zg30
 Experiment: 1D
 Number of Scans: 16
 Receiver Gain: 17.5 db
 Relaxation Delay: 1.0000 s
 Pulse Width: 10.0000 μ s
 Acquisition Time: 3.2768 s
 Acquisition Date: 2019-07-17T12:20:42
 Spectrometer Frequency: 500.13 MHz
 Nucleus: 1H



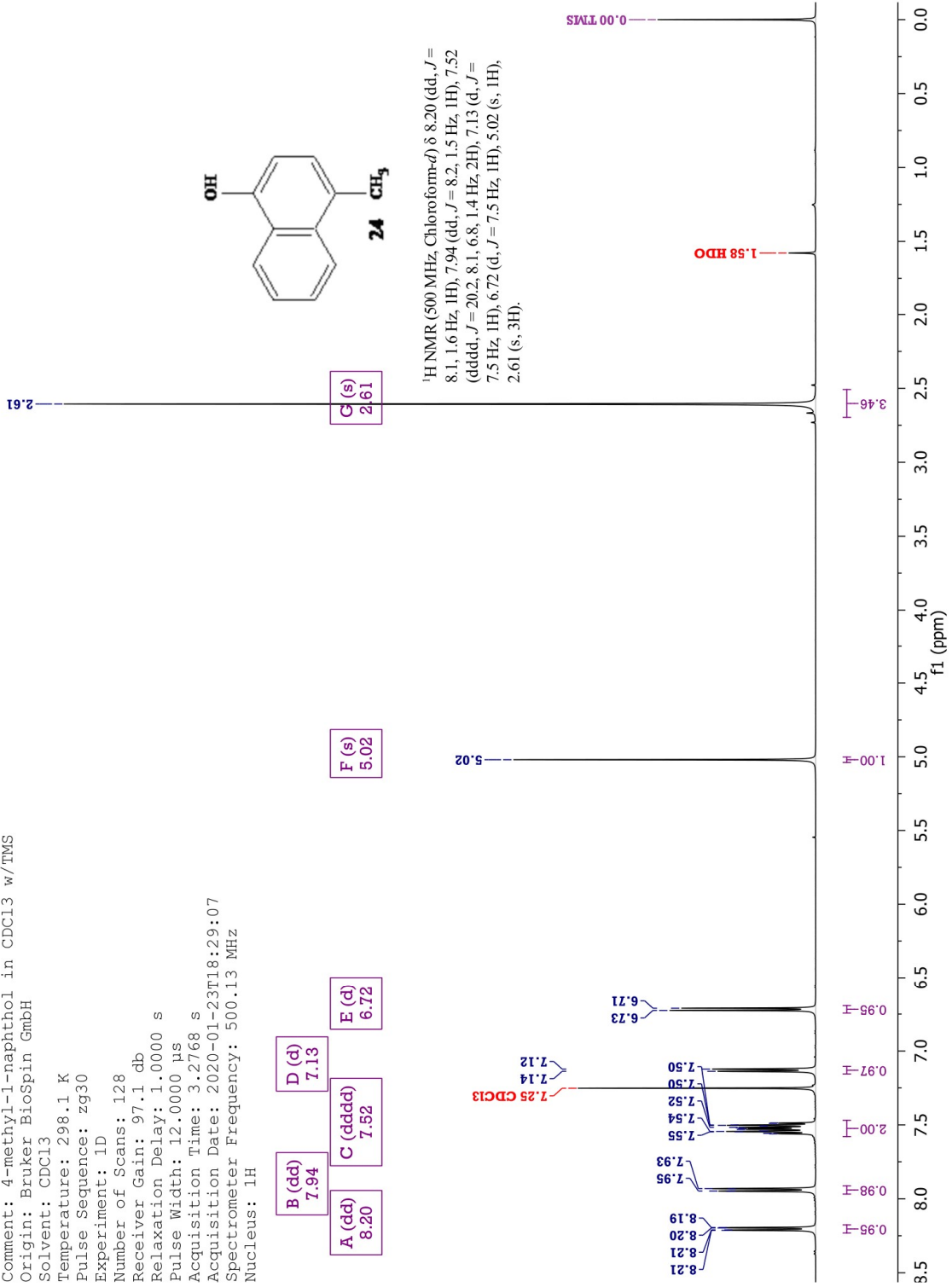
¹H NMR (500 MHz, Chloroform-*d*) δ 7.17 (d, *J* = 6.8 Hz, 1H),
 7.13 (d, *J* = 6.8 Hz, 1H), 7.00 – 6.89 (m, 3H), 6.73 (d, *J* = 5.5 Hz,
 1H), 5.59 (s, 1H), 1.89 (s, 3H).



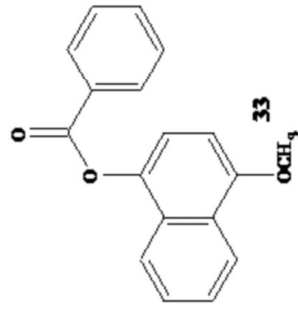
JAJ2-39-A.4.fid
 Comment: 4-methyl-1-naphthol in CDCl3 w/TMS
 Origin: Bruker BioSpin GmbH
 Solvent: CDCl3
 Temperature: 298.1 K
 Pulse Sequence: zg30
 Experiment: 1D
 Number of Scans: 128
 Receiver Gain: 97.1 db
 Relaxation Delay: 1.0000 s
 Pulse Width: 12.0000 μ s
 Acquisition Time: 3.2768 s
 Acquisition Date: 2020-01-23T18:29:07
 Spectrometer Frequency: 500.13 MHz
 Nucleus: 1H



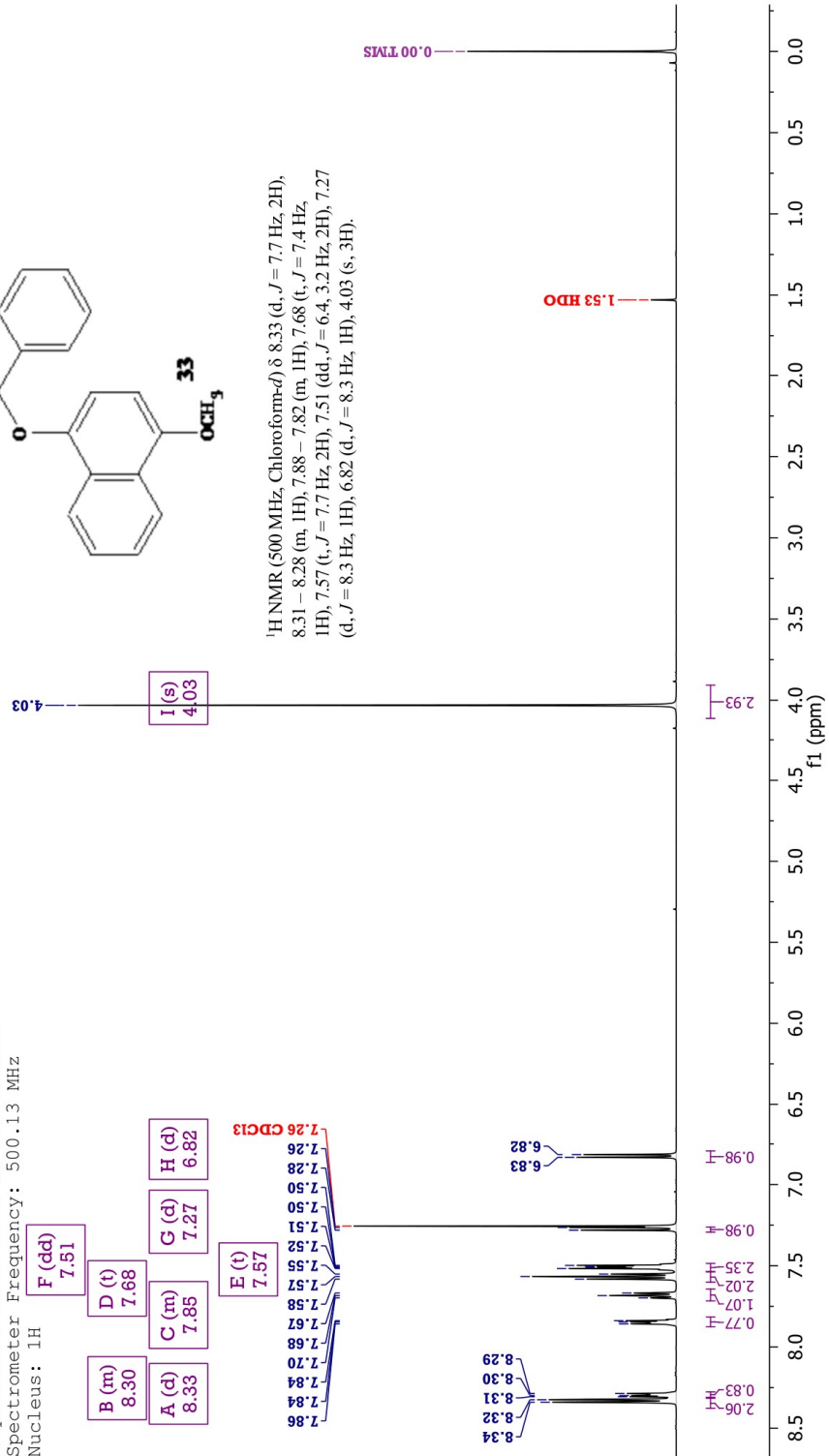
¹H NMR (500 MHz, Chloroform-*d*) δ 8.20 (dd, *J* = 8.1, 1.6 Hz, 1H), 7.94 (dd, *J* = 8.2, 1.5 Hz, 1H), 7.52 (dddd, *J* = 20.2, 8.1, 6.8, 1.4 Hz, 2H), 7.13 (d, *J* = 7.5 Hz, 1H), 6.72 (d, *J* = 7.5 Hz, 1H), 5.02 (s, 1H), 2.61 (s, 3H).



JAJ2-01-A.3.fid
 Comment: 4-methoxyphenyl-1-yl benzoate in CDCl3 w/TMS
 Origin: Bruker BioSpin GmbH
 Solvent: CDCl3
 Temperature: 298.1 K
 Pulse Sequence: zg30
 Experiment: 1D
 Number of Scans: 16
 Receiver Gain: 97.1 db
 Relaxation Delay: 1.0000 s
 Pulse Width: 12.0000 µs
 Acquisition Time: 3.2768 s
 Acquisition Date: 2020-04-22T17:02:56
 Spectrometer Frequency: 500.13 MHz
 Nucleus: 1H

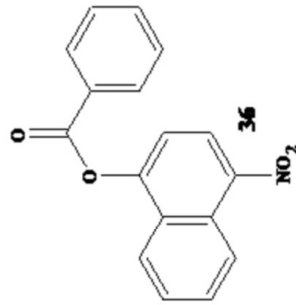


¹H NMR (500 MHz, Chloroform-*d*) δ 8.33 (d, *J* = 7.7 Hz, 2H),
 8.31 – 8.28 (m, 1H), 7.88 – 7.82 (m, 1H), 7.68 (t, *J* = 7.4 Hz,
 1H), 7.57 (t, *J* = 7.7 Hz, 2H), 7.51 (dd, *J* = 6.4, 3.2 Hz, 2H), 7.27
 (d, *J* = 8.3 Hz, 1H), 6.82 (d, *J* = 8.3 Hz, 1H), 4.03 (s, 3H).

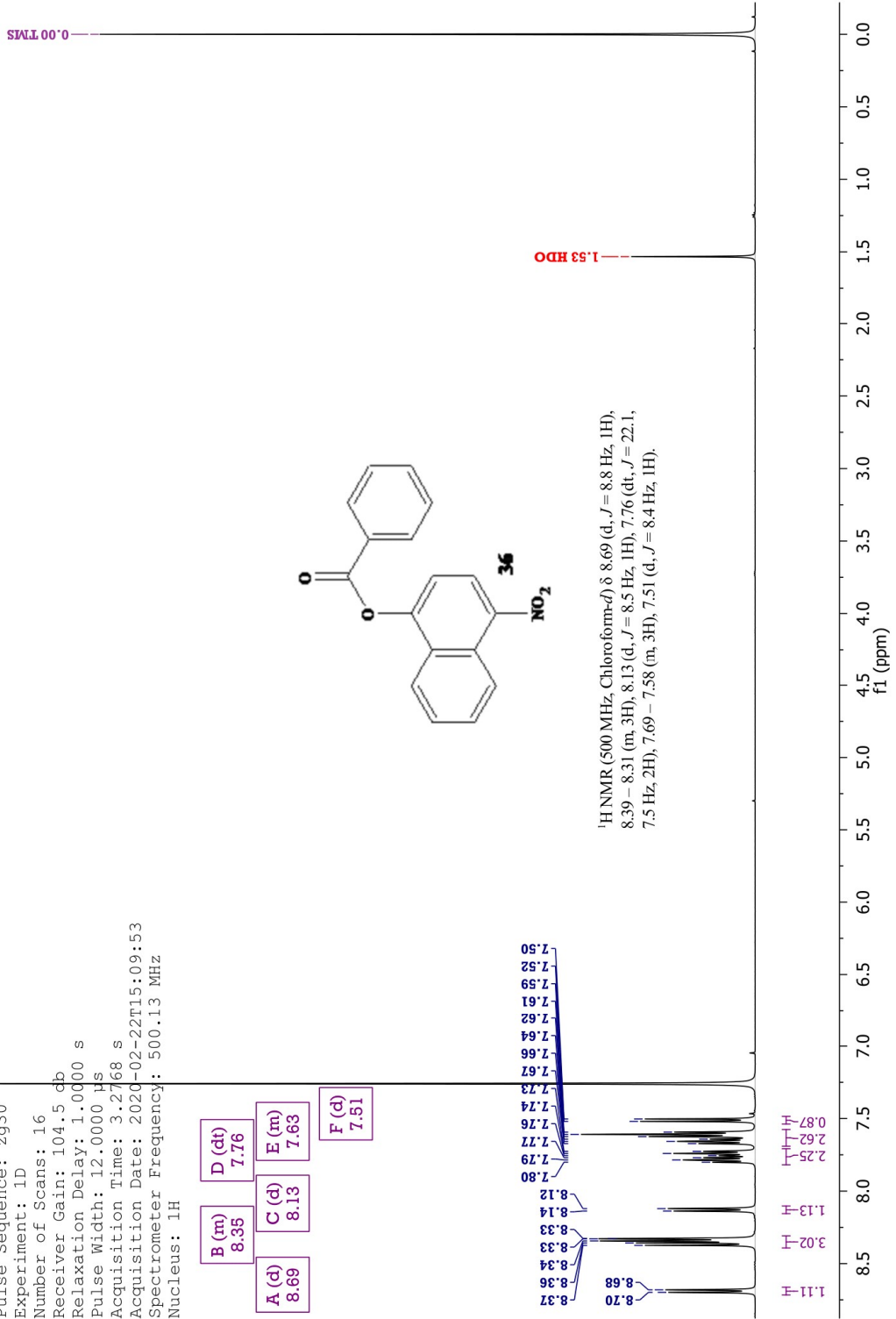


JAJ2-13-A.4.fid
 Comment: 4-nitronaphthalenyl benzoate in CDCl3 w/TMS
 Origin: Bruker BioSpin GmbH
 Solvent: CDCl3
 Temperature: 298.1 K
 Pulse Sequence: zg30
 Experiment: 1D
 Number of Scans: 16
 Receiver Gain: 104.5 db
 Relaxation Delay: 1.0000 s
 Pulse Width: 12.0000 μ s
 Acquisition Time: 3.2768 s
 Acquisition Date: 2020-02-22T15:09:53
 Spectrometer Frequency: 500.13 MHz
 Nucleus: 1H

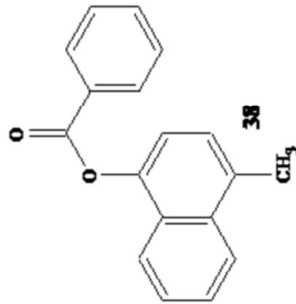
A (d)	8.69
B (m)	8.35
C (d)	8.13
D (dt)	7.76
E (m)	7.63
F (d)	7.51



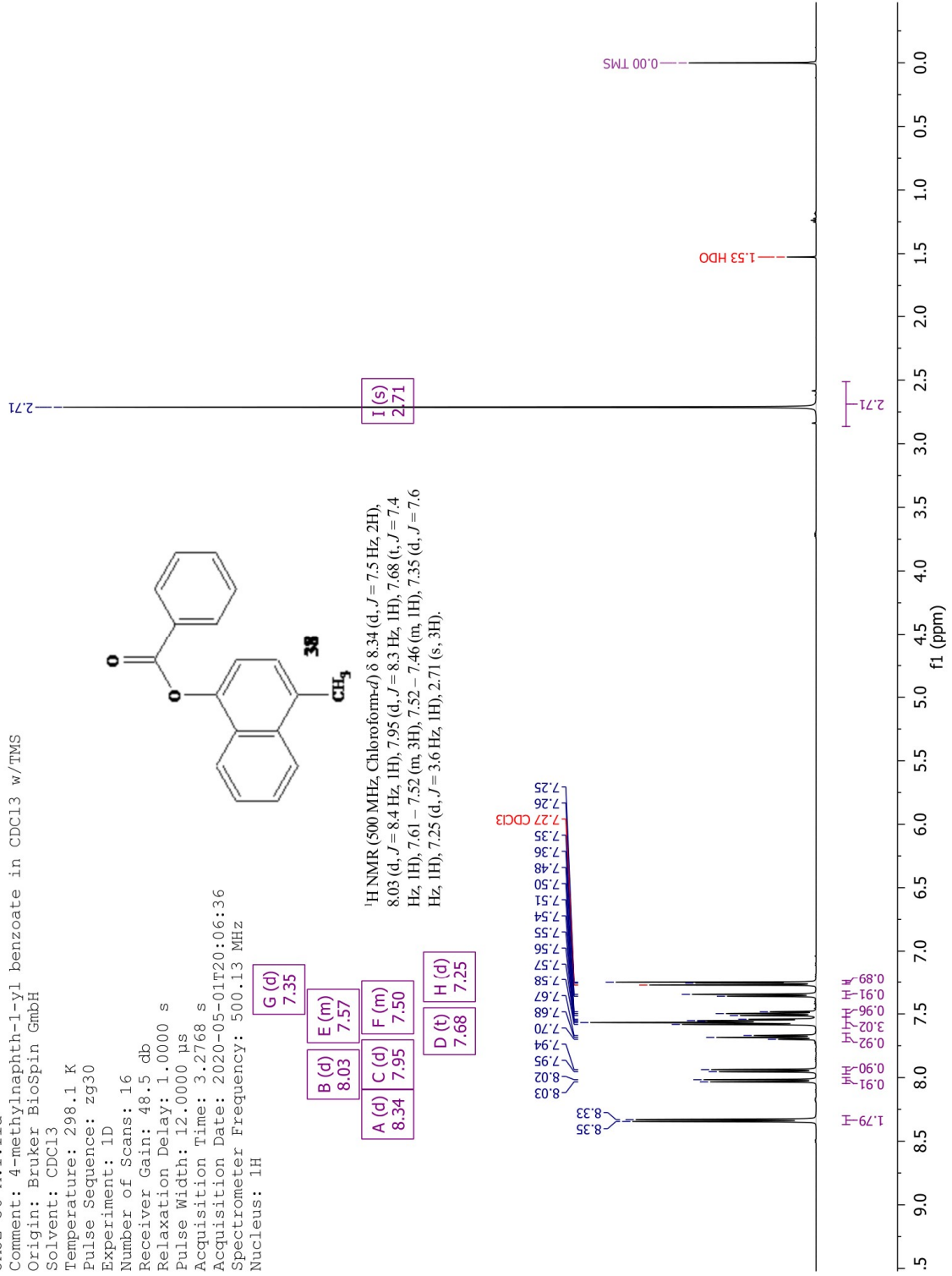
¹H NMR (500 MHz, Chloroform-*d*) δ 8.69 (d, *J* = 8.8 Hz, 1H),
 8.39 – 8.31 (m, 3H), 8.13 (d, *J* = 8.5 Hz, 1H), 7.76 (dt, *J* = 22.1,
 7.5 Hz, 2H), 7.69 – 7.58 (m, 3H), 7.51 (d, *J* = 8.4 Hz, 1H).



JAJ2-56-A.1.fid
 Comment: 4-methylnaphth-1-yl benzoate in CDCl3 w/TMS
 Origin: Bruker BioSpin GmbH
 Solvent: CDCl3
 Temperature: 298.1 K
 Pulse Sequence: zg30
 Experiment: 1D
 Number of Scans: 16
 Receiver Gain: 48.5 db
 Relaxation Delay: 1.0000 s
 Pulse Width: 12.0000 μ s
 Acquisition Time: 3.2768 s
 Acquisition Date: 2020-05-01T20:06:36
 Spectrometer Frequency: 500.13 MHz
 Nucleus: 1H



¹H NMR (500 MHz, Chloroform-*d*) δ 8.34 (d, *J* = 7.5 Hz, 2H),
 8.03 (d, *J* = 8.4 Hz, 1H), 7.95 (d, *J* = 8.3 Hz, 1H), 7.68 (t, *J* = 7.4
 Hz, 1H), 7.61 – 7.52 (m, 3H), 7.52 – 7.46 (m, 1H), 7.35 (d, *J* = 7.6
 Hz, 1H), 7.25 (d, *J* = 3.6 Hz, 1H), 2.71 (s, 3H).



JAJ2-57-A.1.fid
 Comment: 4-nitronaphth-1-yl p-toluate in CDCl3 w/TMS

Origin: Bruker BioSpin GmbH
 Solvent: CDCl3

Temperature: 298.1 K
 Pulse Sequence: zg30

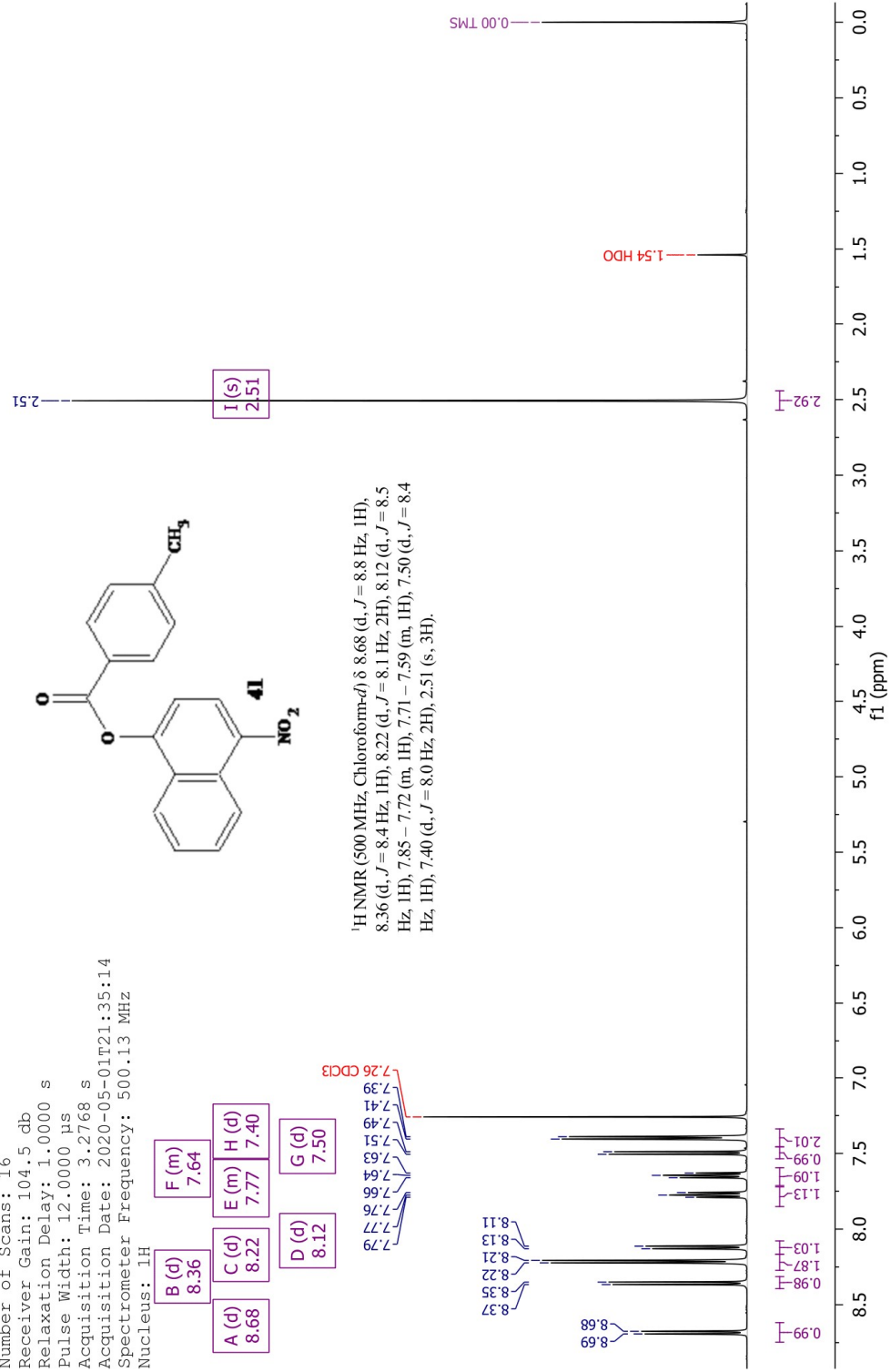
Experiment: 1D
 Number of Scans: 16

Receiver Gain: 104.5 db
 Relaxation Delay: 1.0000 s

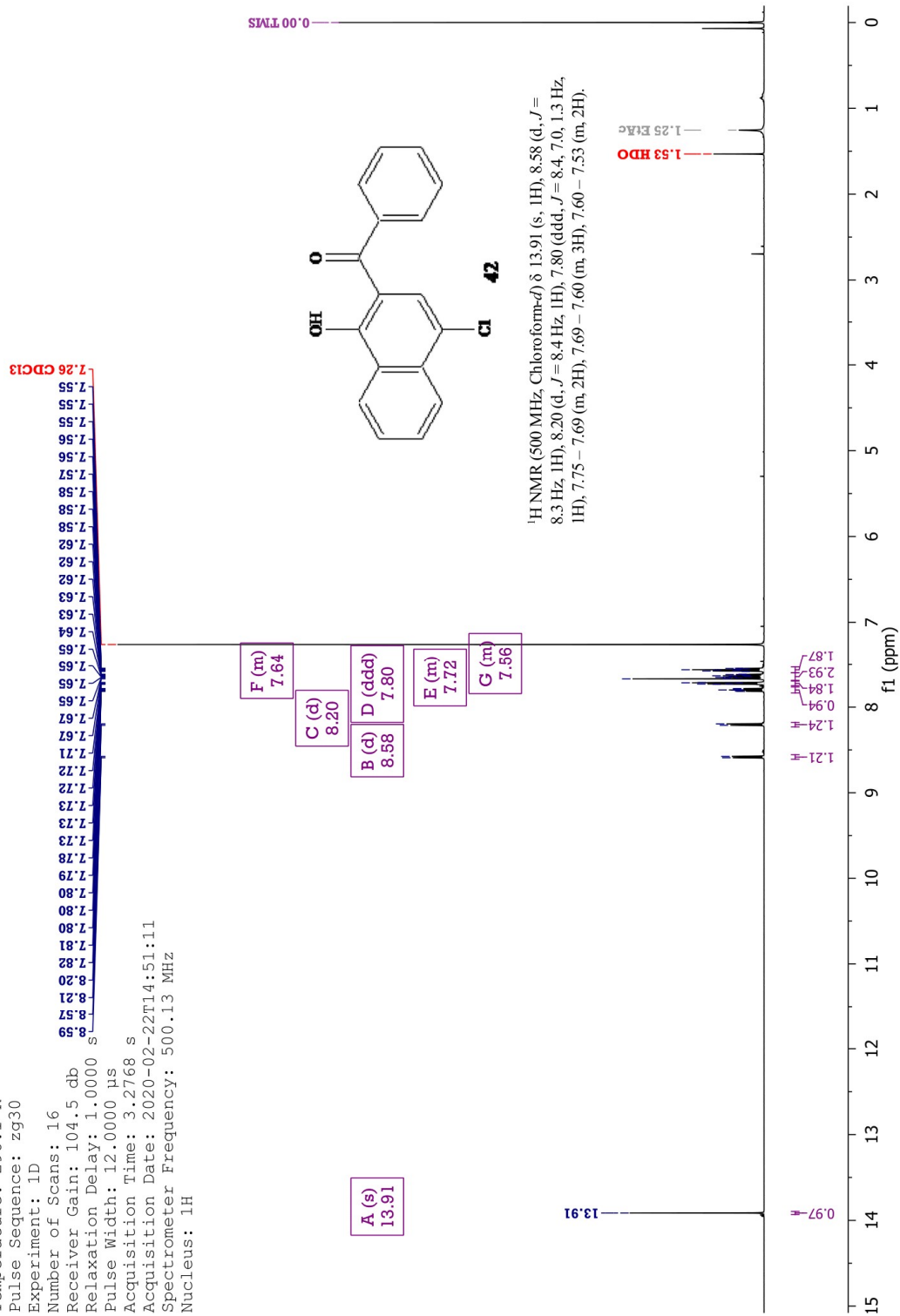
Pulse Width: 12.0000 μ s
 Acquisition Time: 3.2768 s

Acquisition Date: 2020-05-01T21:35:14
 Spectrometer Frequency: 500.13 MHz

Nucleus: 1H



JAJ-2-19-A.1.fid
 Comment: 2-benzoyl-4-chloro-1-naphthol in CDCl3 w/TMS
 Origin: Bruker BioSpin GmbH
 Solvent: CDCl3
 Temperature: 298.1 K
 Pulse Sequence: zg30
 Experiment: 1D
 Number of Scans: 16
 Receiver Gain: 104.5 db
 Relaxation Delay: 1.0000 s
 Pulse Width: 12.0000 µs
 Acquisition Time: 3.2768 s
 Acquisition Date: 2020-02-22T14:51:11
 Spectrometer Frequency: 500.13 MHz
 Nucleus: 1H



JAJ2-53-A.1.fid
 Comment: 5mg 2-benzoyl-4-methoxy-1-naphthol in CDCl3 w/TMS
 Origin: Bruker BioSpin GmbH
 Solvent: CDCl3

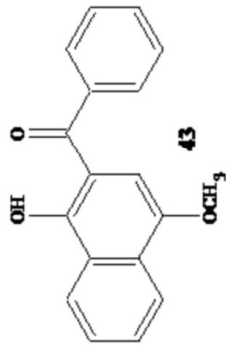
Temperature: 298.1 K
 Pulse Sequence: zg30

Experiment: 1D
 Number of Scans: 256

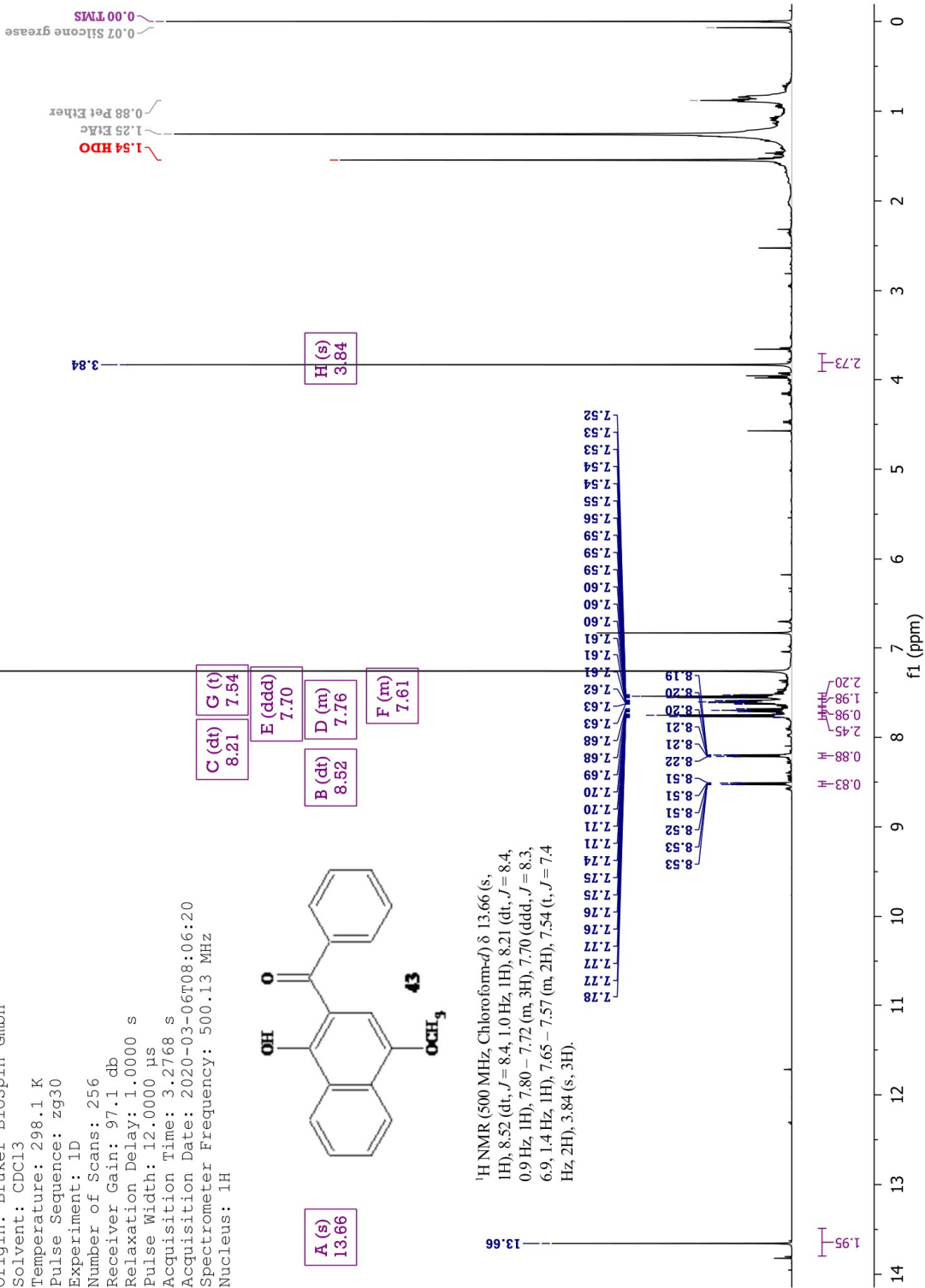
Receiver Gain: 97.1 db
 Relaxation Delay: 1.0000 s

Pulse Width: 12.0000 μ s
 Acquisition Time: 3.2768 s

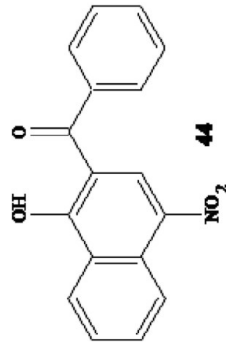
Acquisition Date: 2020-03-06T08:06:20
 Spectrometer Frequency: 500.13 MHz
 Nucleus: 1H



¹H NMR (500 MHz, Chloroform-*d*) δ 13.66 (s, 1H), 8.52 (dt, *J* = 8.4, 1.0 Hz, 1H), 8.21 (dt, *J* = 8.4, 0.9 Hz, 1H), 7.80 – 7.72 (m, 3H), 7.70 (ddd, *J* = 8.3, 6.9, 1.4 Hz, 1H), 7.65 – 7.57 (m, 2H), 7.54 (t, *J* = 7.4 Hz, 2H), 3.84 (s, 3H).

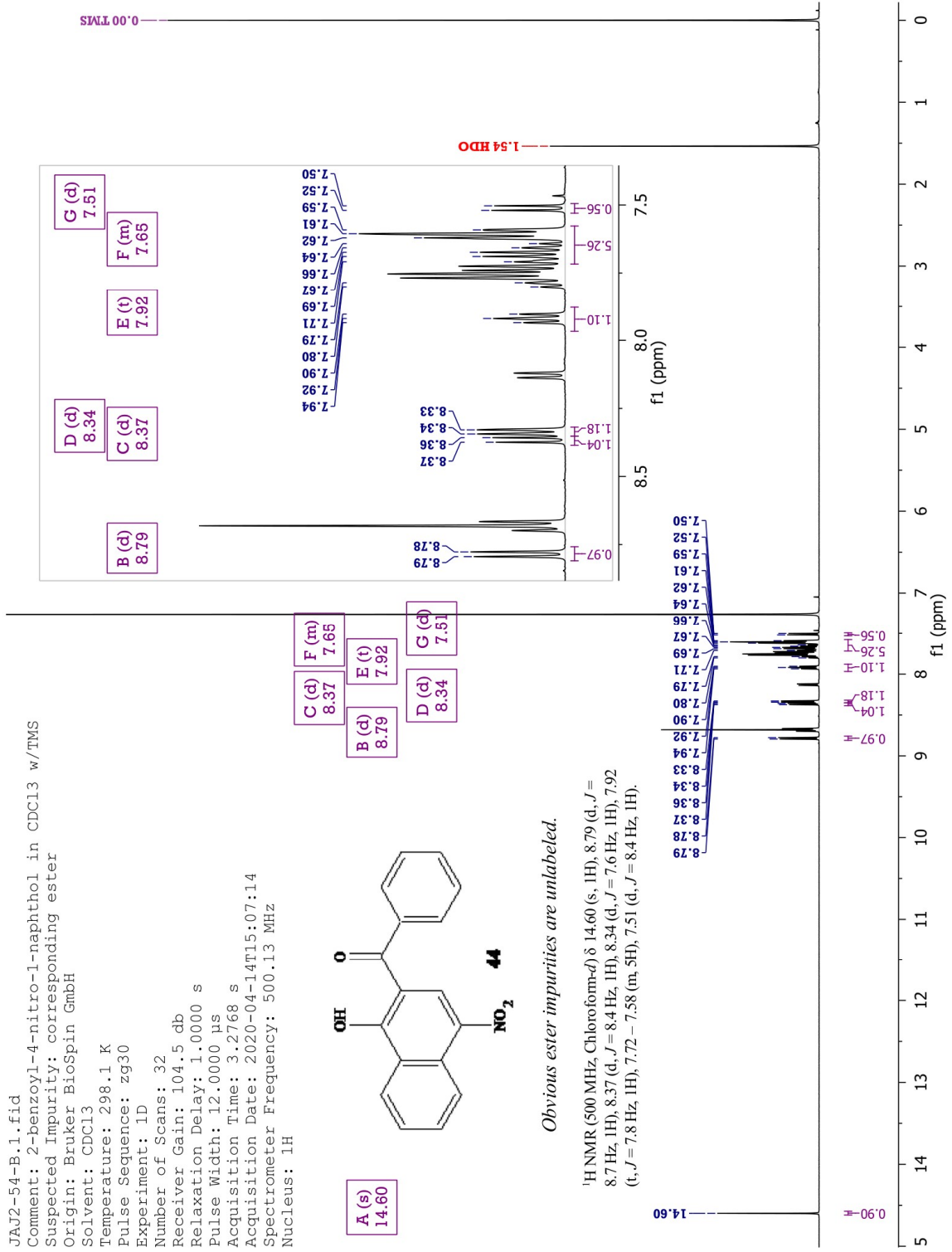


JAJ2-54-B.1.1.fid
 Comment: 2-benzoyl-4-nitro-1-naphthol in CDCl3 w/TMS
 Suspected Impurity: corresponding ester
 Origin: Bruker BioSpin GmbH
 Solvent: CDCl3
 Temperature: 298.1 K
 Pulse Sequence: zg30
 Experiment: 1D
 Number of Scans: 32
 Receiver Gain: 104.5 db
 Relaxation Delay: 1.0000 s
 Pulse Width: 12.0000 μ s
 Acquisition Time: 3.2768 s
 Acquisition Date: 2020-04-14T15:07:14
 Spectrometer Frequency: 500.13 MHz
 Nucleus: 1H



Obvious ester impurities are unlabeled.

¹H NMR (500 MHz, Chloroform-*d*) δ 14.60 (s, 1H), 8.79 (d, *J* = 8.7 Hz, 1H), 8.37 (d, *J* = 8.4 Hz, 1H), 8.34 (d, *J* = 7.6 Hz, 1H), 7.92 (t, *J* = 7.8 Hz, 1H), 7.72 – 7.58 (m, 5H), 7.51 (d, *J* = 8.4 Hz, 1H).



JAJ2-58-A.1.fid
 Comment: 4-bromo-2-benzoyl-1-naphthol in CDCl3 w/TMS

Origin: Bruker BioSpin GmbH

Solvent: CDCl3

Temperature: 298.0 K

Pulse Sequence: zg30

Experiment: 1D

Number of Scans: 16

Receiver Gain: 89.4 db

Relaxation Delay: 1.0000 s

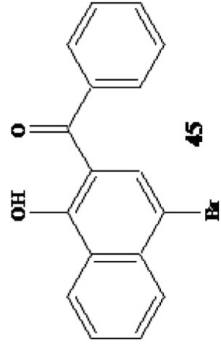
Pulse Width: 12.0000 µs

Acquisition Time: 3.2768 s

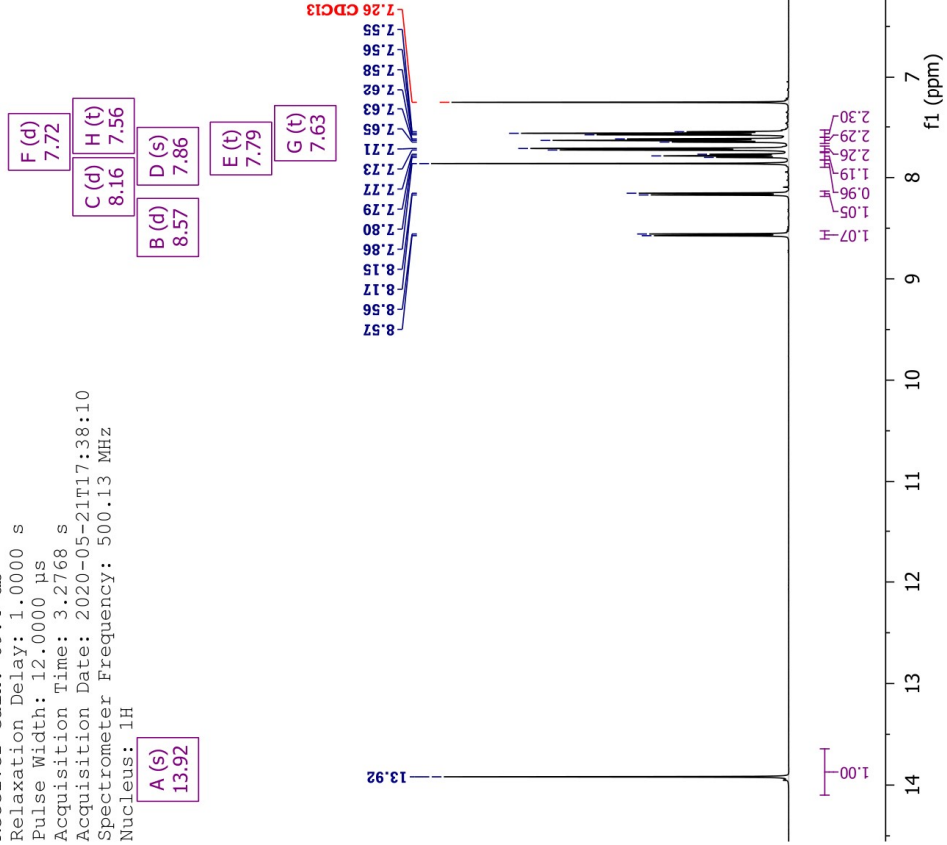
Acquisition Date: 2020-05-21T17:38:10

Spectrometer Frequency: 500.13 MHz

Nucleus: 1H

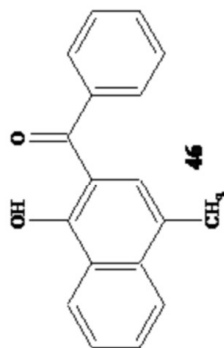


¹H NMR (500 MHz, Chloroform-d) δ 13.92 (s, 1H), 8.57 (d, J = 8.3 Hz, 1H), 8.16 (d, J = 8.4 Hz, 1H), 7.86 (s, 1H), 7.79 (t, J = 7.7 Hz, 1H), 7.72 (d, J = 7.5 Hz, 2H), 7.63 (t, J = 7.7 Hz, 2H), 7.56 (t, J = 7.6 Hz, 2H).

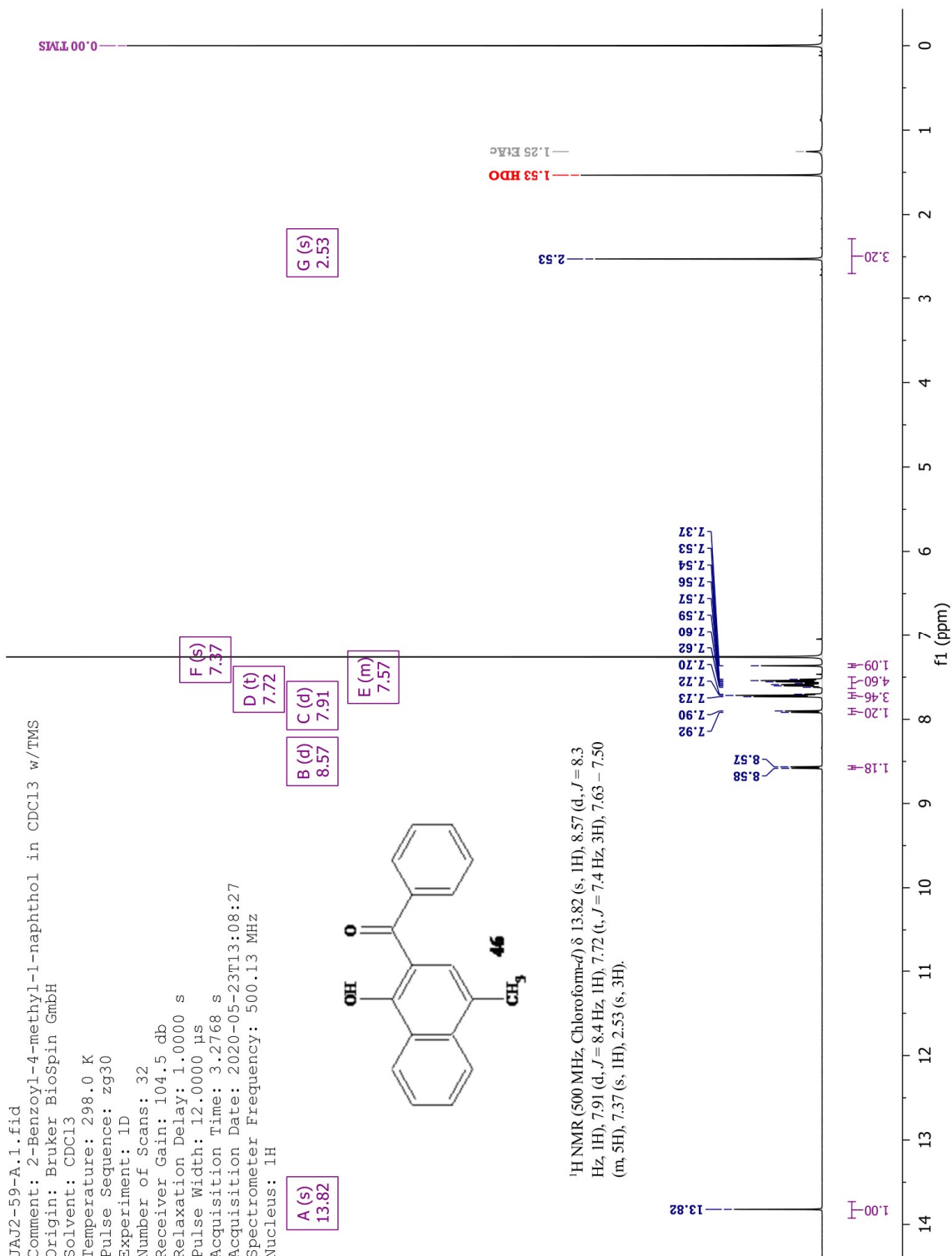


JAJ2-59-A.1.fid
 Comment: 2-Benzoyl-4-methyl-1-naphthol in CDCl3 w/TMS

Origin: Bruker BioSpin GmbH
 Solvent: CDCl3
 Temperature: 298.0 K
 Pulse Sequence: zg30
 Experiment: 1D
 Number of Scans: 32
 Receiver Gain: 104.5 db
 Relaxation Delay: 1.0000 s
 Pulse Width: 12.0000 µs
 Acquisition Time: 3.2768 s
 Acquisition Date: 2020-05-23T13:08:27
 Spectrometer Frequency: 500.13 MHz
 Nucleus: 1H

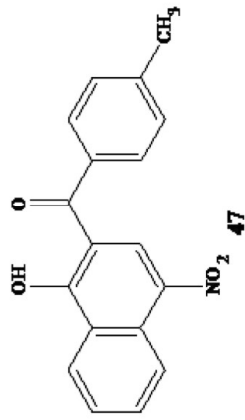


¹H NMR (500 MHz, Chloroform-d) δ 13.82 (s, 1H), 8.57 (d, J = 8.3 Hz, 1H), 7.91 (d, J = 8.4 Hz, 1H), 7.72 (t, J = 7.4 Hz, 3H), 7.63 – 7.50 (m, 5H), 7.37 (s, 1H), 2.53 (s, 3H).



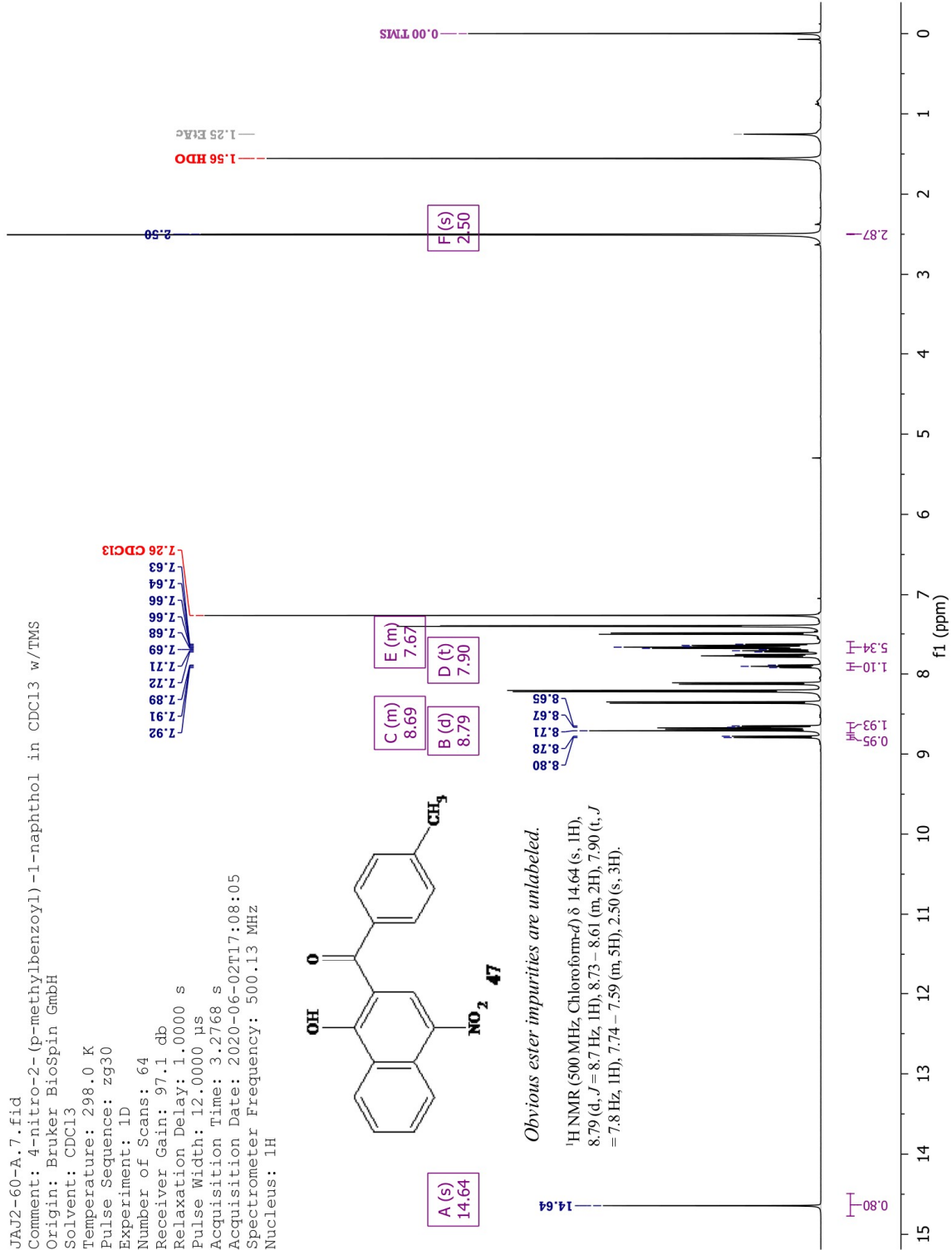
JAJ2-60-A.7.fid
 Comment: 4-nitro-2-(p-methylbenzoyl)-1-naphthol in CDCl3 w/TMS
 Origin: Bruker BioSpin GmbH

Solvent: CDCl3
 Temperature: 298.0 K
 Pulse Sequence: zg30
 Experiment: 1D
 Number of Scans: 64
 Receiver Gain: 97.1 db
 Relaxation Delay: 1.0000 s
 Pulse Width: 12.0000 µs
 Acquisition Time: 3.2768 s
 Acquisition Date: 2020-06-02T17:08:05
 Spectrometer Frequency: 500.13 MHz
 Nucleus: 1H



Obvious ester impurities are unlabeled.

¹H NMR (500 MHz, Chloroform-d) δ 14.64 (s, 1H), 8.79 (d, J = 8.7 Hz, 1H), 8.73 – 8.61 (m, 2H), 7.90 (t, J = 7.8 Hz, 1H), 7.74 – 7.59 (m, 5H), 2.50 (s, 3H).



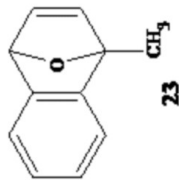
Appendix B: ¹³C NMR Spectra

Spectra taken in CDCl₃ with TMS were corrected (if needed) to have the TMS signal appear at exactly $\delta = 0.00$ ppm. For spectra taken without TMS, referencing was done with the center deuteriochloroform peak corrected to $\delta = 77.36$ ppm for ¹³C spectra (**29**). The NMR spectra were processed using the Mestrelabs Mnova software. In processing, each spectrum had the default automatic phase correction performed, followed by automatic baseline correction using the Whittaker smoother algorithm.

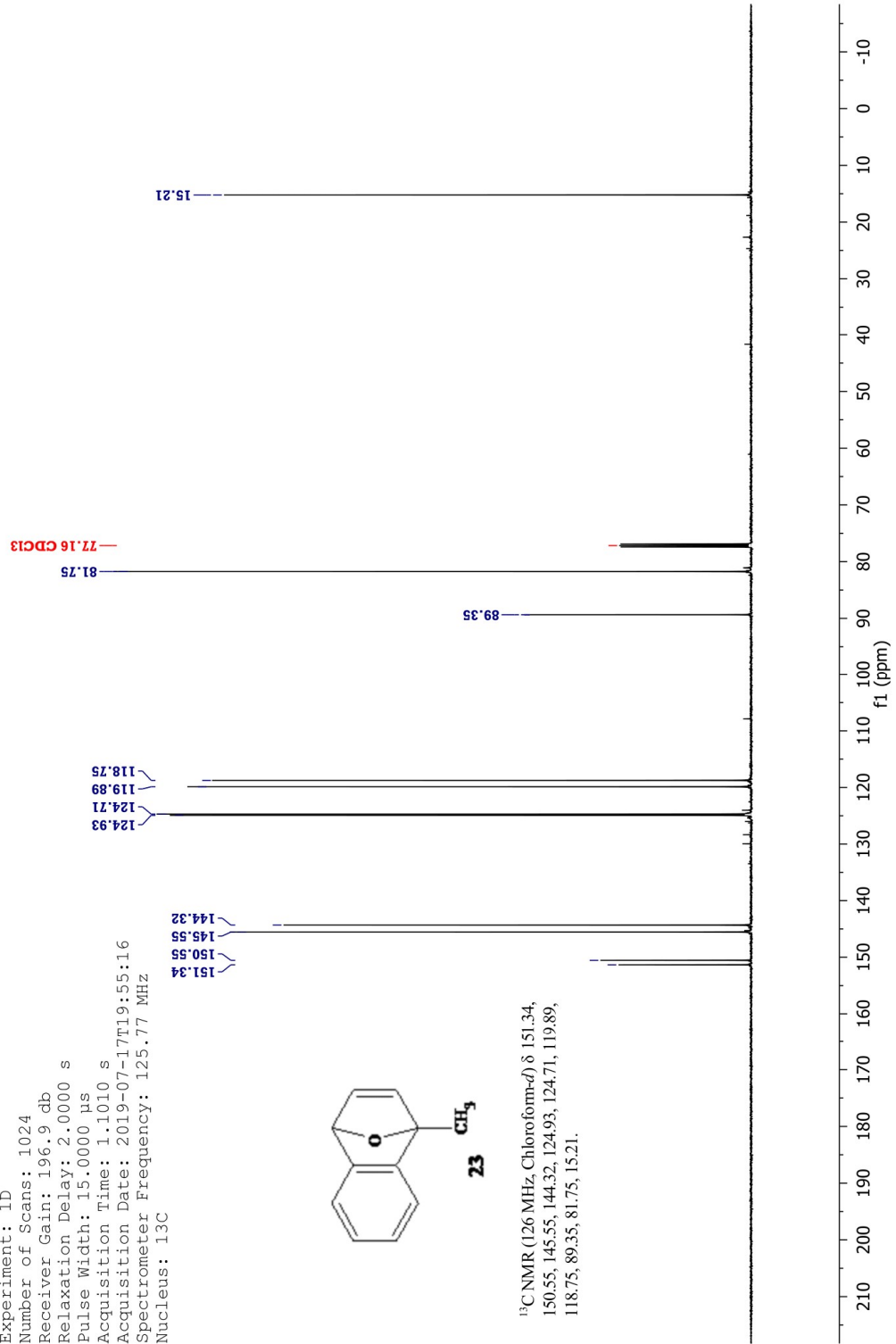
List of ¹³C Spectra in Appendix B

Page 120	1-Methyl-1,4-dihydro-1,4-epoxynaphthalene – JAJ1-54-D
Page 121	4-Methyl-1-naphthol – JAJ2-39-A
Page 122	4-Methoxynaphth-1-yl Benzoate – JAJ2-01-A
Page 123	4-Chloronaphth-1-yl Benzoate – JAJ1-19-A
Page 124	4-Nitronaphth-1-yl Benzoate – JAJ2-13-A
Page 125	4-Bromonaphth-1-yl Benzoate – JAJ2-35-B
Page 126	4-Methylnaphth-1-yl Benzoate – JAJ2-56-A
Page 127	4-Nitronaphth-1-yl p-Toluate – JAJ2-57-A
Page 128	2-Benzoyl-4-chloro-1-naphthol – JAJ2-19-A
Page 129	2-Benzoyl-4-methoxy-1-naphthol – JAJ2-53-B
Page 130	2-Benzoyl-4-nitro-1-naphthol – JAJ2-54-B
Page 131	2-Benzoyl-4-bromo-1-naphthol – JAJ2-58-A
Page 132	2-Benzoyl-4-methyl-1-naphthol – JAJ2-59-A
Page 133	2-(p-Toluoyl)-4-nitro-1-naphthol – JAJ2-60-A

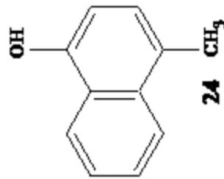
JAJ1-054-D-3.fid
Comment: Distillate 2 in CDCl3 w/TMS
Origin: Bruker BioSpin GmbH
Solvent: CDCl3
Temperature: 298.5 K
Pulse Sequence: zgpg30
Experiment: 1D
Number of Scans: 1024
Receiver Gain: 196.9 db
Relaxation Delay: 2.0000 s
Pulse Width: 15.0000 μ s
Acquisition Time: 1.1010 s
Acquisition Date: 2019-07-17T19:55:16
Spectrometer Frequency: 125.77 MHz
Nucleus: 13C



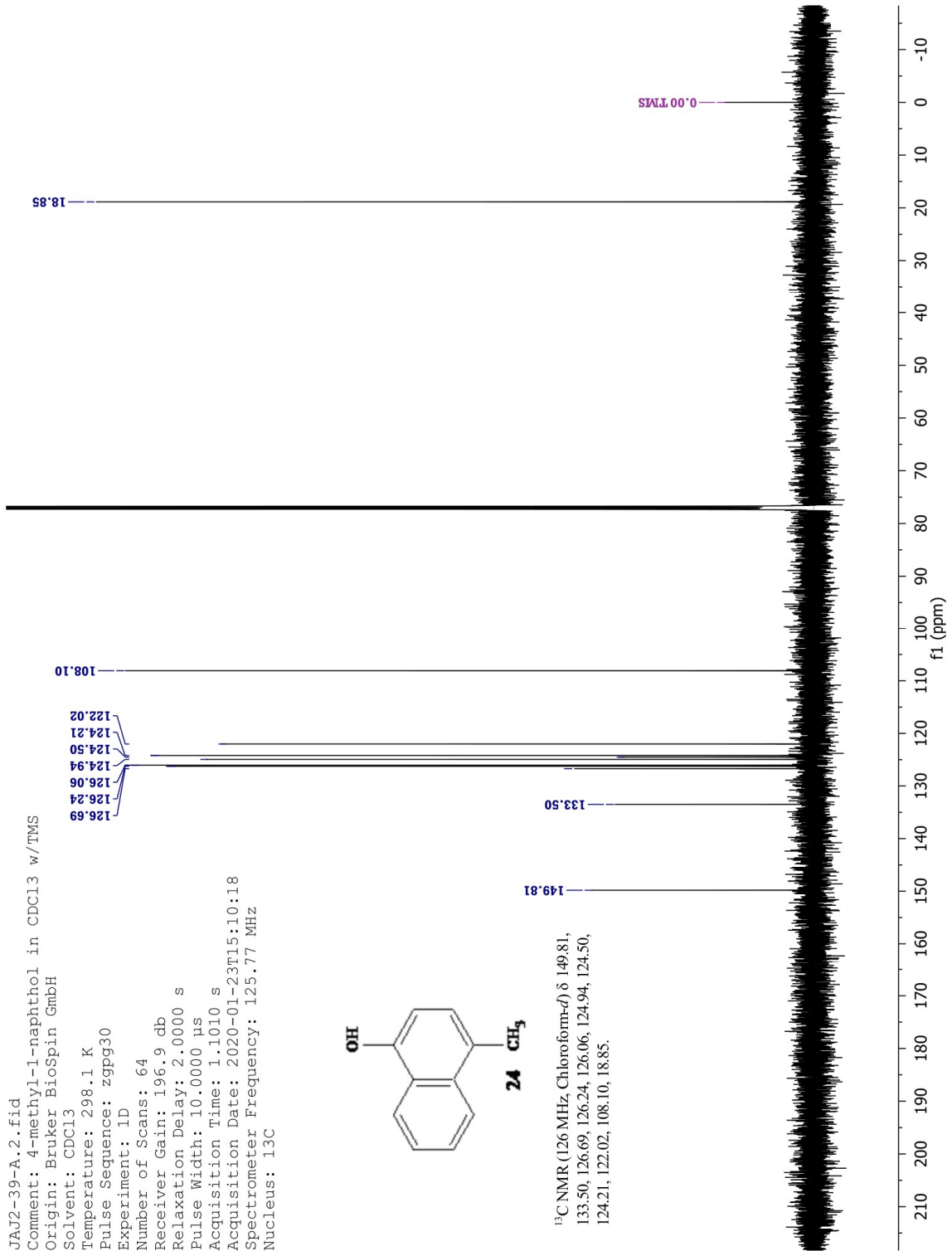
¹³C NMR (126 MHz, Chloroform-*d*) δ 151.34,
150.55, 145.55, 144.32, 124.93, 124.71, 119.89,
118.75, 89.35, 81.75, 15.21.



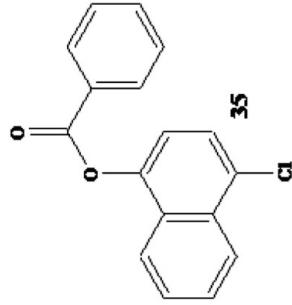
JAJ2-39-A.2.fid
 Comment: 4-methyl-1-naphthol in CDCl3 w/TMS
 Origin: Bruker BioSpin GmbH
 Solvent: CDCl3
 Temperature: 298.1 K
 Pulse Sequence: zgpg30
 Experiment: 1D
 Number of Scans: 64
 Receiver Gain: 196.9 db
 Relaxation Delay: 2.0000 s
 Pulse Width: 10.0000 µs
 Acquisition Time: 1.1010 s
 Acquisition Date: 2020-01-23T15:10:18
 Spectrometer Frequency: 125.77 MHz
 Nucleus: 13C



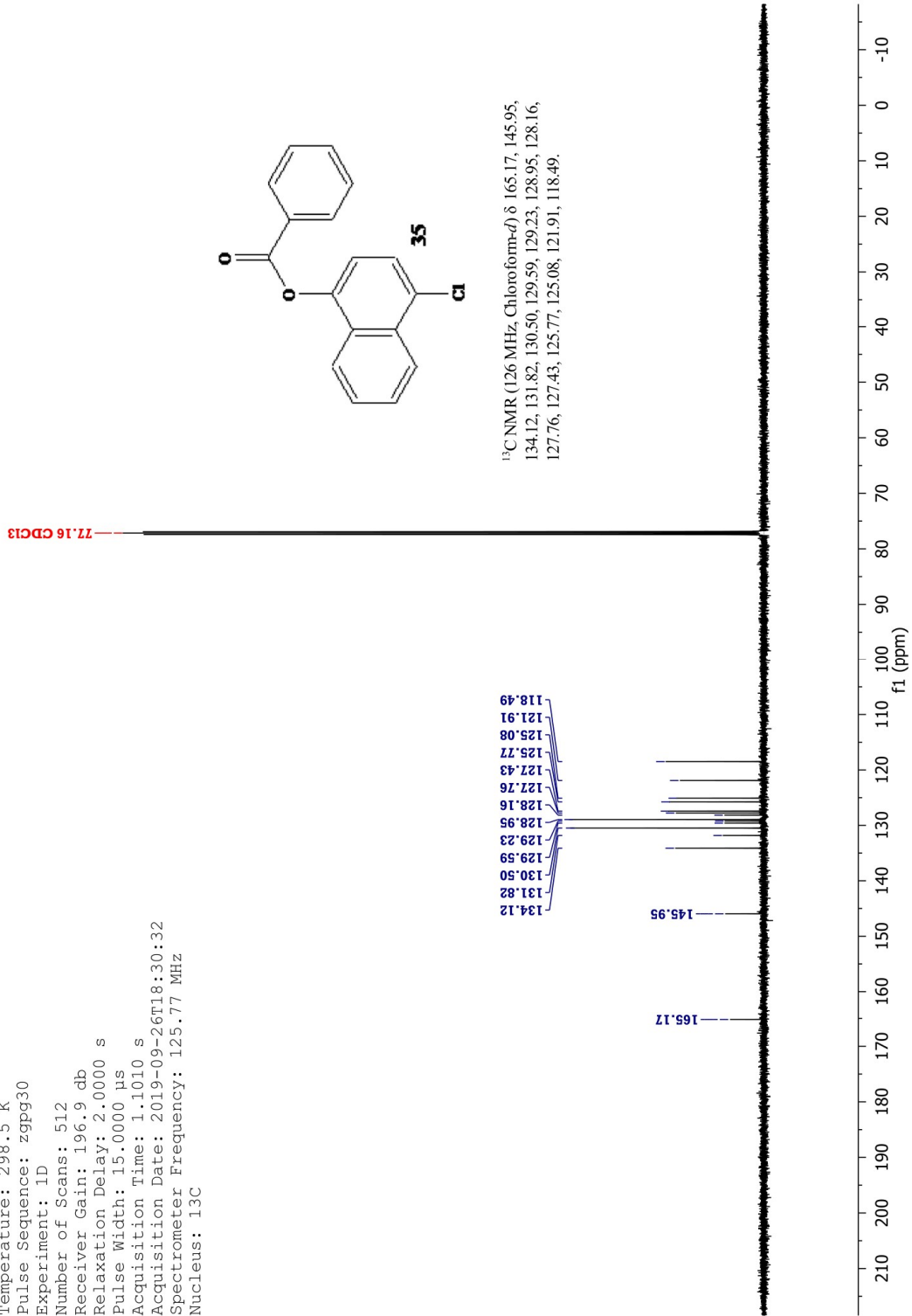
¹³C NMR (126 MHz Chloroform-*d*) δ 149.81,
 133.50, 126.69, 126.24, 126.06, 124.94, 124.50,
 124.21, 122.02, 108.10, 18.85.



JAJ1-019-A.5.fid
Comment: 4-chloronaphth-1-yl benzoate in CDCl3
Origin: Bruker BioSpin GmbH
Solvent: CDCl3
Temperature: 298.5 K
Pulse Sequence: zgpg30
Experiment: 1D
Number of Scans: 512
Receiver Gain: 196.9 db
Relaxation Delay: 2.0000 s
Pulse Width: 15.0000 μ s
Acquisition Time: 1.1010 s
Acquisition Date: 2019-09-26T18:30:32
Spectrometer Frequency: 125.77 MHz
Nucleus: 13C

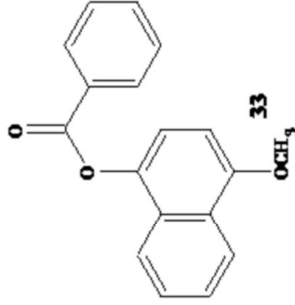


^{13}C NMR (126 MHz, Chloroform-*d*) δ 165.17, 145.95,
134.12, 131.82, 130.50, 129.59, 129.23, 128.95, 128.16,
127.76, 127.43, 125.77, 125.08, 121.91, 118.49.



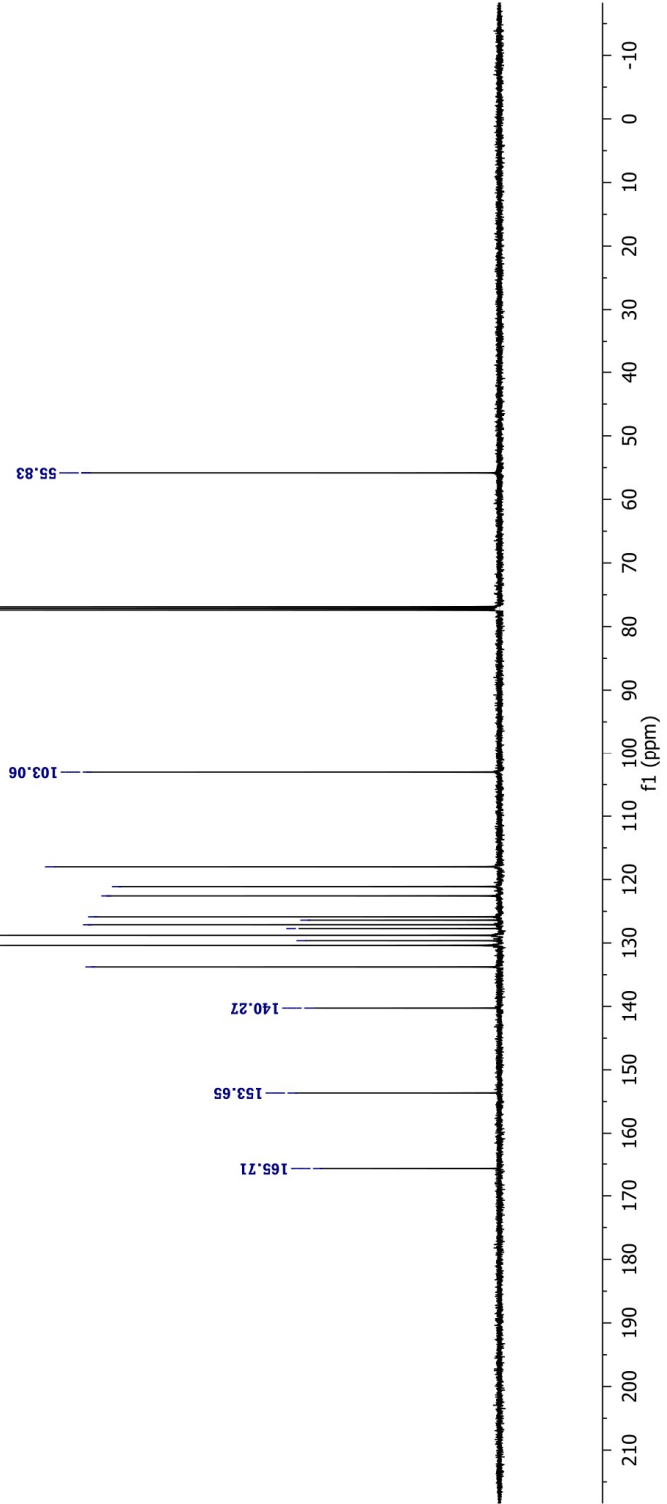
JAJ2-01-A.1.fid
 Comment: 4-methoxy ester in CDCl3
 Origin: Bruker BioSpin GmbH
 Solvent: CDCl3
 Temperature: 298.5 K
 Pulse Sequence: zgpg30
 Experiment: 1D
 Number of Scans: 512
 Receiver Gain: 196.9 db
 Relaxation Delay: 2.0000 s
 Pulse Width: 15.0000 μ s
 Acquisition Time: 1.1010 s
 Acquisition Date: 2019-09-26T20:50:27
 Spectrometer Frequency: 125.77 MHz
 Nucleus: 13C

133.78
 130.38
 129.64
 128.80
 127.73
 127.12
 126.40
 125.88
 122.58
 121.11
 117.99



¹³C NMR (126 MHz, Chloroform-*d*) δ 165.71, 153.65,
 140.27, 133.78, 130.38, 129.64, 128.80, 127.73, 127.12,
 126.40, 125.88, 122.58, 121.11, 117.99, 103.06, 55.83.

77.16 CDCl3



JAJ2-13-A.6.fid
Comment: 4-nitronaphth-1-yl benzoate in CDCl3 w/TMS

Origin: Bruker BioSpin GmbH

Solvent: CDCl3

Temperature: 298.1 K

Pulse Sequence: zgpg30

Experiment: 1D

Number of Scans: 1024

Receiver Gain: 196.9 db

Relaxation Delay: 2.0000 s

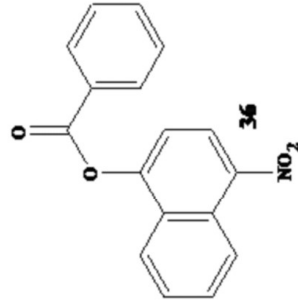
Pulse Width: 10.0000 μ s

Acquisition Time: 1.1010 s

Acquisition Date: 2020-02-22T21:43:30

Spectrometer Frequency: 125.77 MHz

Nucleus: 13C



^{13}C NMR (126 MHz, Chloroform- d) δ 164.36, 151.31, 144.11, 134.40, 130.46, 130.04, 128.97, 128.53, 127.90, 127.75, 126.70, 124.66, 123.72, 122.09, 116.93.

134.40
130.46
130.04
128.97
128.53
127.90
127.75
126.70
124.66
123.72
122.09
116.93

164.36
151.31
144.11

0.00 TMS

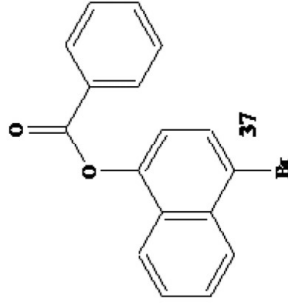
210 200 190 180 170 160 150 140 130 120 110 100 90 80 70 60 50 40 30 20 10 0 -10

f1 (ppm)

JAJ2-35-B.6.fid
Comment: 4-bromonaphth-1-yl benzoate in CDCl3 with TMS
Origin: Bruker BioSpin GmbH
Solvent: CDCl3

Temperature: 298.1 K
Pulse Sequence: zgpg30
Experiment: 1D
Number of Scans: 256
Receiver Gain: 196.9 db
Relaxation Delay: 2.0000 s
Pulse Width: 10.0000 μ s
Acquisition Time: 1.1010 s
Acquisition Date: 2020-02-01T17:00:20
Spectrometer Frequency: 125.77 MHz
Nucleus: 13C

134.00
132.92
130.37
129.33
129.08
128.81
128.20
127.93
127.62
127.32
121.79
119.94
118.86



^{13}C NMR (126 MHz, Chloroform-*d*) δ 164.94, 146.55, 134.00, 132.92, 130.37, 129.33, 129.08, 128.81, 128.20, 127.93, 127.62, 127.32, 121.79, 119.94, 118.86.

0.00 TMS

164.94
146.55

f1 (ppm)

JAJ2-56-A.2.fid
Comment: 4-methylnaphth-1-yl benzoate in CDCl3 w/TMS

Origin: Bruker BioSpin GmbH

Solvent: CDCl3

Temperature: 298.1 K

Pulse Sequence: zgpg30

Experiment: 1D

Number of Scans: 1024

Receiver Gain: 196.9 db

Relaxation Delay: 2.0000 s

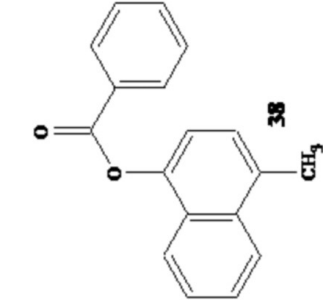
Pulse Width: 10.0000 μ s

Acquisition Time: 1.1010 s

Acquisition Date: 2020-05-01T21:01:35

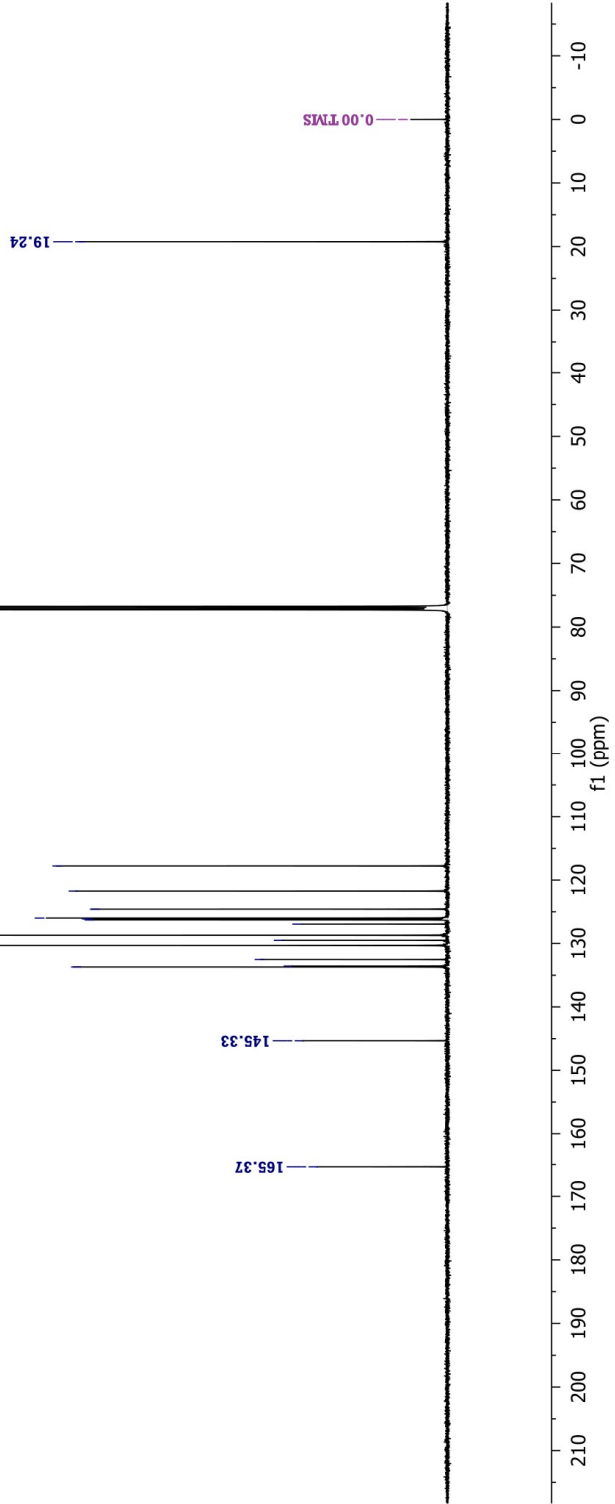
Spectrometer Frequency: 125.77 MHz

Nucleus: 13C

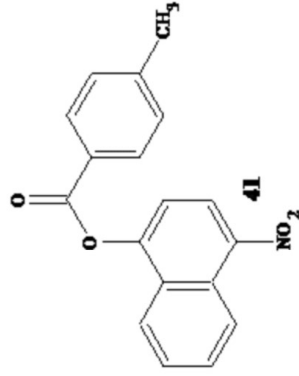


^{13}C NMR (126 MHz, Chloroform- d) δ 165.37, 145.33, 133.71, 133.56, 132.54, 130.32, 129.51, 128.71, 126.95, 126.29, 126.13, 125.99, 124.59, 121.74, 117.78, 19.24.

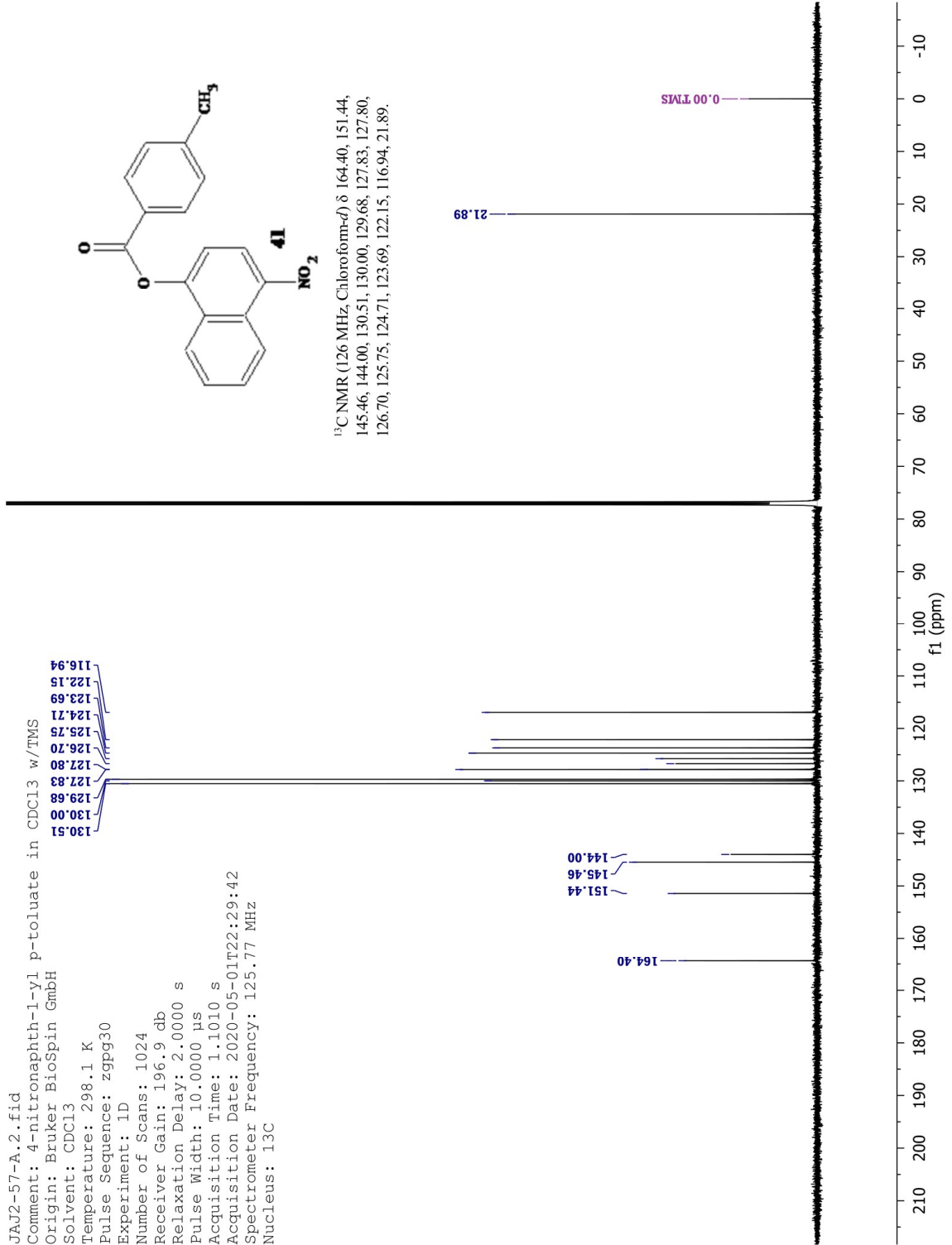
133.71
133.56
132.54
130.32
129.51
128.71
126.95
126.29
126.13
125.99
124.59
121.74
117.78



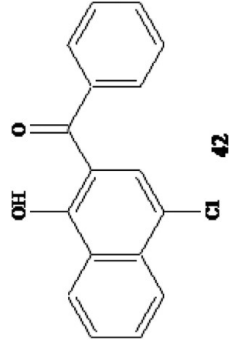
JAJ2-57-A.2.fid
 Comment: 4-nitronaphth-1-yl p-toluate in CDCl3 w/TMS
 Origin: Bruker BioSpin GmbH
 Solvent: CDCl3
 Temperature: 298.1 K
 Pulse Sequence: zgpg30
 Experiment: 1D
 Number of Scans: 1024
 Receiver Gain: 196.9 db
 Relaxation Delay: 2.0000 s
 Pulse Width: 10.0000 μ s
 Acquisition Time: 1.1010 s
 Acquisition Date: 2020-05-01T22:29:42
 Spectrometer Frequency: 125.77 MHz
 Nucleus: 13C



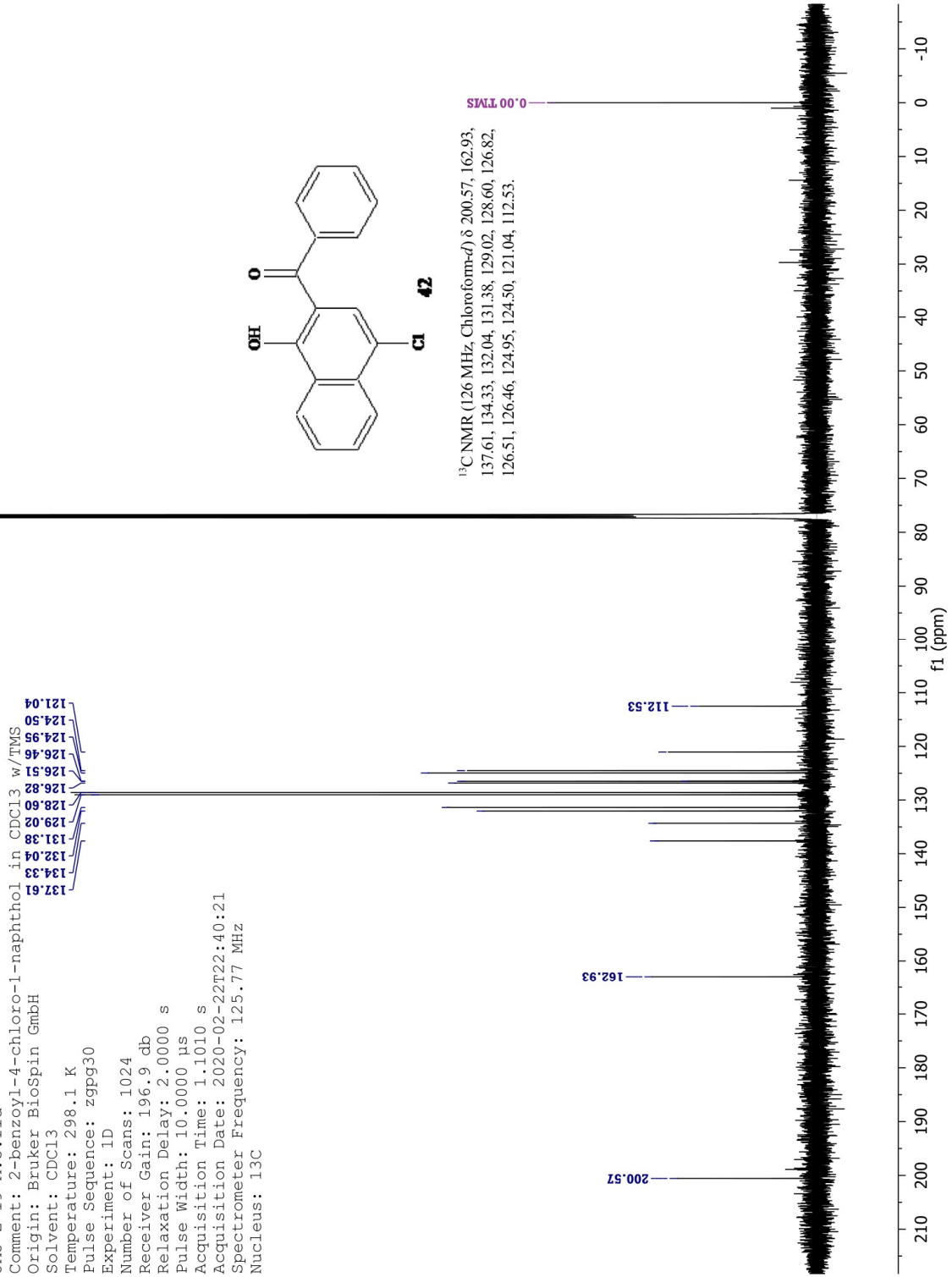
^{13}C NMR (126 MHz, Chloroform- d) δ 164.40, 151.44, 145.46, 144.00, 130.51, 130.00, 129.68, 127.83, 127.80, 126.70, 125.75, 124.71, 123.69, 122.15, 116.94, 21.89.



JAJ-2-19-A.3.fid
 Comment: 2-benzoyl-4-chloro-1-naphthol in CDCl3 w/TMS
 Origin: Bruker BioSpin GmbH
 Solvent: CDCl3
 Temperature: 298.1 K
 Pulse Sequence: zgpg30
 Experiment: 1D
 Number of Scans: 1024
 Receiver Gain: 196.9 db
 Relaxation Delay: 2.0000 s
 Pulse Width: 10.0000 µs
 Acquisition Time: 1.1010 s
 Acquisition Date: 2020-02-22T22:40:21
 Spectrometer Frequency: 125.77 MHz
 Nucleus: 13C

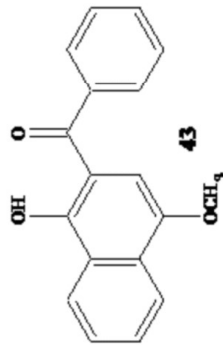


¹³C NMR (126 MHz, Chloroform-d) δ 200.57, 162.93,
 137.61, 134.33, 132.04, 131.38, 129.02, 128.60, 126.82,
 126.51, 126.46, 124.95, 124.50, 121.04, 112.53.

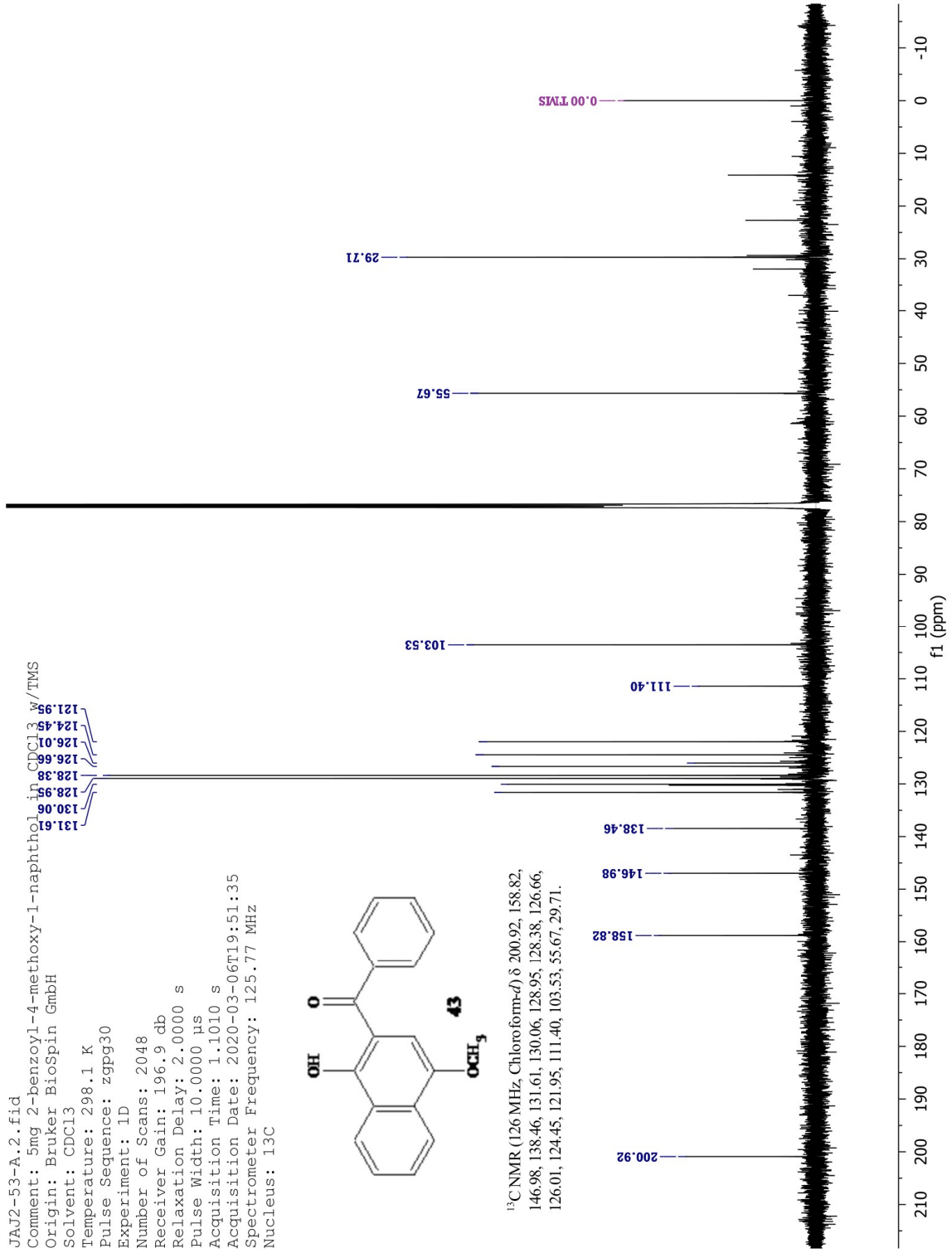


JAJ2-53-A.2.fid
Comment: 5mg 2-benzoyl-4-methoxy-1-naphthol in CDCl3 w/TMS

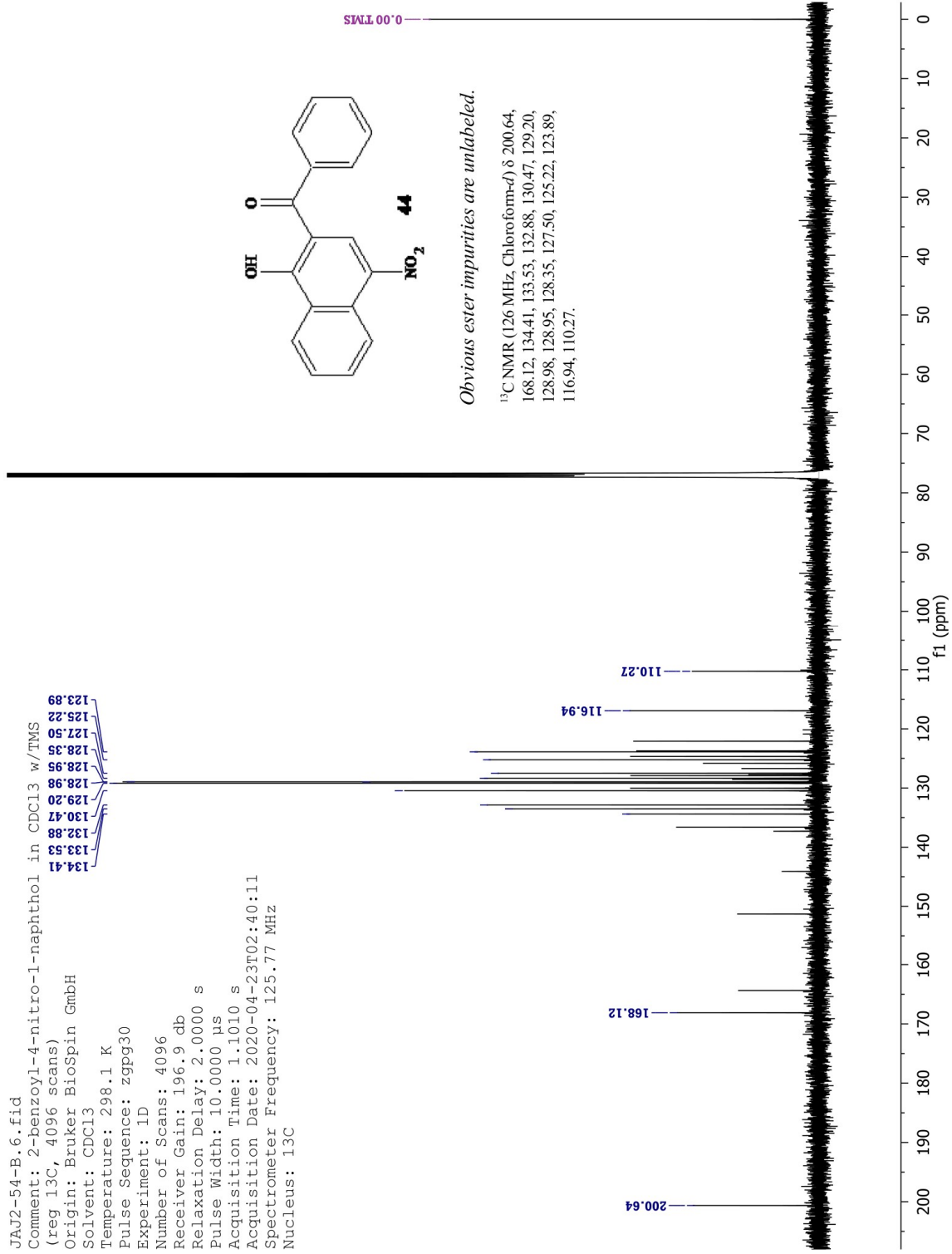
Origin: Bruker BioSpin GmbH
Solvent: CDCl3
Temperature: 298.1 K
Pulse Sequence: zgpg30
Experiment: 1D
Number of Scans: 2048
Receiver Gain: 196.9 db
Relaxation Delay: 2.0000 s
Pulse Width: 10.0000 µs
Acquisition Time: 1.1010 s
Acquisition Date: 2020-03-06T19:51:35
Spectrometer Frequency: 125.77 MHz
Nucleus: 13C



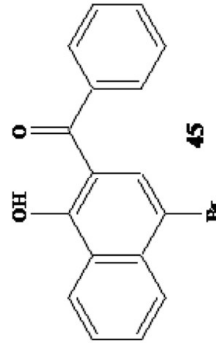
¹³C NMR (126 MHz, Chloroform-d) δ 200.92, 158.82, 146.98, 138.46, 131.61, 130.06, 128.95, 128.38, 126.66, 126.01, 124.45, 121.95, 111.40, 103.53, 55.67, 29.71.



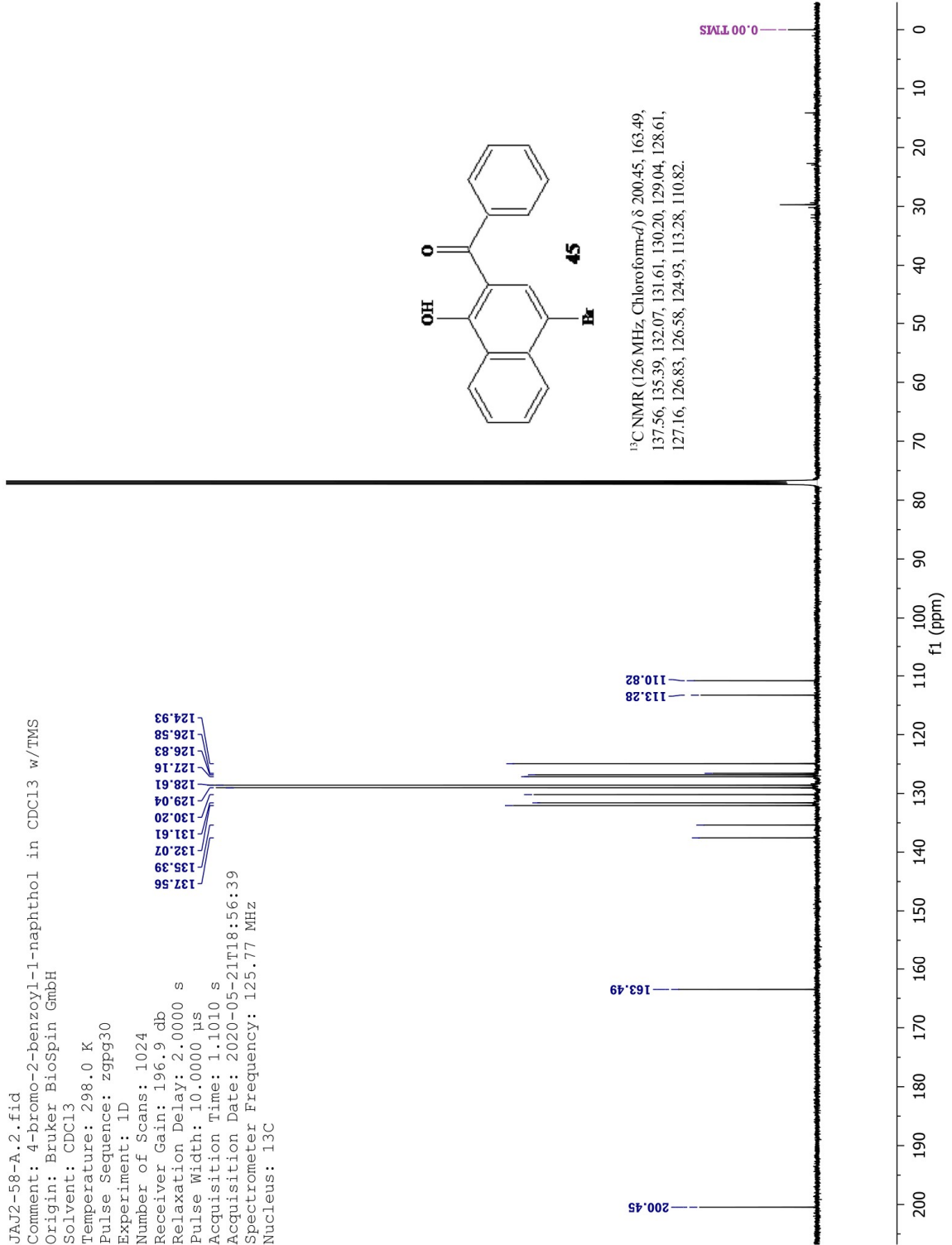
JAJ2-54-B.6.fid
 Comment: 2-benzoyl-4-nitro-1-naphthol in CDCl3 w/TMS
 (reg 13C, 4096 scans)
 Origin: Bruker BioSpin GmbH
 Solvent: CDCl3
 Temperature: 298.1 K
 Pulse Sequence: zgpg30
 Experiment: 1D
 Number of Scans: 4096
 Receiver Gain: 196.9 db
 Relaxation Delay: 2.0000 s
 Pulse Width: 10.0000 μ s
 Acquisition Time: 1.1010 s
 Acquisition Date: 2020-04-23T02:40:11
 Spectrometer Frequency: 125.77 MHz
 Nucleus: 13C



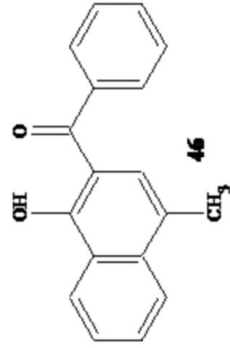
JAJ2-58-A.2.fid
 Comment: 4-bromo-2-benzoyl-1-naphthol in CDCl3 w/TMS
 Origin: Bruker BioSpin GmbH
 Solvent: CDCl3
 Temperature: 298.0 K
 Pulse Sequence: zgpg30
 Experiment: 1D
 Number of Scans: 1024
 Receiver Gain: 196.9 db
 Relaxation Delay: 2.0000 s
 Pulse Width: 10.0000 µs
 Acquisition Time: 1.1010 s
 Acquisition Date: 2020-05-21T18:56:39
 Spectrometer Frequency: 125.77 MHz
 Nucleus: 13C



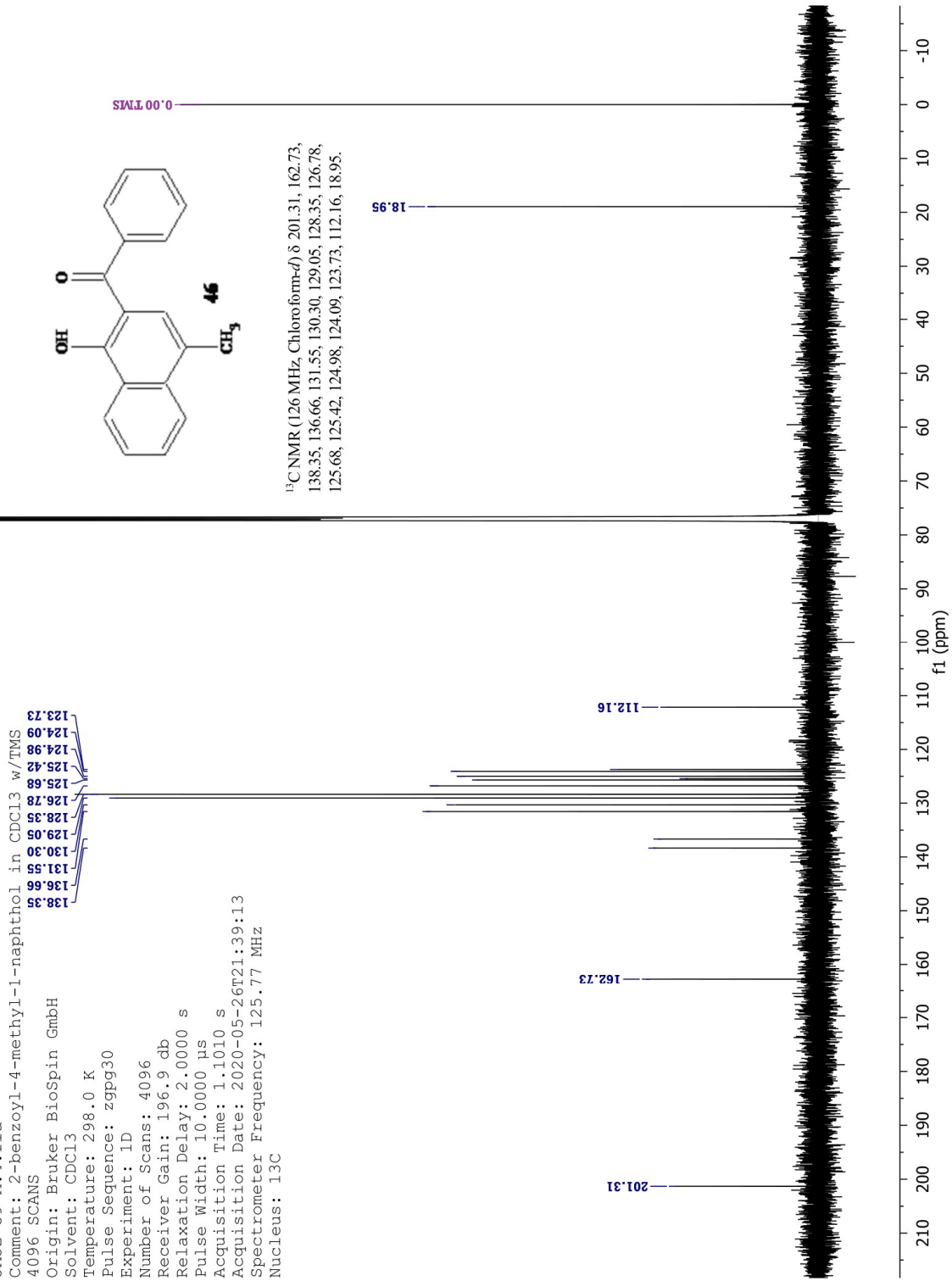
¹³C NMR (126 MHz, Chloroform-d) δ 200.45, 163.49,
 137.56, 135.39, 132.07, 131.61, 130.20, 129.04, 128.61,
 127.16, 126.83, 126.58, 124.93, 113.28, 110.82.



JAJ2-59-A.4.fid
 Comment: 2-benzoyl-4-methyl-1-naphthol in CDCl3 w/TMS
 4096 SCANS
 Origin: Bruker BioSpin GmbH
 Solvent: CDCl3
 Temperature: 298.0 K
 Pulse Sequence: zgpg30
 Experiment: 1D
 Number of Scans: 4096
 Receiver Gain: 196.9 db
 Relaxation Delay: 2.0000 s
 Pulse Width: 10.0000 μ s
 Acquisition Time: 1.1010 s
 Acquisition Date: 2020-05-26T21:39:13
 Spectrometer Frequency: 125.77 MHz
 Nucleus: 13C

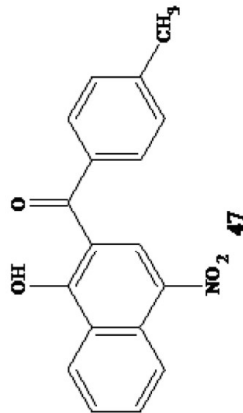


¹³C NMR (126 MHz, Chloroform-d) δ 201.31, 162.73, 138.35, 136.66, 131.55, 130.30, 129.05, 128.35, 126.78, 125.68, 125.42, 124.98, 124.09, 123.73, 112.16, 18.95.



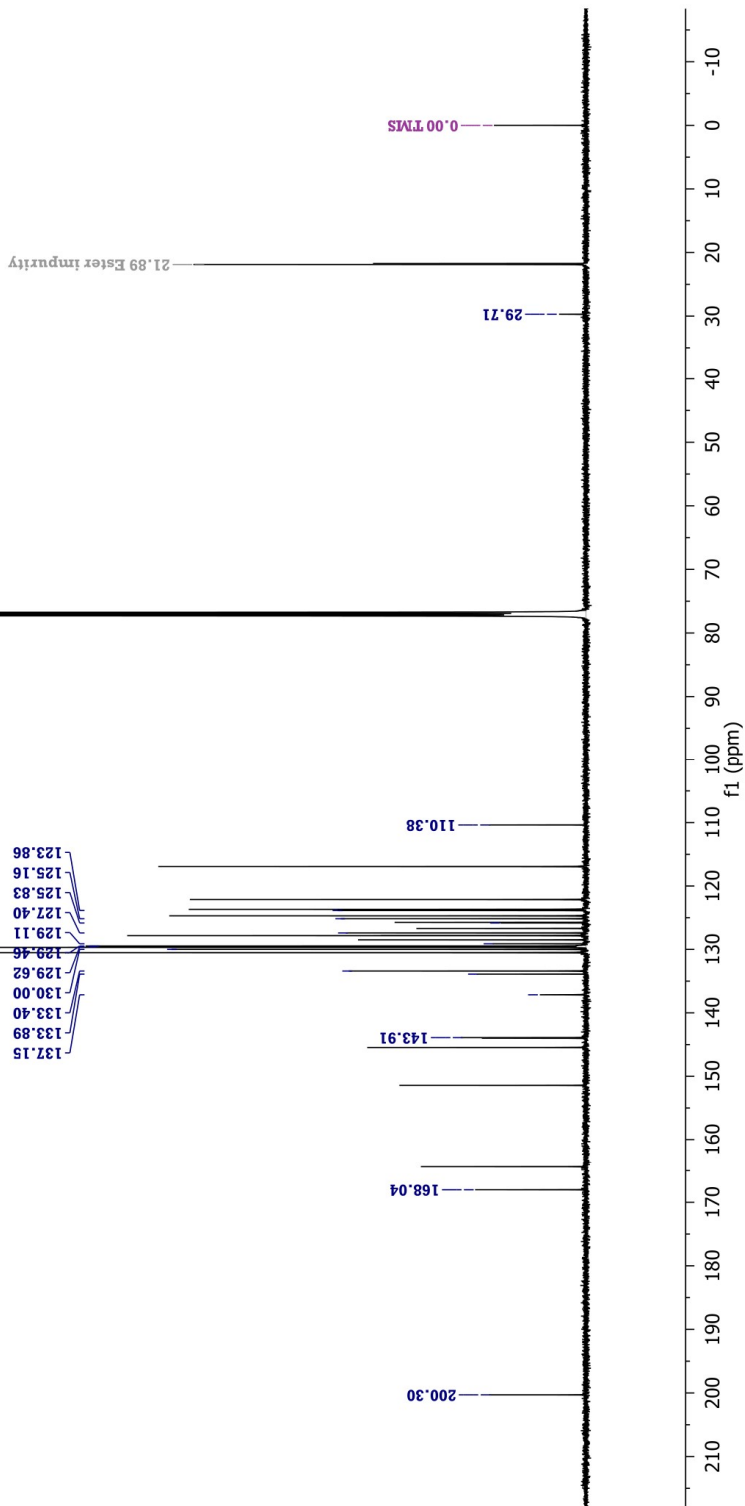
JAJ2-60-A.10.fid
Comment: 4-nitro-2-(p-methylbenzoyl)-1-naphthol in CDCl3 w/TMS
4096 scans

Origin: Bruker BioSpin GmbH
Solvent: CDCl3
Temperature: 298.0 K
Pulse Sequence: zgpg30
Experiment: 1D
Number of Scans: 4096
Receiver Gain: 196.9 db
Relaxation Delay: 2.0000 s
Pulse Width: 10.0000 μ s
Acquisition Time: 1.1010 s
Acquisition Date: 2020-06-02T23:36:44
Spectrometer Frequency: 125.77 MHz
Nucleus: 13C



Obvious ester impurities are unlabeled.

¹³C NMR (126 MHz, Chloroform-d) δ 200.30, 168.04, 143.91, 137.15, 133.89, 133.40, 130.00, 129.62, 129.46, 129.11, 127.40, 125.83, 125.16, 123.86, 110.38, 29.71.

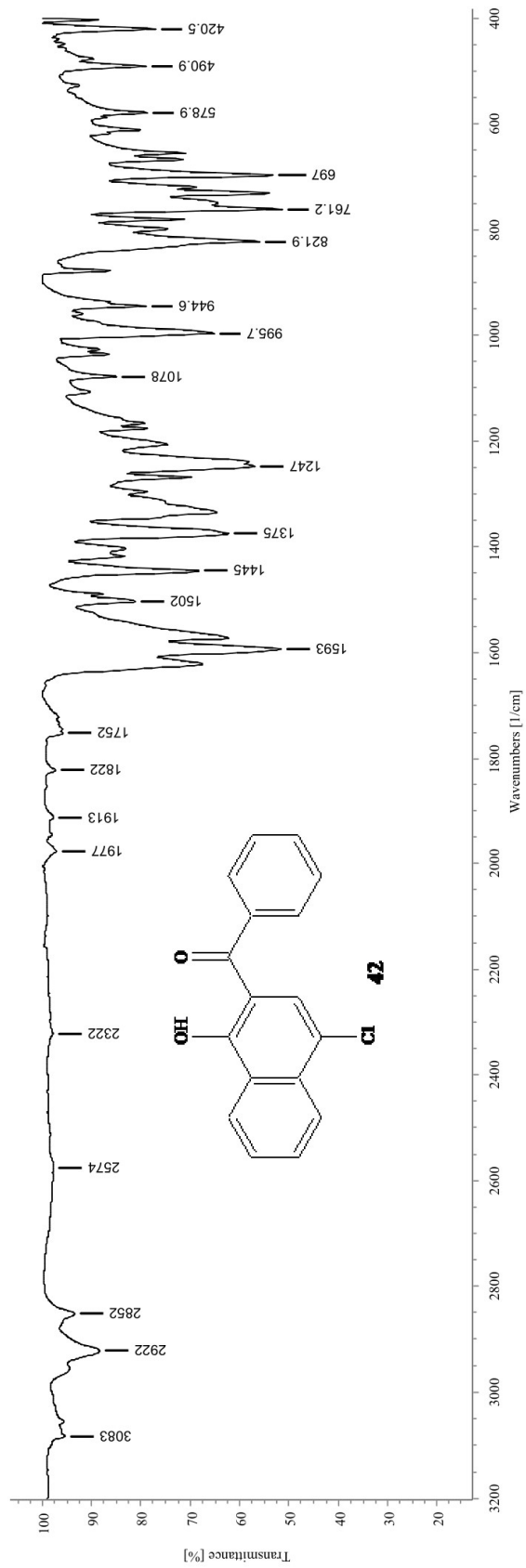


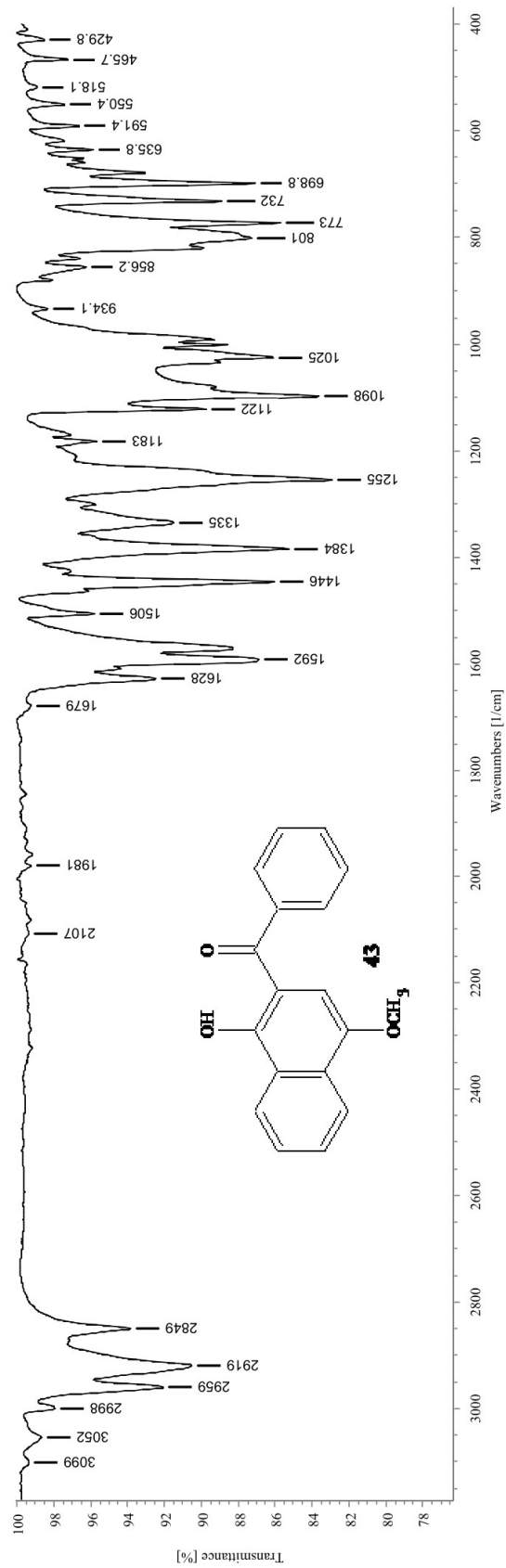
Appendix C: FT-IR Spectra

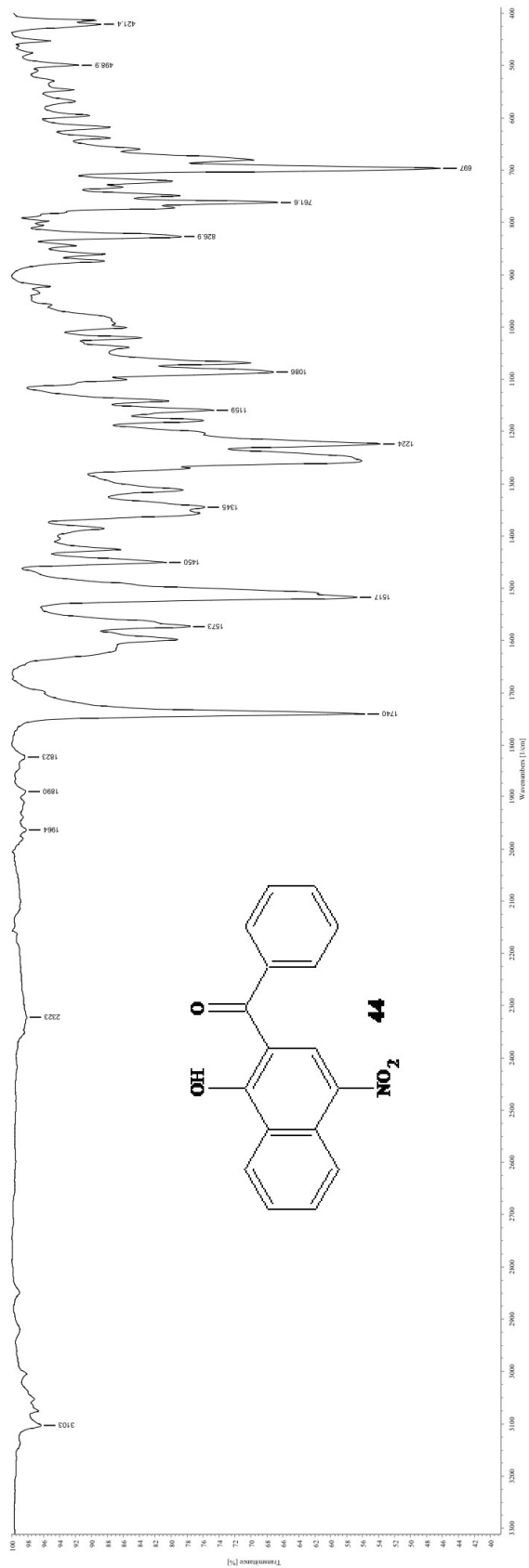
Infrared spectra were obtained on a Perkin-Elmer Spectrum Two FT-IR spectrometer with an attenuated total reflection (ATR) sampling apparatus, with the ATR set to a 1 cm pathlength. The FT-IR spectra were collected by accumulating eight scans at 4 cm^{-1} resolution with the samples compressed onto the ATR crystal under at least 100 Newtons of force using the anvil. Spectra were processed using the instrument's software to execute an ATR correction. Finally, using the freely available Spectragryph software, a baseline correction was performed and peaks were picked using the Spectragryph software (30).

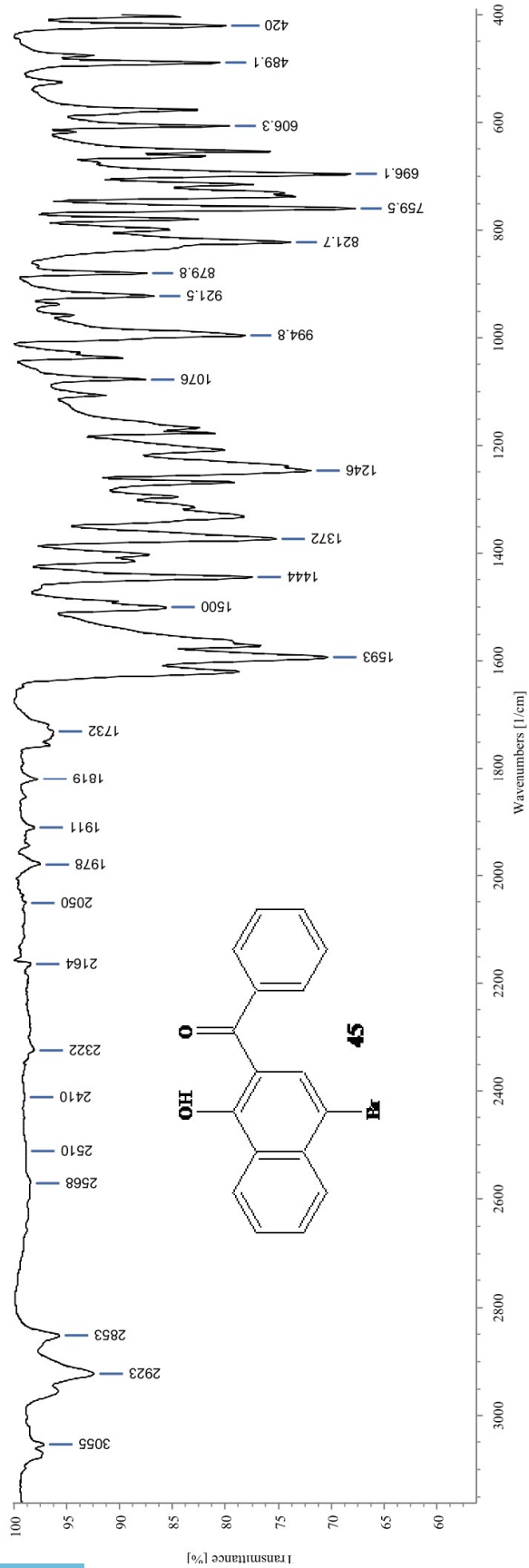
List of FT-IR Spectra in Appendix C

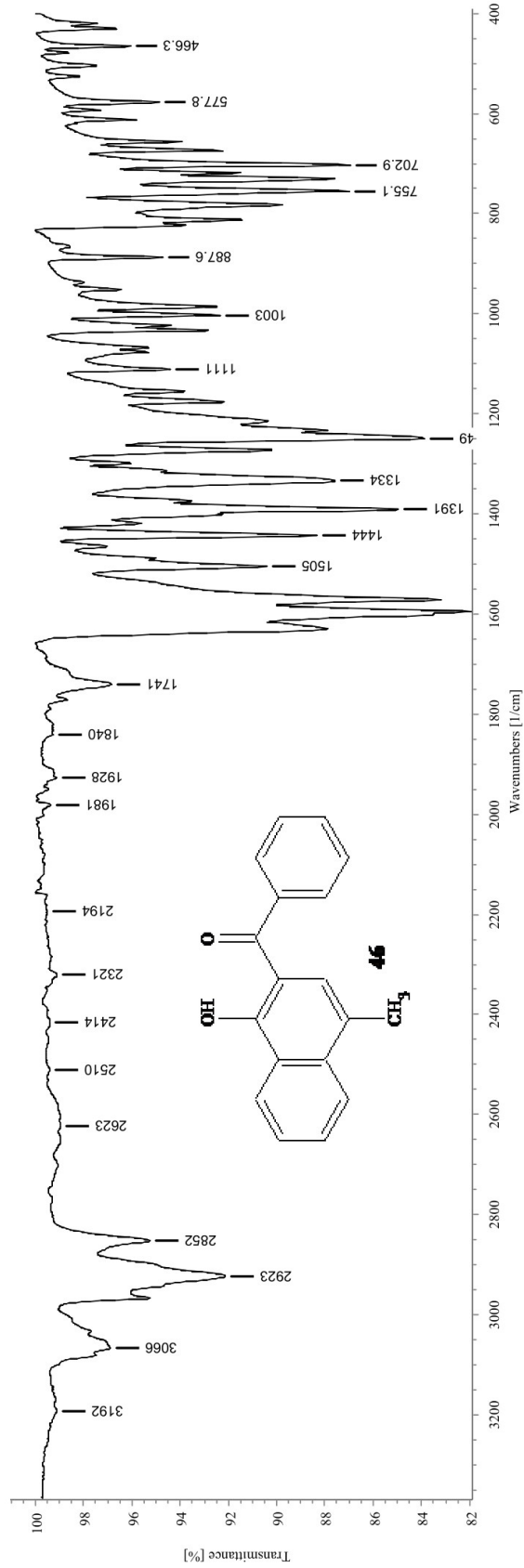
Page 135	2-Benzoyl-4-chloro-1-naphthol – JAJ2-19-A
Page 136	2-Benzoyl-4-methoxy-1-naphthol – JAJ2-53-B
Page 137	2-Benzoyl-4-nitro-1-naphthol – JAJ2-54-B
Page 138	2-Benzoyl-4-bromo-1-naphthol – JAJ2-58-A
Page 139	2-Benzoyl-4-methyl-1-naphthol – JAJ2-59-A
Page 140	2-(<i>p</i> -Toluoyl)-4-nitro-1-naphthol – JAJ2-60-A

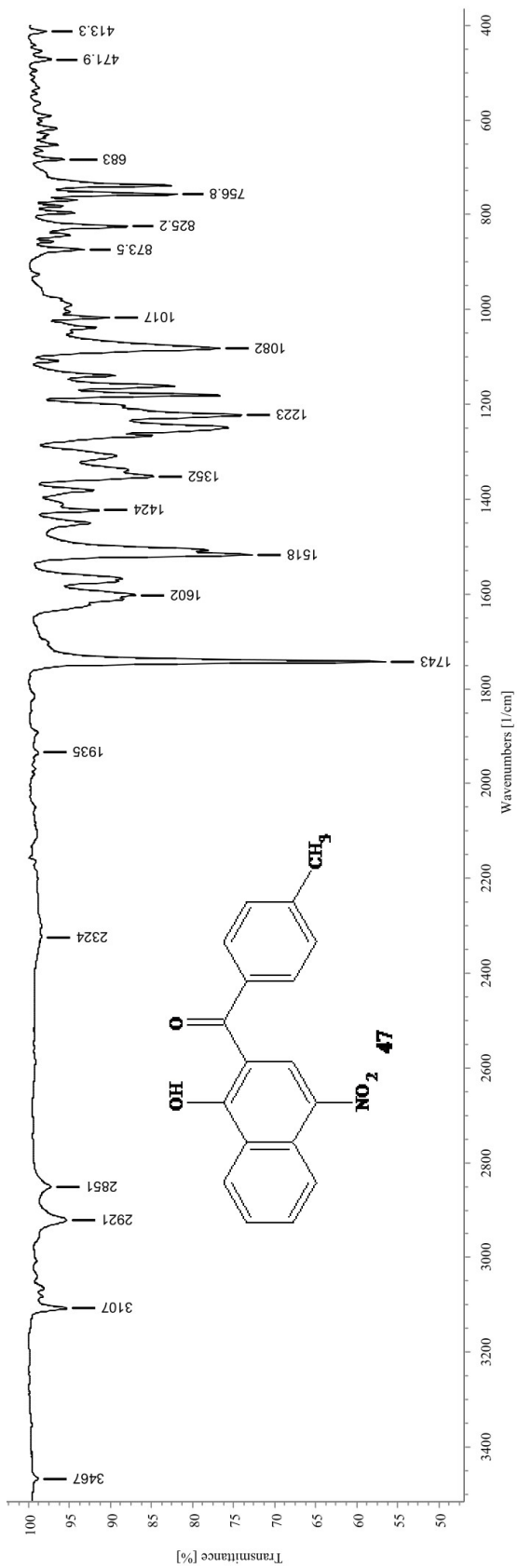










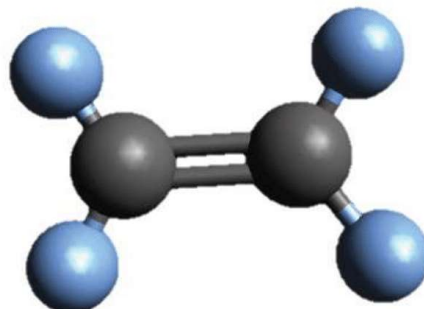


Appendix D: The Avogadro Exercise

The text of the Avogadro exercise appears on the following pages. This material comes directly from the CHEM-1120 lab manual, 2020 edition (57).

EA

Avogadro Exercise



INTRODUCTION

In recent years, the field of computational chemistry has emerged, which utilizes computers to perform complex calculations to model chemical substances and processes. Computational studies can be carried out on chemical systems that would otherwise be impossible to analyze with current technologies, or in support of traditional laboratory analyses. Many computational studies are directed at determining the shapes of molecules, which involves calculating the lowest energy configuration of the atoms in the substance. In this experiment, students will gain experience in modeling chemical compounds using a freely available software, Avogadro, to review concepts of bonding covered in CHEM 1110.

VSEPR THEORY & HYBRIDIZATION

Valence Shell Electron Pair Repulsion (VSEPR) theory provides a relatively simple framework to predict the arrangement of outer atoms around a given central atom. The basic premise of the theory is that electrons in the valence (outer) shell of an atom tend to be as far away from each other in space as possible. Specifically, electrons concentrated in a region of space (electron domains (EDs)) will arrange such that the overall structure has the lowest net repulsive interactions between the EDs. EDs can be any type of bond (single, double, or triple) or a nonbonding electron (as in an odd-electron species, or radical) or electron pair. The electron domain geometry (EDG) describes the arrangement of EDs around a central atom (A), while the molecular geometry (MG) establishes the arrangement of the bonded atoms (B) around the central atom, taking into account the influence of the nonbonding EDs (U). There are characteristic bond angles associated with each of the geometrical arrangements of EDs, which are generally compressed when nonbonding EDs are present, due to the larger repulsive interactions between nonbonding EDs as compared to bonding EDs.

As part of valence bond theory, atomic orbitals undergo hybridization in order to achieve the directional bonding predicted as part of VSEPR theory. The hybridization of the central atom is a function of the EDG, and is identified by describing the number of each orbital hybridized on the atom (*e.g.*,

133 ■

■ Avogadro Ex.

Table A - VSEPR & Hybridization Summary					
Class.	Total # of EDs	EDG	MG	Bond Angle(s)	Hybridization
AB ₂	2	Linear	Linear	180°	sp
AB ₃	3	Trigonal planar	Trigonal planar	120°	sp ²
AB ₂ U	3	Trigonal planar	Bent	<120°	sp ²
AB ₄	4	Tetrahedral	Tetrahedral	109.5°	sp ³
AB ₃ U	4	Tetrahedral	Trigonal pyramidal	<109.5°	sp ³
AB ₂ U ₂	4	Tetrahedral	Bent	<109.5°	sp ³
AB ₅	5	Trigonal bipyramidal	Trigonal bipyramidal	120°, 90°	sp ³ d
AB ₄ U	5	Trigonal bipyramidal	See-saw		sp ³ d
AB ₃ U ₂	5	Trigonal bipyramidal	T-shape		sp ³ d
AB ₂ U ₃	5	Trigonal bipyramidal	Linear		sp ³ d
AB ₆	6	Octahedral	Octahedral	90°	sp ³ d ²
AB ₅ U	6	Octahedral	Square pyramidal		sp ³ d ²
AB ₄ U ₂	6	Octahedral	Square planar		sp ³ d ²

sp³d² hybridization indicates the central atom has hybridized one s orbital, three p orbitals, and two d orbitals). Table A summarizes the EDGs, MGs, bond angles, and hybridizations covered in CHEM 1110 & 1120.

ORGANIC COMPOUNDS & FUNCTIONAL GROUPS

The element carbon (C, Z = 6) forms bonds to a great many elements, including itself. Organic chemistry is the study of compounds containing carbon-hydrogen bonds (at least one carbon atom bonded to a hydrogen atom). The simplest organic compounds contain only carbon and hydrogen, and are therefore known as hydrocarbons. Since carbon-hydrogen bonds themselves are relatively inert, owing to the similar electronegativities of the two elements, transformations of organic molecules generally involve functional groups, which are common structural motifs found in many organic molecules.

As part of this exercise, students will investigate molecular shapes using different organic functional groups as examples. The following section will introduce common functional groups found in organic chemistry (note that the structures are

not drawn to imply any particular geometry):

- Alkyl groups are generally considered to be those containing only carbon-carbon and carbon hydrogen bonds. The "R" designates a variable group (generally an alkyl group of some type), with the subscripts (1 - 4) indicating that they can be different. Saturated hydrocarbons contain only carbon-carbon single bonds.

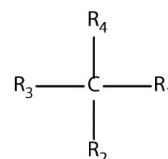


Figure EA1 - An alkyl group (R)

- Unsaturated hydrocarbons contain carbon-carbon double bonds (alkenes) or carbon-carbon triple bonds (alkynes).

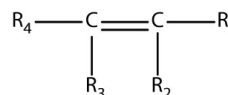


Figure EA2 - An alkene

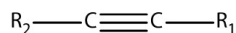


Figure EA3 - An alkyne

- Alkyl halides (R-X, where X = F, Cl, Br, or I) groups involve a carbon atom bonded to a halogen (Group 17 (VIIA)) element.

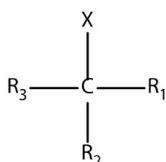


Figure EA4 - An alkyl halide (RX)

- Alcohols (R-OH) involve a hydroxyl (OH) group attached to a carbon atom. In contrast to metal (ionic) hydroxides, aqueous solutions of alcohols tend not to be basic.

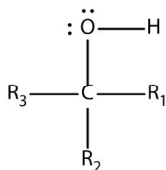


Figure EA5 - An alcohol (ROH)

- Ethers (R-O-R) contain an oxygen atom bonded to two alkyl groups.

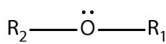


Figure EA6 - An ether (ROR)

- Aldehydes (RC(O)H) contain a carbon atom which has a double bond to an oxygen atom and a single bond to a hydrogen atom. In organic chemistry, the C=O portion itself is referred to as a carbonyl group.

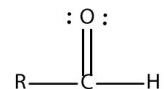


Figure EA7 - An aldehyde (RC(O)H)

- Ketones (RC(O)R) are visually similar to aldehydes, but have the central carbon atom doubly bonded to an oxygen atom with bonds to two other carbon atoms.

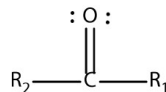


Figure EA8 - A ketone (RC(O)R)

- Carboxylic acids (RC(O)OH) contain a carbonyl group with a hydroxyl group attached to the carbon atom of the carbonyl. As the name implies, carboxylic acids are the most common class of organic acids. The acid behavior of the carboxylic acids is due to resonance stabilization of the resulting anion when the proton is donated.

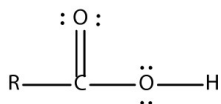


Figure EA9 - A carboxylic acid (RC(O)OH)

- Esters (RC(O)OR) contain a carbonyl group with its carbon atom bonded to another alkyl group and an oxygen atom, which is then bonded to another alkyl group. Esters commonly have pleasant, fruity aromas.

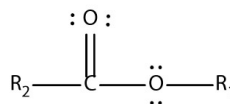


Figure EA10 - An ester (RC(O)OR)

- Amines (NR₃) are organic derivatives of ammonia, NH₃, where one or more of the hydrogen atoms are replaced by alkyl groups. Like ammonia, most amines are weak bases in aqueous solution.

■ Avogadro Ex.

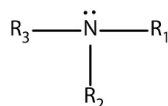


Figure EA11 - An amine (NR_3)

- Amides (RC(O)NR_2) contain a carbonyl group linked with an amine group. Amides are of vital importance in biochemistry, forming the basis of protein structures.

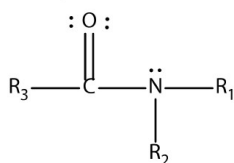


Figure EA12 - An amide (RC(O)NR_2)

AVOGADRO EXERCISE

Avogadro is a free software program that can be used to perform basic computational chemistry processes and modeling. Students are encouraged to download and install Avogadro on their own computers, but it can also be accessed on campus computers, specifically those in Foster 414. Detailed installation instructions, walkthroughs, and video tutorials (for the Windows version) are available on the lab iLearn website. Using a computer with a mouse is **strongly** recommended.

Once you are acclimated to the program, use your knowledge of VSEPR theory, hybridization, and the Avogadro program to complete the associated worksheet.

I. Analysis of Lewis Structures

Using your knowledge of VSEPR theory and hybridization, predict the electron domain geometry (EDG), molecular geometry (MG), and hybridization of the circled atoms in each of the Lewis structures provided. Record your answers in spaces provided on the worksheet.

II. Modeling in Avogadro

For this section, you will build a molecule in Avogadro and optimize the structure to see how the bond lengths and angles change.

For Part A, select one of the four molecules shown in Figure EA13 (the circled atoms indicate which atoms will be used to determine the bond angles). Write the name of the molecule you have chosen to build in Table 1 on the worksheet. In Avogadro, build the molecule, and measure the indicated bond angles and lengths **prior to optimization**. Record these values in the "Pre-Optimization" columns in Table 1 on the worksheet. Then, optimize the structure using Avogadro, and report the optimized bond angles and lengths for the circled atoms. Record these values in the "Post-Optimization" columns Table 1 on the worksheet.

Repeat the above paragraph for Parts B and C, selecting one molecule from Figure EA14 and Figure EA15, respectively.

III. Combined Functional Groups

Using your knowledge of VSEPR theory and hybridization, predict the electron domain geometry (EDG), molecular geometry (MG), and hybridization of the circled atoms in the Lewis structures provided. Record your answers in spaces provided on the worksheet.

Repeat the procedure in Part II to build the molecule in Avogadro and report the Pre-Optimization and Post-Optimization parameters in the appropriate spaces in Table 2. For this structure, report the carbon-nitrogen bond length.

Answer all additional questions and submit your worksheet at the beginning of the pre-lab lecture on the day of the submission deadline.

Acknowledgements - Jordan A. Jones contributed significantly to the development and implementation of this exercise.

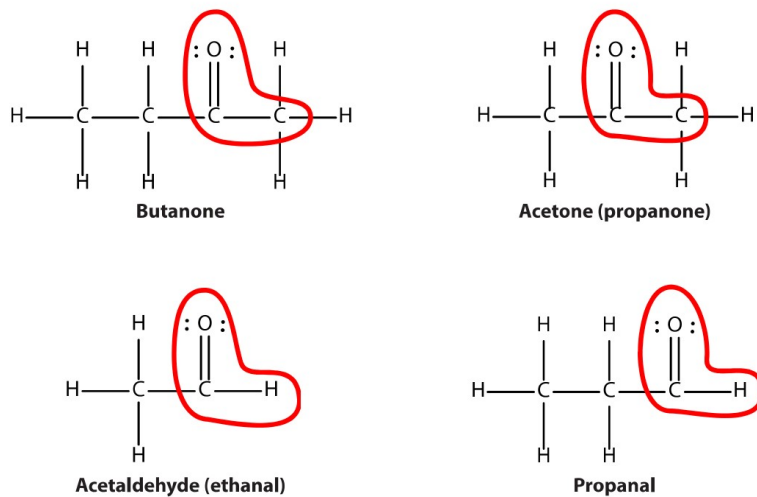


Figure EA13 - Aldehydes and ketones for use in Part A
Report length of circled C=O bond

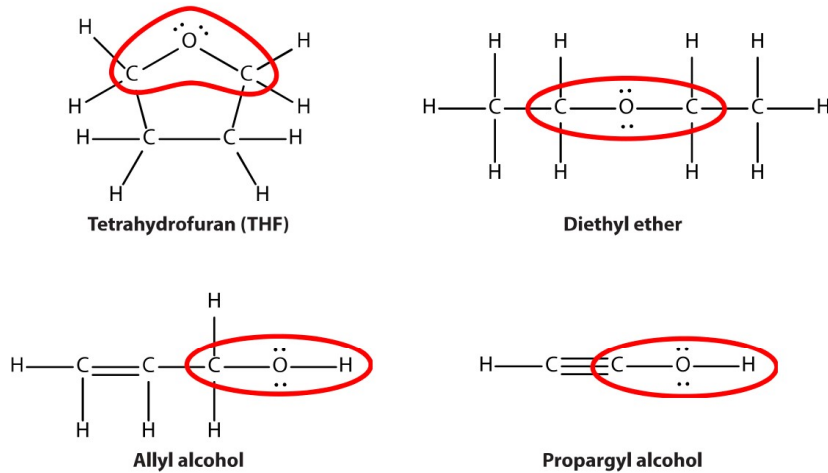


Figure EA14 - Alcohols and ethers for use in Part B
Report length of circled C-O bond

■ Avogadro Ex.

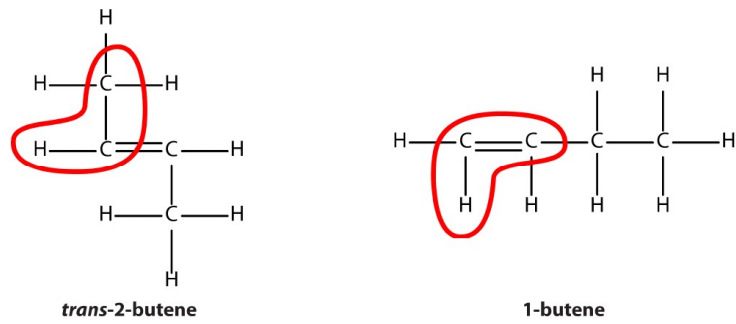


Figure EA15 - Alkenes for use in Part C
Report length of circled C-H bond

■138

EA - Avogadro Exercise - Worksheet

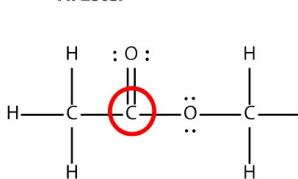
Name _____

Lab Section _____

I. Analysis of Lewis Structures

Examine the Lewis Structures below and answer the corresponding questions using your knowledge of VSEPR theory. All questions below refer to the circled atoms in the Lewis Structure.

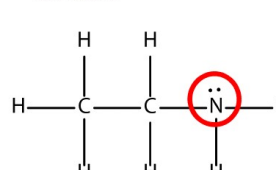
A. Ester



Methyl acetate

EDG of circled carbon atom:	
MG of circled carbon atom:	
Hybridization of circled carbon atom:	

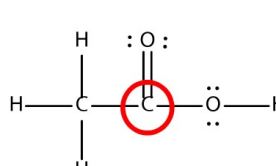
B. Amine



Ethanamine

EDG of circled nitrogen atom:	
MG of circled nitrogen atom:	
Hybridization of circled nitrogen atom:	

C. Carboxylic Acid



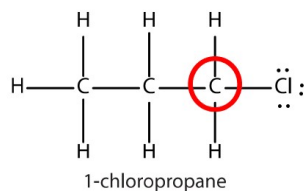
Acetic acid

EDG of circled carbon atom:	
MG of circled carbon atom:	
Hybridization of circled carbon atom:	

139 ■

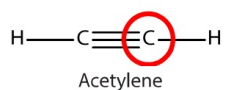
■ Avogadro Ex.

D. Alkyl Halide



EDG of circled carbon atom:	
MG of circled carbon atom:	
Hybridization of circled carbon atom:	

E. Alkyne



EDG of circled carbon atom:	
MG of circled carbon atom:	
Hybridization of circled carbon atom:	

II. Modeling in Avogadro

For Part A, B, and C, choose one of the molecules given in the procedure to build in Avogadro and fill in the table below.

Table 1 - Pre- and Post-Optimization Parameters in Avogadro					
Part	Name of Molecule	Pre-Optimization		Post-Optimization	
		Bond Angle (°)	Bond Length (Å)	Bond Angle (°)	Bond Length (Å)
A					
B					
C					

III. Combined Functional Groups

Based on the Lewis Structure of formamide below

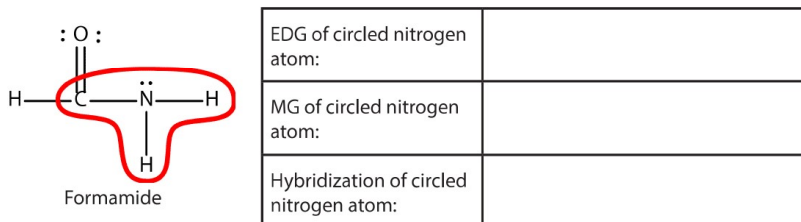


Table 2 - Pre- and Post-Optimization Parameters of Formamide			
Pre-Optimization		Post-Optimization	
Bond Angle (°)	C-N Bond Length (Å)	Bond Angle (°)	C-N Bond Length (Å)

IV. Additional Questions

- Does the observed geometry for formamide (in Part III) match up with what you predicted based on VSEPR theory? If not, what might explain this observation?

Appendix E: The Avogadro Exercise Pre-Quiz

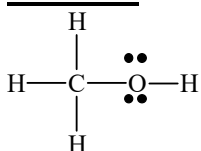
Answers are circled using a box in the quiz below.

CODE: _____ **Please, record this code for your post-quiz.**

Directions: circle one answer for each multiple-choice question below. **DO NOT WRITE YOUR NAME ON THIS QUIZ.**

Note: the Lewis structures provided are not intended to convey any particular geometry.

Methanol



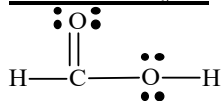
- 1) What is the hybridization of the **oxygen atom** in methanol?
 - A. sp
 - B. sp^2
 - C. sp^3
- 2) Use VSEPR to predict the **molecular geometry** around the **oxygen atom** in methanol.
 - A. Square Planar
 - B. Tetrahedral
 - C. Bent
 - D. Trigonal Planar
- 3) Which of these is the best approximation of the **bond angle between C–O–H** for methanol?
 - A. 104.5°
 - B. 90°
 - C. 109.5°
 - D. 120°

(Flip the page)

Directions: circle one answer for each multiple-choice question below. DO NOT WRITE YOUR NAME ON THIS QUIZ.

Note: the Lewis structures provided are not intended to convey any particular geometry.

Formaldehyde



4) What is the hybridization of the **carbon atom** in formaldehyde?

- A. sp
- B. sp^2
- C. sp^3

5) Use VSEPR to predict the molecular geometry around the **carbon atom** in formaldehyde.

- A. Bent
- B. Trigonal Planar
- C. Tetrahedral
- D. Trigonal Pyramidal

6) Which of these is the best approximation of the **bond angle between O–C–O** for formaldehyde?

- A. 180°
- B. 90°
- C. 104.5°
- D. 120°

Appendix F: The Avogadro Exercise Post-Quiz

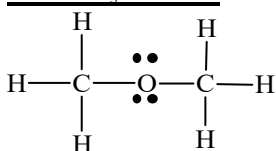
Answers are circled using a box in the quiz below.

CODE: _____ **Enter the code from your pre-test last week.**

Directions: circle one answer for each multiple-choice question below. **DO NOT WRITE YOUR NAME ON THIS QUIZ.**

Note: the Lewis structures provided are not intended to convey any particular geometry.

Dimethyl Ether



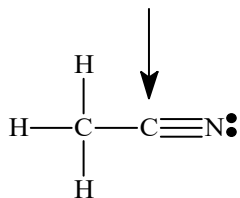
- 1) What is the hybridization of the **oxygen atom** in dimethyl ether?
 - A. sp
 - B. sp^2
 - C. sp^3
- 2) Use VSEPR to predict the **molecular geometry** around the **oxygen atom** in dimethyl ether.
 - A. Square Planar
 - B. Tetrahedral
 - C. Bent
 - D. Trigonal Planar
- 3) Which of these is the best approximation of the **bond angle between C–O–C** for dimethyl ether?
 - A. 104.5°
 - B. 90°
 - C. 109.5°
 - D. 120°

(Flip the page)

Directions: circle one answer for each multiple-choice question below. DO NOT WRITE YOUR NAME ON THIS QUIZ.

Note: the Lewis structures provided are not intended to convey any particular geometry.

Acetonitrile



4) What is the hybridization of the **indicated carbon atom** in acetonitrile?

- A. sp
- B. sp^2
- C. sp^3

5) Use VSEPR to predict the molecular geometry around the **indicated carbon atom** in acetonitrile?

- A. Bent
- B. Linear
- C. Tetrahedral
- D. Trigonal Pyramidal

6) Which of these is the best approximation of the **bond angle between C–C–N** for acetonitrile?

- A. 180°
- B. 90°
- C. 104.5°
- D. 120°

Appendix G: The Avogadro Exercise Student Survey

Students were first informed of how their responses would be used and asked to provide their consent for the author to use their responses. If they refused, the survey terminated there. If they agreed, it went on to ask the student asked to enter their pre-test code. The next page then asked them to indicate their level of agreement with the following statements. Levels of agreement included strongly agree, somewhat agree, neutral, somewhat disagree, and strongly disagree. Finally, the students were given a space to respond with any comments. The results of this survey can be found in **Table 7.12** (pp.93) and **Figure 7.31** (pp. 94).

- The experiment write-up in the lab manual provided sufficient background.
- The instructions in the procedure were easy to follow.
- The video tutorial was helpful in completing the exercise.
- I was provided enough resources to complete the exercise.
- The questions on the worksheet were fair.
- I learned how to construct molecules in Avogadro through this exercise.
- This exercise helped me review VSEPR theory.
- This exercise helped me review hybridization.
- I enjoyed this exercise.
- I think this exercise was a waste of my time.

References

1. Gilli, G.; Gilli, P. *The Nature of the Hydrogen Bond: Outline of a Comprehensive Hydrogen Bond Theory*; Oxford University Press: Oxford, 2009.
2. Gilli, P.; Bertolasi, V.; Pretto, L.; Lyčka, A.; Gilli, G. The Nature of Solid-State N–H···O/O–H···N Tautomeric Competition in Resonant Systems. Intramolecular Proton Transfer in Low-Barrier Hydrogen Bonds Formed by the $\cdots\text{OC}=\text{CN}-\text{NH}\cdots \rightleftharpoons \cdots\text{HO}-\text{CC}=\text{NN}\cdots$ Ketohydrazone–Azoenol System. A VT XRC and DFT Study. *Journal of the American Chemical Society* **2002**, *124* (45), 13554-13567.
3. Huggins, C. M.; Pimentel, G. C.; Shoolery, J. N. Proton Magnetic Resonance Studies of chloroform in solution: Evidence for hydrogen bonding. *J. Chem. Phys.* **1956**, *23*, 1311-1314.
4. Jeffrey, G. A.; Saenger, W. *Hydrogen Bonding in Biological Structures*; Springer-Verlag: Berlin, Heidelberg, 1991.
5. Tran, H. A. Erlenmeyer Flask. *The Journal of Clinical Endocrinology & Metabolism* **2004**, *89* (10), 4827–4828.
6. Bio-Rad Laboratories, Inc. Acetylacetone - ¹H NMR Chemical Shifts - SpectraBase. <https://spectrabase.com/spectrum/EONbc6IZImr> (accessed April 10, 2019).
7. Schmidt, E. A.; Hoffmann, H. M. Thermodynamically unstable enols. 2-Methyl-2-penten-3-ols from 4-isopropylidene-5,5-dimethyl-2-dimethylamino-1,3-dioxolane. *J. Am. Chem. Soc.* **1972**, *94* (22), 7832-7837.
8. Solomons, T. W. G.; Fryhle, C. B. *Organic Chemistry*, 10th ed.; Wiley: Hoboken, N.J., 2011.

9. Silverstein, R. M.; Webster, F. X.; Kiemle, D. J. *Spectrometric Identification of Organic Compounds*, 7th ed.; Wiley: Hoboken, NJ, 2005.
10. Crouse, D. J.; Hurlbut, S. L.; Wheeler, D. M. Photo Fries rearrangements of 1-naphthyl esters in the synthesis of 2-acylnaphthoquinones. *Journal of Organic Chemistry* **1981**, *46* (11), 364-378.
11. Basheer, A.; Mishima, M.; Rappoport, Z. Enols of 2-nitro- and related 2-substituted malonamides. *J. Phys. Org. Chem.* **2010**, *23* (3), 255-265.
12. Gilli, G.; Bellucci, F.; Ferretti, V.; Bertolasi, V. Evidence for Resonance-Assisted Hydrogen Bonding from Crystal-Structure Correlations on the Enol Form of the β -Diketone Fragment. *J. Am. Chem. Soc.* **1989**, *111*, 1023-1028.
13. Gilli, P.; Bertolasi, V.; Ferretti, V.; Gilli, G. Evidence for resonance-assisted hydrogen bonding. 4. Covalent nature of the strong homonuclear hydrogen bond. Study of the O-H--O system by crystal structure correlation methods. *J. Am. Chem. Soc.* **1994**, *116* (3), 909-915.
14. Wells, P. R. Linear Free Energy Relationships. *Chem. Rev.* **1963**, *63* (2), 171-219.
15. Hammett, L. P. Some Relations Between Reaction Rates and Equilibrium Constants. *Chem. Rev.* **1935**, *17* (1), 125-136.
16. Hammett, L. P. The Effect of Structure upon the Reactions of Organic Compounds. Benzene Derivatives. *J. Am. Chem. Soc.* **1937**, *59* (1), 96-103.
17. Spraul, B. K.; Suresh, S.; Jin, J.; Smith, D. Synthesis and Electronic Factors in Thermal Cyclodimerization of Functionalized Aromatic Trifluorovinyl Ethers. *J. Am. Chem. Soc.* **2006**, *128* (21), 7055-7064.

18. Charton, M.; Charton, B. I. The mode of transmission of electrical effects: evidence from infrared stretching frequencies. *Journal of Physical Organic Chemistry* **2001**, *14* (11), 832-838.
19. Mathis, T. M. *Synthesis and Characterization of o-Acylnaphthols*; Tennessee Technological University via ProQuest: Cookeville, Tennessee, 2009.
20. T. Cohen, A. G. D. J.; Miser, J. R. A simple preparation of phenols from diazonium ions via the generation and oxidation of aryl radicals by copper salts. *J. Org. Chem.* **1977**, *42* (12), 2053-2058.
21. Furwson, R. C.; Horning, E. C.; Rowland, S. P.; Ward, M. L. Mesitaldehyde. *Organic Syntheses* **1943**, *23*, 549.
22. Read, R. R.; Wood, J. J. o-n-HEPTYLPHENOL. *Organic Syntheses* **1940**, *20*, 57.
23. Mirsadeghi, S.; Rickborn, B. Trapping Reactive Intermediate Carbanions Generated by Lithium Tetramethylpiperidide Treatment of 7-Oxabicyclo[2.2.1]heptenes in the Presence of Trimethylsilyl Chloride. *J. Org. Chem* **1986**, *51* (7), 986-992.
24. Dougherty, C. M.; Baumgarten, R. L.; A. Sweeney, J.; Concepcion, E. Phthalimide, Anthranilic Acid, Benzyne: An undergraduate organic laboratory sequence. *J. Chem. Ed.* **1977**, *54* (10), 643-644.
25. E. Wolthuis, B. B.; DeWall, G.; Geels, E.; Leegwater, A. Reactions of Methyl-substituted 1,4-Epoxy-1,4-dihydronaphthalenes. *J. Org. Chem.* **1963**, *28* (1), 144-158.
26. Ballantine, M.; Menard, M. L.; Tam, W. Isomerization of 7-Oxabenzonorbordienes into Naphthols Catalyzed by $[RuCl_2(CO)_3]_2$. *J. Org. Chem.* **2009**, *74* (19), 7570-7573.

27. Armarego, W. L. F.; Chai, C. *Purification of Laboratory Chemicals*, 6th ed.; Butterworth–Heinemann Inc.: Burlington, Massachusetts, USA, 2009.
28. Still, W. C.; Kahn, M.; Mitra, A. Rapid Chromatographic Technique for Preparative Separations with Moderate Resolution. *J. Org. Chem.* **1978**, *43* (14), 2923-2925.
29. Fulmer, G. R.; Miller, A. J.; Sherden, N. H.; Gottlieb, H. E.; Nudelman, A.; Stoltz, B. M.; Bercaw, J. E.; Goldberg, K. I. NMR Chemical Shifts of Trace Impurities: Common Laboratory Solvents, Organics, and Gases in Deuterated Solvents Relevant to the Organometallic Chemist. *Organometallics* **2010**, *29* (9), 2176-2179.
30. Menges, F. Spectragryph - optical spectroscopy software.
<https://www.effemm2.de/spectragryph/> (accessed June 2, 2020).
31. Mirsadeghi, S.; Rickborn, B. Trapping reactive intermediate carbanions generated by lithium tetramethylpiperidide treatment of 7-oxabicyclo[2.2.1]heptenes in the presence of trimethylsilyl chloride. *J. Org. Chem.* **1986**, *51* (7), 986-992.
32. Wolthius, E.; Bossenbroek, B.; DeWall, G.; Geels, E.; Leegwater, A. Reactions of Methyl-substituted 1,4-Epoxy-1,4-dihydronaphthalenes. *J. Org. Chem.* **1963**, *28* (1), 148-152.
33. Villeneuve, K.; Tam, W. Ruthenium-Catalyzed Isomerization of Oxa/Azabicyclic Alkenes: an Expedient Route for the Synthesis of 1,2-Naphthalene Oxides and Imines. *J. Am. Chem. Soc.* **2006**, *128* (11), 3514-3515.
34. Shriner, R. L.; Hermann, C. K. F.; Morrill, T. C.; Curtin, D. Y.; Fuson, R. F. *The Systematic Identification of Organic Compounds*; John Wiley & Sons, Inc.: New York City, 1998; pp 239-247.

35. Ungnade, H. E.; Orwoll, E. F. 3-BROMO-4-HYDROXYTOLUENE. *Organic Syntheses* **1943**, No. 23, 11.
36. Crouse, D. J. *STUDIES IN THE SYNTHESIS OF ADRIAMYCIN ANALOGS*; The University of Nebraska - Lincoln via ProQuest: Lincoln, Nebraska, USA, 1980.
37. Wolthuis, E.; Bossenbroek, B.; DeWall, G.; Geels, E.; Leegwater, A. Reactions of Methyl-substituted 1,4-Epoxy-1,4-dihydronaphthalenes. *J. Org. Chem.* **1963**, 28 (1), 148-152.
38. Sonntag, N. O. V. The Reactions of Aliphatic Acid Chlorides. *Chem. Rev.* **1953**, 52 (2), 237-416.
39. Anderson, J. C.; Reese, C. B. Photoinduced Fries Rearrangement. *Proc. Chem. Soc.* **1960**, 1960 (June), 217.
40. Kobsa, H. Rearrangement of Aromatic Esters by Ultraviolet Radiation. *J. Org. Chem.* **1962**, 27 (7), 2293-2298.
41. Hansch, C.; Leo, A.; Taft, R. W. A Survey of Hammett Substituent Constants and Resonance and Field Parameters. *Chem. Rev.* **1991**, 91 (2), 165-195.
42. Mertler, C. A.; Reinhart, R. V. *Advanced and Multivariate Statistical Methods: Practical Application and Interpretation*, 6th ed.; Routledge: New York, 2016.
43. Gillespie, R. J.; Nyholm, R. S. Inorganic Stereochemistry. *Chemical Society Quarterly Reviews* **1957**, 11 (4), 339-380.
44. Gillespie, R. J. Fifty years of the VSEPR model. *Coordination Chemistry Reviews* **2008**, 252 (12-14), 1315-1327.
45. Esselman, B. J.; Block, S. B. VSEPR-Plus: Correct Molecular and Electronic Structures Can Lead to Better Student Conceptual Models. *J. Chem. Ed.* **2019**, 96 (1), 75-81.

46. Burke, K.; Wagner, L. O. DFT in a nutshell. *International Journal of Quantum Chemistry* **2012**, *113* (2), 96-101.
47. Case, D. A.; Cheatam III, T. E.; Darden, T.; Gohkle, H.; Luo, R.; Merz Jr., K. M.; Onufriev, A.; Simmerling, C.; Wang, B.; Woods, R. The Amber biomolecular simulation programs. *J. Computat. Chem.* **2005**, *26* (16), 1668-1688.
48. Chan, H. S.; Dill, K. A. The Protein Folding Problem. *Physics Today*, February 1993, 24-32.
49. Acuna, V. V.; Hopper, R. M.; Yoder, R. J. Computer-Aided Drug Design for the Organic Chemistry Laboratory Using Accessible Molecular Modeling Tools. *J. Chem. Educ.* **2020**, *97* (3), 760-763.
50. Durrant, J. M.; McCammon, J. A. Molecular dynamics simulations and drug discovery. *BMC Biology* **2011**, *9* (1).
51. Hii, K. K.; Rzepa, H. S.; Smith, E. H. Asymmetric Epoxidation: A Twinned Laboratory and Molecular Modeling Experiment for Upper-Level Organic Chemistry Students. *J. Chem. Educ.* **2015**, *92* (8), 1385-1389.
52. O'Brien, M. Creating 3-Dimensional Molecular Models to Help Students Visualize Stereoselective Reaction Pathways. *J. Chem. Educ.* **2016**, *93* (9), 1663-1666.
53. Tantillo, D. J.; Siegel, J. B.; Saunders, C. M.; Palazzo, T. A.; Painter, P. P.; O'Brien, T. E.; Nuñez, N. N.; Nouri, D. H.; Lodewyk, M. W.; Hudson, B. M.; Hare, S. R.; Davis, R. L. Computer-Aided Drug Design for Undergraduates. *J. Chem. Educ.* **2019**, *96* (5), 920-925.
54. Phillips, A.; Ludowieg, H.; Swihart, S.; Autschbach, J.; Zurek, E. The Computational Design of Two-Dimensional Materials. *J. Chem. Educ.* **2019**, *96* (10), 2308-2314.

55. Avogadro Chemistry. Avogadro - Free cross-platform molecular editor - Avogadro.
<https://avogadro.cc/> (accessed May 20, 2020).
56. Allwright, J. C. Conjugate gradient versus steepest descent. *Journal of Optimization Theory and Applications* **1976**, 20 (1), 129-124.
57. Rezsnyak, C. E. *General Chemistry 1120 Laboratory Manual 2020*; XanEdu: Cookeville, TN, 2020.

Vita

Jordan Anthony Jones was born on June 3, 1996. He was raised in Lexington, TN, where he attended Westover Elementary School and graduated from Lexington High School in May 2014. The following August, he entered undergraduate study at Tennessee Technological University, where he eventually chose to major in Applied Chemistry. He received the degree of Bachelor of Science in Applied Chemistry in May 2018. He continued his studies at Tennessee Technological University, working under D. Crouse, Ph.D., and C. Rezsnyak, Ph.D., to earn the degree of Master of Science in Chemistry in August 2020.